THE UNIVERSITY *of* EDINBURGH

Analysis of the function of LSH in DNA Damage Repair

Joseph Burrage

Thesis presented for the degree of Doctor of Philosophy

University of Edinburgh

2012

Declaration

I declare that this thesis was composed by myself, the research presented is my own except where otherwise stated and this work has not been submitted for any other degree or professional qualification.

Joseph Burrage

September 2012

Abstract

DNA damage from both normal metabolic activities and environmental factors such as UV and radiation can cause as many as 1 million individual lesions to the DNA per cell per day (Lodish *et al* 2004). Cells respond to this continuous damage by employing many, highly efficient DNA repair mechanisms and undergo apoptosis when normal DNA repair fails. Of the many types of DNA damage that can occur, double strand breaks (DSBs) are the most toxic (Featherstone & Jackson 1999). A single unrepaired DSB is enough to induce cellular apoptosis and several mechanisms have developed to repair DSBs. The recognition, signalling and repair of DSBs involve large multi-subunit complexes that bind to both the DNA and modified histone tails, which require modification of the chromatin in order to access their bind sites and function effectively (Allard *et al* 2004). Consequently several chromatin-remodelling proteins have been implicated in DSB repair (van Attikum *et al* 2004, Chai *et al* 2005).

LSH (Lymphoid specific helicase) is a putative chromatin-remodelling enzyme that interacts with DNA methyltransferases and has been connected to DNA methylation (Myant & Stancheva, 2008). Knockouts of LSH or its homologues in *A. thaliana* and *M. musculus* show a reduction in DNA methylation of 60-70% (Jeddeloh *et al* 1999, Dennis *et al* 2001). However in addition to this phenotype, knockout *A. thaliana* also have an increased sensitivity to DNA damage (Shaked *et al* 2006). A homologue of LSH has also been identified in *S. cerevisiae*, which interacts with known repair proteins (Collins *et al* 2007) and may be involved in DSB repair. Although the majority of $Lsh^{-/-}$ mice die shortly after birth, 40% of the line produced by Sun *et al* survive and show unexplained premature aging (Sun *et al* 2004). As premature aging is a hallmark of increased acquisition of DNA damage there is the possibility of a conserved role for LSH in mammalian DNA damage repair.

Here I show that LSH depleted mammalian cells have an increased sensitivity specifically to DSB inducing agents and show increased levels of apoptosis. Further analysis shows that cells lacking LSH repair DSBs slower, indicating a novel role for LSH in mammalian repair of DSB. I performed an in depth analysis of the DSB defects in LSH depleted cells in an attempt to elucidate the function of LSH in DSB repair. I found that LSH depleted cells can correctly recognise DSBs but recruit downstream signalling and repair factors, such as γH2AX, less efficiently. I show that reduced recruitment of downstream DSB repair factors is not accompanied by extended cell cycle checkpoint signalling. This suggests that LSH depleted cells continue through the mitosis with unrepaired DSBs, which most likely leads to apoptosis and the increased sensitivity to DSB inducing agents. These experiments also showed that recruitment of DSB signalling and repair factors is not impaired equally at all breaks, and I present a model system created to quantitatively compare individually breaks between WT and LSH depleted cells to identify DSB that require LSH for efficient repair. I also preformed an analysis of *Lsh*$^{-/-}$ MEFs containing WT or catalytic null mutant LSH rescue constructs and I show that WT but not catalytic null LSH can restore efficient DSB repair. These studies identify a novel role for LSH in mammalian DSB repair and demonstrate the importance of its catalytic activity.

Introduction - Chapter One

1.1 DNA Damage Repair

1.1.2 DNA damage repair mechanisms

As many as 1 million individual DNA lesions can occur per cell per day (Lodish *et al* 2004). These arise from normal metabolic activities and environmental factors such as UV or radiation. This large array of damaging agents can cause a wide variety of DNA lesions ranging from mismatches caused by replication errors to double strand breaks from exposure to ionising radiation. Cells have developed many different repair mechanisms to cope with these different types of damage. These mechanisms are highly efficient and usually incorporate backup repair pathways because unrepaired DNA damage can induce potentially harmful mutations affecting transcript integrity and genome fidelity.

1.1.2.1 Base excision repair (BER)

BER repairs damage to bases resulting from oxidation, deamination, the addition of non-bulky side groups or loss of the base (Memisoglu *et al* 2000). There are 2 BER pathways (Figure 1.1) "short-patch", which represents approximately 80-90% of all BER and "long-patch", which corrects the remaining damage resistant to “short-patch” repair. Both are initiated by cleavage of the N-glycosidic bond between the damaged base and the sugar phosphate backbone. In humans, this cleavage is carried out by one of eight DNA glycosylase, each specific to a different type of damage (Schärer & Jiricny 2001). Cleavage creates an abasic site in the DNA. Subsequent processing of the abasic site by Endonuclease 1 (APE1) nicks the DNA by cleaving the phosphodiester backbone immediately 5' of the site. This leaves a 3' hydroxyl group and 5' abasic deoxyribose phosphate (dRP). The dRP is removed by DNA polymerase beta (DNA Pol β). DNA Pol β also adds a nucleotide to the 3' end of the nick (Matsumoto & Kim 1995). The single strand nick in the DNA can then be repaired by DNA ligase.

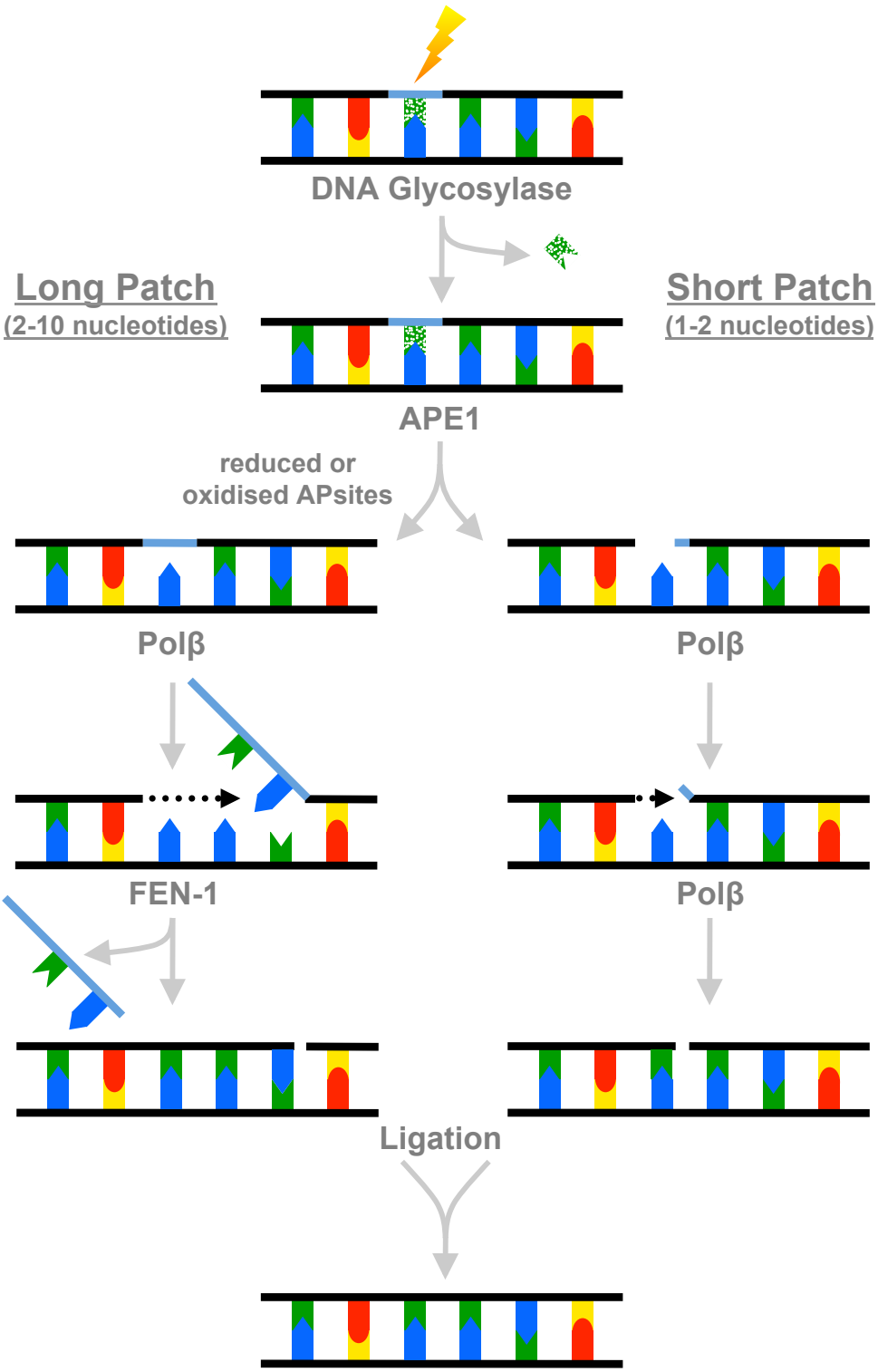

Figure 1.1: A model of BER showing short patch (left) and long patch (right) pathways. "Short-patch" refers to the single new nucleotide replacement of the damaged base, where as "long patch" replaces the lesion with between 2-10 nucleotides (modified from R&D Systems 2011).

The second BER pathway requires many of the same factors involved in “short-patch” repair. "Long-patch" is used when modification of a base makes the abasic site resistant to the abasic lyase activity of DNA Pol β (Matsumoto *et al* 1994). “Long-patch” repair results in the replacement of between 2-10 nucleotides by PCNA-dependent DNA polymerase activity, which displaces the dRP. The resulting oligonucleotide overhang is excised by Flap endonuclease FEN-1 prior to repair of the nick by a DNA ligase.

1.1.2.2 Nucleotide excision repair (NER)

NER repairs a variety of DNA lesions including intrastrand crosslinks, pyrimidine dimers caused by UV exposure and the addition of side groups too large to be removed by BER. NER recognize DNA damage that causes helical distortion of the DNA duplex (Hess *et al* 1997). NER is a complex process that requires correct recognition of the damage followed by unzipping of the DNA double helix around the lesion (Figure 1.2). The damaged DNA strand is then incised and replaced by gap repair synthesis (Batty & Wood 2000). Finally the ends are joined by strand ligation. More than 30 proteins have so far been identified to be involved in NER. There are two NER pathways, global genomic NER (GG-NER) and transcription coupled NER (TC-NER). GG-NER repairs damages in transcriptionally silent areas of the genome where as TC-NER repairs damage to actively transcribed DNA. Both pathways rely on the same repair mechanism, but vary in their method of DNA damage recognition.

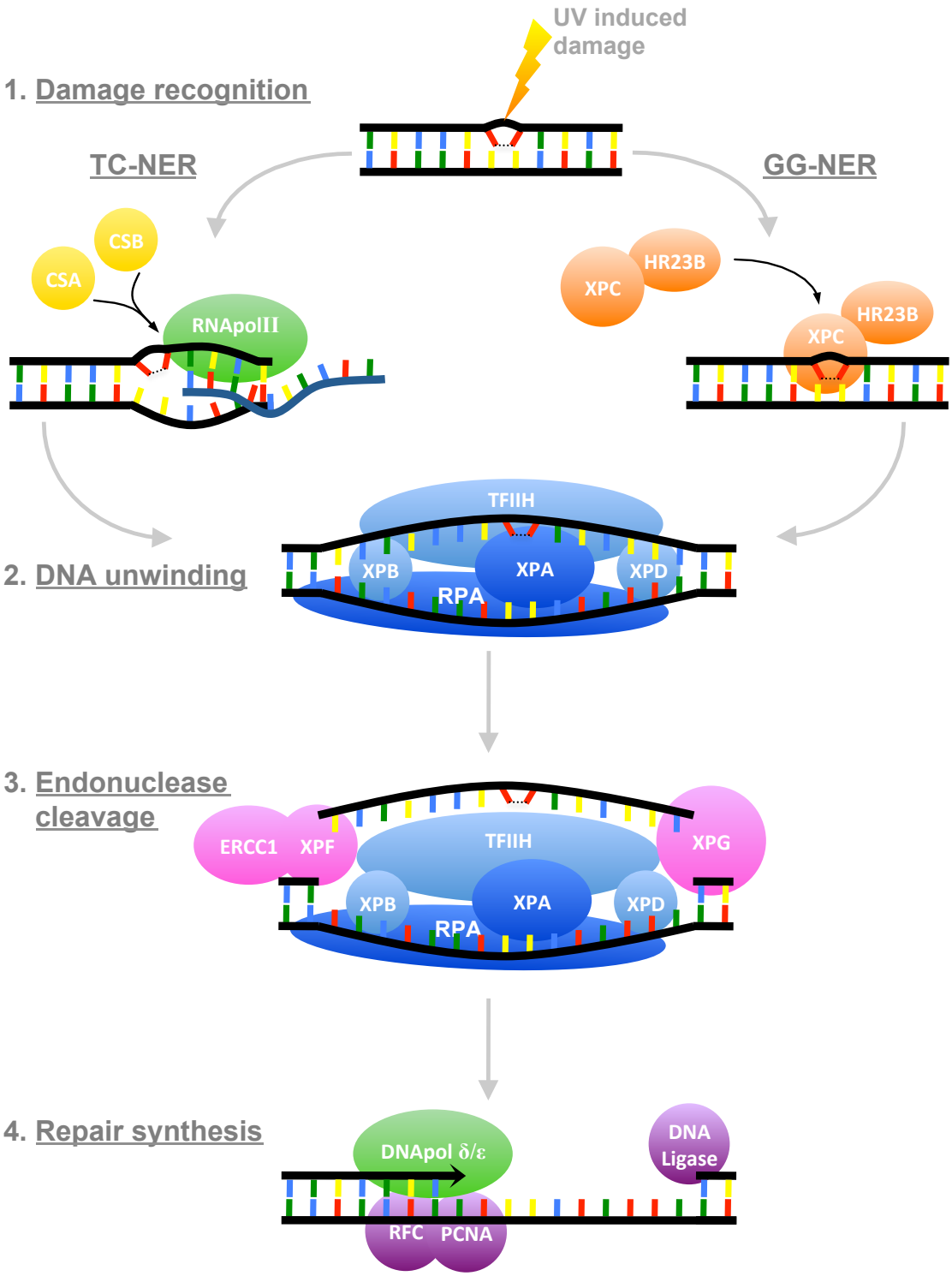

Figure 1.2: A model of NER showing the steps of GG and TC DNA damage recognition (1), DNA unwinding (2), strand incision (3) and repair synthesis and ligation (4).

GG-NER relies on the XPC-HR23B complex to recognize the damage and unwind the DNA. TC-NER does not require XPC, but is thought to rely on stalling of the transcription machinery at sites of DNA damage. The stalled RNA polymerase complex is then displaced by CSA and CSB proteins together with other TC-NER specific factors. The following repair steps are carried out the same in GG- and TC-NER. XPA and replication protein A (RPA) bind the lesion and aid in damage recognition. The helicases XPB and XPD unwind the DNA double helix around the lesion allowing access to endonucleases XPG and ERCC1/XPF. These cleave the damaged strand at positions 3' and 5' of the damage, creating an oligonucleotide approximately 30 bases in length that contains the lesion. The oligonucleotide is displaced and the space filled by DNA Pol δ & ε with the aid of replication accessory factors. The ends of the newly synthesized DNA are then joined to the original strand by DNA ligase.

1.1.2.3 The DNA mismatch repair (MMR)

MMR is essential for correcting replication errors caused by DNA polymerase during replication such as mismatches and insertion/deletion loops (IDLs). MMR also repairs mismatches generated by spontaneous deamination of 5-methylcytosine and heteroduplexes formed by recombination. Defects in MMR result in a mutator phenotype that increases the frequency of spontaneous mutations and causes microsatellite instability (Peltomäki 2001). This can result in a variety of sporadic tumours. MMR is similar to "long-patch" BER and NER, which also rely on excision repair to correct DNA lesions. First the mismatch or IDL is recognised, then a section of DNA containing the lesion is excised and the gap filled by DNA repair synthesis followed by ligation of the DNA nicks (Figure 1.3) (Marti *et al* 2002).

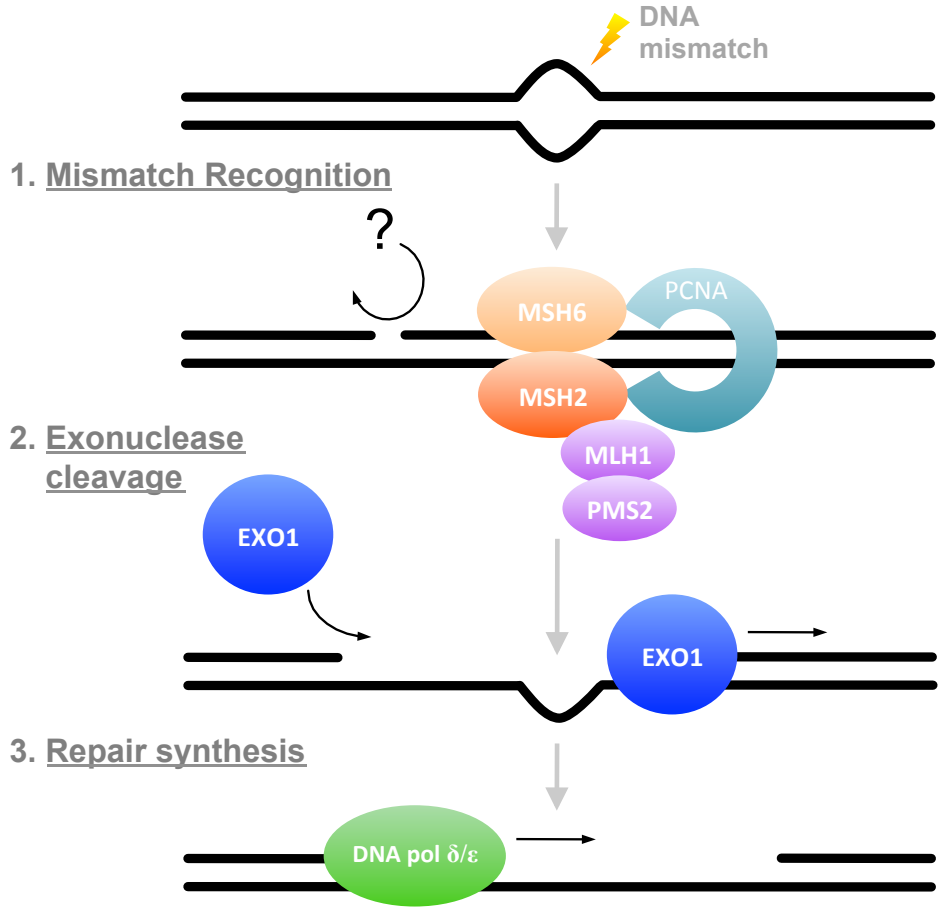

Figure 1.3: A model of mammalian MMR, showing mismatch recognition by MutS alpha (MSH6-MSH2) and strand discrimination followed by excision of the mismatched base and strand resynthesis (modified from Martin & Scharff 2002).

In mammals, MMR is initiated by recognition of the damage by heterodimer MutS alpha or beta. Mismatch and single-base IDL recognition is carried out by MutS alpha, where as MutS beta recognizes larger IDLs (Genschel *et al* 1998). MutS alpha or beta then bind ATP and undergo a conformational change. They can then translocate along DNA until additional MMR proteins are encountered (Gradia *et al* 1999, Blackwell *et al* 1998). MMR proteins make contact with the replication machinery through interactions with the replication accessory factor PCNA (Umar *et al* 1996). This interaction allows strand discrimination to occur and may provide the link for mismatch recognition of newly synthesized DNA. A nick forms in the DNA of the newly synthesized strand. In bacteria this is carried out by endonuclease MutH, but in eukaryotes its unclear if a nick is already present at the replication fork or produced by an unknown homologue of MutH. Excision of the damage is carried out by a number of proteins including Exonuclease I (Figure 1.3). The resulting gap is filled by DNA Pol δ & ε (Buermeyer *et al* 1999). DNA ligase then repairs the nicks in the DNA.

1.1.2.4 Repair of DNA double-strand breaks (DSBs)

DSBs are the most serious form of DNA damage because they pose problems to replication and chromosome segregation. Failure to repair these defects can lead to chromosomal instability and loss of chromosome arms, which can result in miss regulated gene expression and carcinogenesis (Hoeijmakers *et al* 2001). DSBs can be caused by a variety of exogenous agents such as ionizing radiation and genotoxic chemicals as well as from endogenous sources like reactive oxygen species, replication across single-strand DNA breaks and chromosomal stress (Featherstone & Jackson 1999, Kuzminov 2001). DSBs differ from other DNA lesions as they affect both strands of the DNA. Therefore the complementary strand is unavailable as a template for DNA repair synthesis as seen in BER, NER, and MMR.

To repair DSBs cells have developed two DSB repair pathways, homologous recombination (HR) and non-homologous end joining (NHEJ) (Jackson *et al* 2002). HR corrects DSB defects in an error-free manner by using the homologous chromosome as a template. Repair by HR takes place in late S/G2 phases when a sister chromatid is available for use as a repair template. NHEJ takes place throughout the cell cycle and does not require a homologous template for repair, but simply connects two broken ends. NHEJ is often referred to as error-prone as unlike HR there is no checking mechanism to ensure that the correct DNA ends have been connected.

The decision of which pathway to use for DSB repair is influenced by cell cycle stage (Takata *et al* 1998). Repair by HR requires displacement of the Ku70/80 heterodimer on the broken DNA ends and resection of the broken end to leave a 3' single-stranded (ssDNA) overhang. Resection has been found to be dependent on recruitment of CtIP, which in turn has been shown to require deacetylation by Sirtuin 6 (SIRT6) and phosphorylation by cyclin dependent kinases (Kaidi *et al* 2010). Cyclin dependent kinases and SIRT6 are both expressed in a cell cycle dependent manner. They regulate at what point of the cell cycle HR occurs by control of resection.

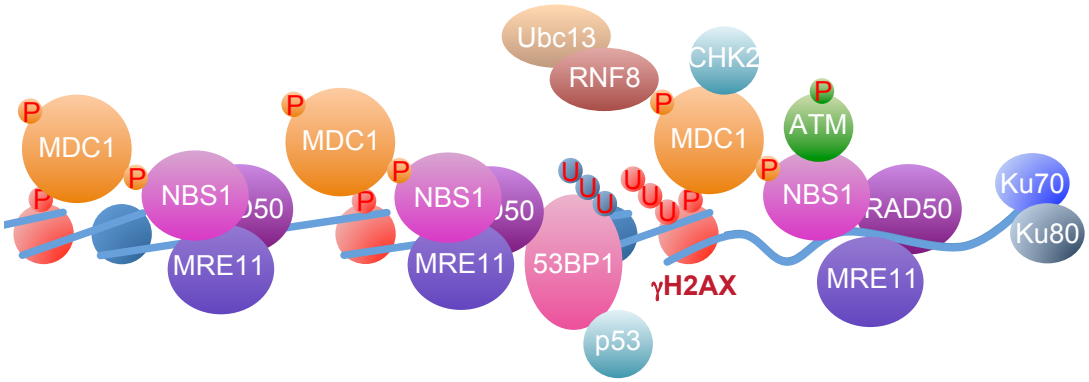

Figure 1.4: Schematic representation of the main mediator complex proteins involved in binding the broken DNA end to facilitate repair and cell cycle check point signalling. Phosphorylation marks are show with a P and U's indicate polyubiquitination of histone tails by Ubc13.

Initial detection of DSBs and checkpoint signalling is carried out in a similar manner in both HR and NHEJ pathways. Initial DSB detection is carried out by the MRN complex, comprised of MRE11, RAD50 and NBS1, which binds to the broken end and recruits activated ATM kinase (Figure 1.4). ATM is activated through auto-phosphorylation of inactive ATM dimers at serine residue 1981 by trans acting ATM kinase domains (Bakkenist & Kastan 2003), although how DNA damage stimulates auto-phosphorylation of inactive ATM dimers is not understood. Ku70/Ku80 heterodimers also bind the broken DNA ends to protect them from endonuclease degradation. ATM in turn phosphorylates histone variant H2AX, which is found throughout the genome at approximately every fifth nucleosome. Phosphorylated H2AX (γH2AX) is recognized as a key marker of DSB repair and is crucial for mediator complex assembly and the recruitment of many downstream repair factors and checkpoint signalling proteins (Figure 1.4). For example MDC1 binds γH2AX, this in turn recruits the checkpoint signalling kinases CHK1 and 2. CHK recruitment to DSBs is essential for their activation and correct cell cycle arrest (Lou *et al* 2003, Xiao *et al* 2003).

Following initial DSB recognition additional protein kinases are recruited that facilitate the DSB response, such as DNA-PK in the case of NHEJ and ATR for repair by HR (Durocher 2001). The phosphorylation of H2AX and associated protein complexes can spread for several megabases on either side of the break. The exact reason for this is unclear, although it has been postulated that γH2AX spreading is required to facilitate access to the broken DNA ends and to stabilise the repair machinery (Savic *et al* 2009)

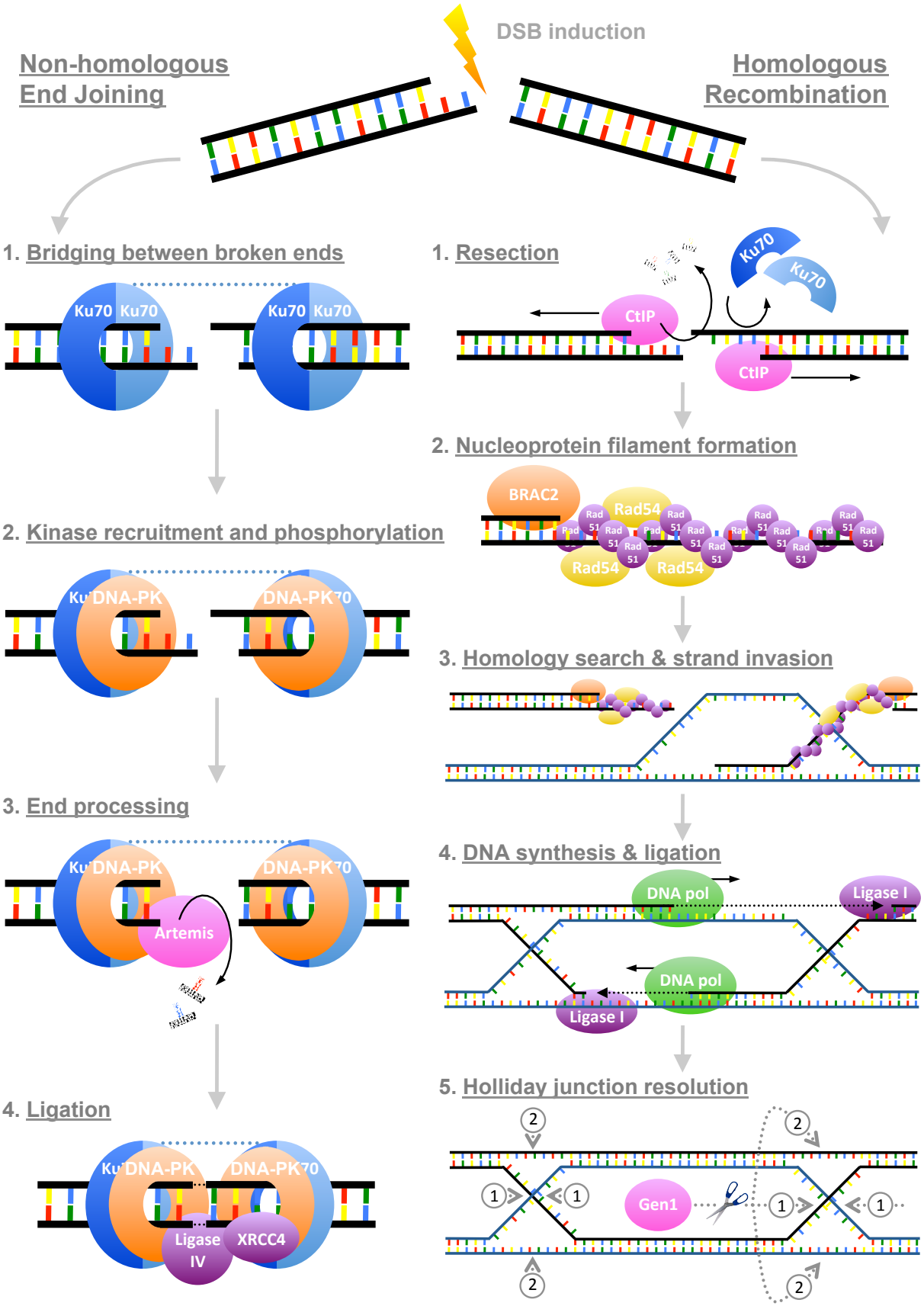

Figure 1.5: An overview of the main steps and factor required for DNA DSB repair by homologous recombination and non-homologous end joining.

Repair by NHEJ relies on the Ku70/Ku80 heterodimer bound to the broken DNA end to recruit NHEJ factors such as DNA-dependent protein kinase (DNA-PK), XRCC4, and DNA Ligase IV (Jackson *et al* 2009, Featherstone & Jackson 1999). Upon binding to Ku70/Ku80, DNA-PK can interact with other Ku70/Ku80 bound DNA-PKs to bridge the gap between broken DNA ends (Figure 1.5, NHEJ 2.). This triggers phosphorylation of DNA-PKs, which in turn can phosphorylate a number of substrates including cell cycle checkpoint proteins such as p53. Most DSBs generated by genotoxic agents have damaged ends that are unable to be directly ligated, they therefore undergo processing by nucleases such as Artemis to create compatible ends (Moshous *et al* 2001, Petrini 2000, Wu *et al* 1999). To complete the repair, DNA Ligase IV is recruited together with its cofactor XRCC4, which ligates the processed ends and repairs the lesion (Figure 1.5, NHEJ 4.).

In contrast to NHEJ, repair by HR requires displacement of the Ku70/Ku80 heterodimer and resection of the broken DNA to leave a 3' ssDNA overhang. The 3' ssDNA overhang is bound by RAD51 to form a nucleoprotein filament (Figure 1.5, HR 2.). Several additional proteins including RPA, RAD52 and BRCA1 & 2, serve as accessory factors in filament assembly and aid in searching the sister chromatid for a homologous repair template (Jackson *et al* 2009). The nucleoprotein filament invades the undamaged DNA duplex forming a D-loop (Figure 1.5, HR 3.). DNA polymerase is then able to extend the 3' end of the damaged strand using the complementary strand on the homologous sister chromatid as a template (Figure 1.5, HR 4.). Following synthesis of the missing sequence, DNA Ligase I closes the nicks the DNA, resulting in the formation of a Holliday junction. Dissolution of the Holliday junction can be achieved by topoisomerase 3 and orthologues of the *S. cerevisiae* helicase SGS1 to unwind the DNA and cut the intertwined strands. Alternatively the resolvase Gen1 can resolve the Holliday junction by cleaving the DNA at 2 sites, resulting in the formation of either a crossover or non-crossover product depending on the orientation of the 2 cleavage sites (Figure 1.5, HR 5.). Finally the nicks in the DNA are ligated to complete repair of the DSB.

1.1.3 Checkpoint signalling

If DNA lesions are allowed to persist through mitosis, they can contribute to genome instability and carcinogenesis. Therefore in addition to repair, correct checkpoint signalling is also important in the DNA damage response (Figure 1.6). By stalling the cell cycle, time is allowed for the repair machinery to correct any DNA lesions, which prevents DNA damage from becoming worse by progression through the cell cycle. For example, if mitosis occurs while unrepaired DSB are present, it can lead to loss of chromosomal arms or, if transcription is carried out across a single stranded DNA nick, a more serious double strand break can form. Another important function of checkpoint signalling is to facilitate apoptosis when DNA lesions cannot be repaired, thus preventing the potential onset of carcinogenesis.

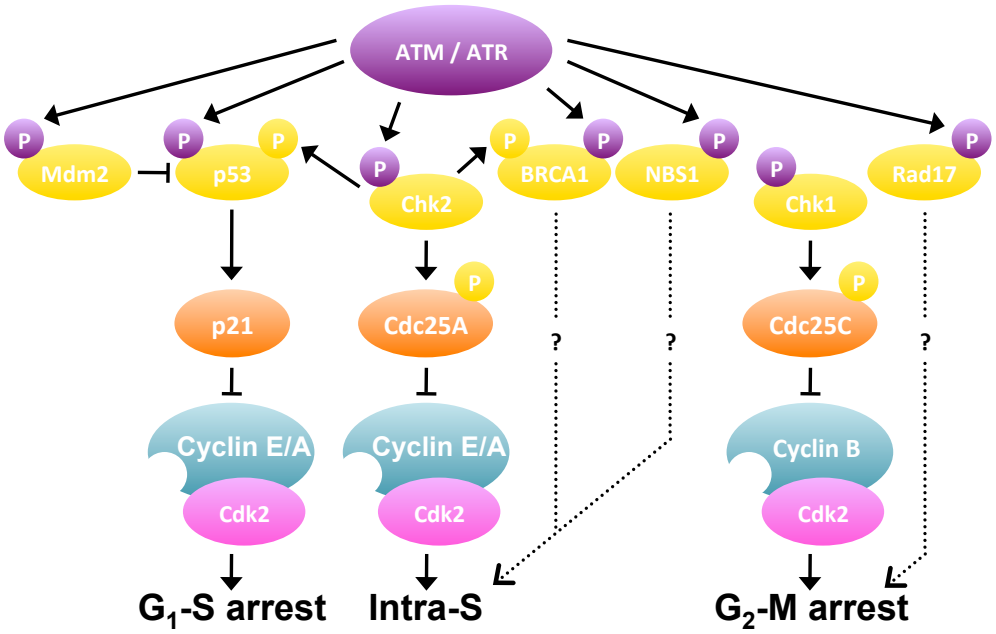

Figure 1.6: An overview of cell cycle checkpoints leading to G1, S, or G2 cell cycle rest in response to ATM / ATR activation (modified from Khanna & Tibbetts 2006).

1.1.3.1 The role of CHK 1 and 2 in checkpoint signalling

Upon induction of DNA damage, kinases CHK1 and 2 are activated by ATM and ATR, which in turn phosphorylate phosphatase Cdc25 (Peng *et al* 1997, Xiao *et al* 2003). Activation of CHK kinases is aided by sequestering CHK proteins to sites of DNA damage such as transient recruitment of CHK2 to DSB by the DSB mediator complex protein MDC1 (Lou *et al* 2003). Phosphorylation of Cdc25

creates a binding site for 14-3-3 proteins, which sequesters Cdc25 in the cytoplasm leading to its targeted degradation by the proteasome. The result is that Cdc25 is unable to dephosphorylate cyclin dependent kinases, which causes G2/S phase arrest and blocks entry into mitosis. This delay gives the repair machinery time to correct the DNA lesion. However failure to repair the damage results in persistent CHK signalling, which can active p53 leading to apoptosis.

1.1.3.2 The role of p53 in checkpoint signalling

Transformation related protein 53 (p53) is a tumour suppressor gene that responds to cellular stresses to regulate the expression of genes involved in cell cycle arrest, apoptosis, senescence and DNA repair. In normal dividing cells p53 levels are kept low by MDM2 targeted degradation, which exports p53 to the cytoplasm for degradation by the proteasome (Alarcon-Vargas & Ronai 2002). Upon induction of DNA damage, kinases phosphorylate a number of sites within p53 leading to its stabilisation and activation. For example, phosphorylation of residue S20 by CHK2 blocks the interaction between p53 and MDM2, preventing nuclear export of p53 and subsequent degradation by the proteasome, increasing p53 levels (Matsuoka *et al* 2000). ATM also phosphorylates MDM2, which blocks its ability to export p53 from the nucleus further stabilizing the increase in p53 levels in response to DNA damage (Cheng *et al* 2011).

ATM and ATR also phosphorylate p53 on residue S15 of p53, allowing it to function as a transcriptional activator to up-regulate a variety of target genes involved in the DNA damage response and cell cycle arrest. These include the cyclin-dependent kinase inhibitor p21, which accumulates and suppresses Cdk2 kinase activity resulting in G1 arrest (Bartek & Lukas 2001). Failure to repair the damage and alleviate checkpoint signalling results in a persistence of high levels of active p53. This in turn leads to p53 mediated apoptosis. Apoptosis acts as a fail-safe mechanism to prevent the persistence of DNA lesions through cell division leading to potentially harmful mutations and carcinogenesis. p53 is the most commonly mutated tumour suppressor genes in human cancer, which demonstrates the importance of p53 mediated cell cycle arrest and apoptosis in preventing the propagation of potentially deleterious mutations.

1.2 Chromatin remodelling

DNA coiling around histones to produce a compact chromatin structure is vital for organising DNA molecules to fit inside the nucleus. However, this coiled structure greatly limits how accessible the DNA is to protein complexes. This impacts on how processes such as recombination, transcription, replication and DNA repair are regulated to allow access to the DNA. There are two mechanisms for relaxing the chromatin to overcoming the barrier posed by a compact chromatin structure. Firstly, modification of histone tails can alter the charged DNA:histone contacts or secondly direct manipulation of DNA:histone interactions by ATP hydrolysis driven chromatin remodelling proteins.

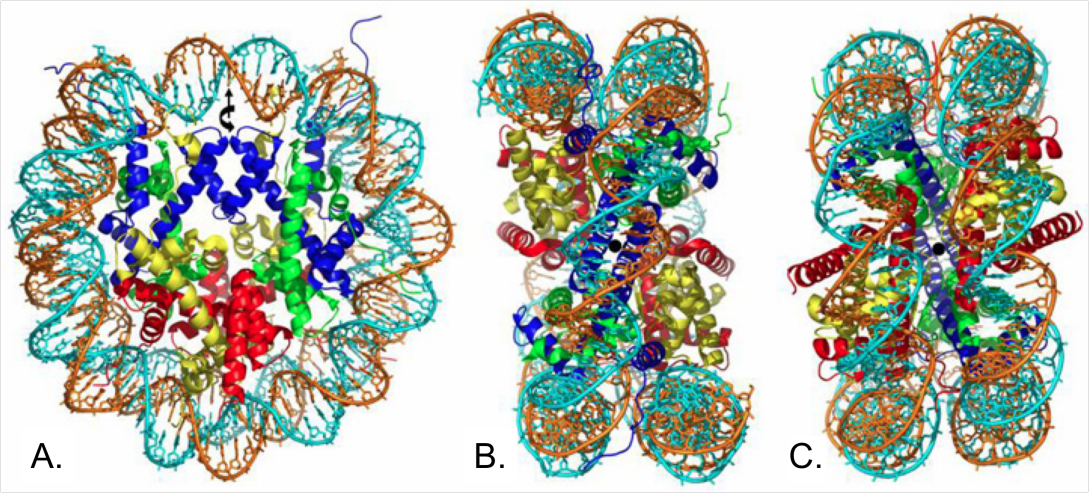

Figure 1.7: Structure of the histone core particle. Side (A.), top (B.), and bottom (C.) views of the 1.9 Å resolution crystal structure of the nucleosome core particle bound to 147 base pairs of DNA (Davey et al 2002).

1.2.1 Histone modifications

Post-translational modification of histone N-terminal tails can affect the DNA: histone contacts resulting in stronger or weaker interactions. This, in turn leads to a more or less condensed chromatin structure. The most well characterised histone N-terminal tail modifications are methylation, acetylation and phosphorylation (Kouzarides 2007), although several other types of post-translational modification also occur, such as ubiquitination and sumoylation. Lysine acetylation has an especially potent effect as it neutralises a basic charge, which is required to maintain the structure of the 30 nm chromatin fibre (Dorigo *et al* 2004, Shogren-Kraak *et al* 2006).

Histone modifications not only alter chromatin compaction but also serve as recognition sequences to recruit other proteins to sites of compact or open chromatin (Dillon 2004, Gelato & Fischle 2008). Specific, conserved protein motifs have evolved to recognise and bind specific histone modifications. Histone acetylation serves as the recruitment factor for bromodomain containing proteins. Likewise histone methylation is recognized by chromodomains and phosphorylation by 14-3-3 proteins (Kouzarides 2007). For example, HP1 localises to heterochromatin by binding di and tri methylated H3K9 through its chromodomain (Bannister *et al* 2001). HP1 can then influence chromatin structure by recruiting other chromatin modifying enzymes such as Dnmt1 & 3b and the H3K9 methyltransferase Suv39h1, which aid transcriptional silencing (Nakayama *et al* 2001). This example demonstrates how histone modifications can indirectly bring about changes in chromatin state in addition to altering charge state to directly effect DNA: histone contacts.

1.2.2 ATP dependent chromatin remodelling

ATP hydrolysing chromatin remodelers are a family of enzymes that use energy from ATP hydrolysis to disrupt DNA: histone contacts and alter chromatin structure. The function of ATP dependent chromatin remodelling enzymes varies greatly, however they all use ATP hydrolysis to alter the DNA: histone contacts within a nucleosome. Several outcomes are linked with ATP-dependent chromatin remodelling including nucleosome eviction, exchange and sliding (Dechassa *et al* 2010, Mizuguchi *et al* 2004, Whitehouse *et al* 1999) (Figure 1.8).

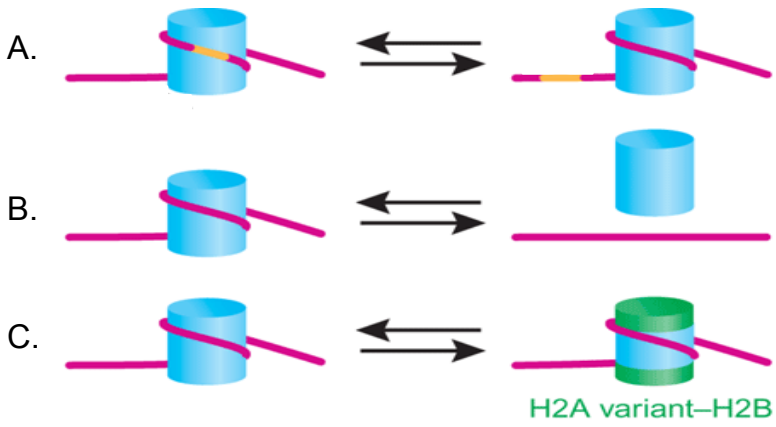

Figure 1.8: Schematic representation of the effects of nucleosome sliding (A.), eviction (B.) and exchange (C.) on chromatin structure. (modified from Cairns 2007).

It is not clear if these represent distinct reactions or are alternative outcomes of a common mechanism of contact disruption. Several models of ATP-dependent chromatin remodelling have been proposed. In the Bulge Diffusion model a small number of DNA: histone contacts are disrupted followed by rebinding of a more distal DNA sequence. A loop of DNA forms which moves around the nucleosome, repositioning it upon the DNA (Strohner *et al* 2005). Alternatively the Twist Defect Diffusion model suggests that by introducing twist defects into the DNA, histone contacts are disrupted (Havas *et al* 2000). The twist moves along the DNA and over the nucleosome disrupting contacts and replacing them with neighbouring ones, which repositions the nucleosome. Both of these mechanisms rely on ATP-dependent disruption of DNA: histone contacts by chromatin remodelling enzymes, and result in changes in DNA accessibility. It has been show by *in vitro* nucleosome positioning assays that different chromatin remodelling complexes can either promote equal spacing of nucleosomes on the DNA (Langst et al 1999) or randomise equally spaced nucleosomes (Whitehouse *et al* 1999). These different states may represent different roles for ATP-dependent chromatin remodelling enzymes, creating either compact or relaxed chromatin.

1.2.3 Classes of ATP hydrolysing chromatin remodelers

ATP hydrolysing chromatin remodelers were identified in yeast genetic screens for proteins involved in mating type switching (SWI) and sucrose fermentation (SNF). Many classes of ATP hydrolysing chromatin remodelers have subsequently been identified that share a core SNF2 domain homologous to the large helicase super family (Eisen *et al* 1995, Flaus *et al* 2006). The SWI/SNF subclass shares seven conserved helicase motifs involved in binding DNA and ATP hydrolysis. SWI/SNF chromatin remodelers have been categorised into subfamilies depending on other domains within the protein. The four main subfamilies are the SNF2, ISWI, CHD1 and INO80 (Figure 1.9).

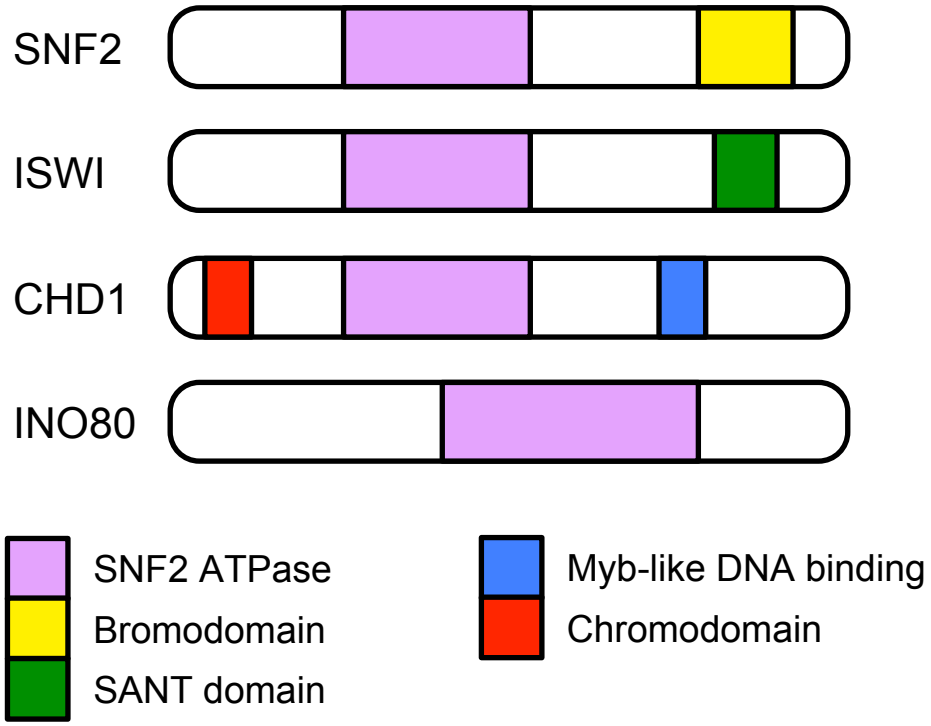

Figure 1.9: SWI/SNF subfamilies showing conserved domain structures that help define the 4 groups; SNF2, ISWI, CHD1 and INO80 (Hogan & Varga-Weisz 2007).

SNF2 proteins have a conserved bromodomain at their C-terminus and generally form part of large multi-subunit protein complexes (Narlikar *et al* 2002). *In vitro* these proteins bind acetylated nucleosomes and *in vivo* promote transcriptional activation. They include members of the yeast SWI2/SNF2 and RSC (restructure of chromatin) complex, which include RSC in yeast and BRG1 (Brahma-related gene 1) in mammals.

The ISWI (imitation SWI) class also act as the chromatin remodelling ATPase component in a number of different complexes such as yeast ISW1 & 2 and human CHRAC (chromatin-accessibility complex) and NoRC (nuclear remodelling complex). They contain SANT domains, which facilitate histone binding (Boyer *et al* 2002). The function of ISWI chromatin remodelers can vary depending on the complex. For example, in the context of the NoRC they promote transcriptional silencing (Santoro *et al* 2002), yet the CHRAC forms regularly spaced nucleosomes in *in vitro* nucleosome positioning assays, suggesting a role in heterochromatin formation (Langst and Becker 2001).

The CHD1 class contain members that form the NuRD (nucleosome remodelling and deacetylation) complex. They form large complexes with transcriptional repressors and co-repressors like histone deacetylases (HDACs), which introduce additional silencing marks such as histone tail deacetylation (Le Guezennec *et al* 2006). They cause transcriptional silencing *in vivo* and regularly spaced nucleosomal arrays in *in vitro* nucleosome positioning assays (Tong *et al* 1998, Zhang *et al* 1998).

The INO80 family have an insertion between their ATPase domains and do not share homology to other SNF2 family members. They catalyse histone dimer exchange and can evict nucleosomes (Mizuguchi *et al* 2004).

SWI/SNF proteins are involved in a wide range of processes, such as transcription, replication, recombination and DNA repair. They promote alterations in chromatin structure to either relax the chromatin and allow proteins to gain access to the DNA or compact the chromatin, which can lead to transcriptional silencing (Flaus & Owen-Huges 2004).

1.2.4 Components of remodelling complexes can modify the function of ATP hydrolysing chromatin remodeler enzymes

The majority of SWI/SNF chromatin remodelers display remodelling activity when isolated from other components of their respective complexes. However, other parts of the complex can play critical roles in targeting and modulating the activity of the chromatin-remodelling enzyme. For example, the ISWI containing CHRAC complex also contains Acf1 (ATP-utilizing chromatin assembly and remodelling factor) (Poot *et al* 2000), which enhances the chromatin remodelling ability of ISWI and alters the position to which the nucleosome are moved in *in vivo* nucleosome positioning assays (Langst *et al* 1999, Yang *et al* 2006). Other components may aid in targeting of the chromatin-remodelling enzyme through recognition of specific histone modifications or sequence specific transcription factors. The composition of protein components within a chromatin-remodelling complex can greatly influence the targeting and function of the chromatin-remodelling enzyme.

1.2.5 Functions of ATP hydrolysing chromatin remodelers

SWI/SNF enzymes are vital for coordinating processes such as transcription, replication, recombination and DNA repair. They ensure that the chromatin either remains compact or the necessary machinery can gain access to the DNA. As may be expected for such a fundamental process, mutations in SWI/SNF family members cause embryonic lethality in mice (Stopka & Skoultchi 2003) and larval lethality in *Drosophila* (Deuring *et al* 2000). Chromatin remodelling ATPase defects have also been linked to human diseases such as Cockayne Syndrome B, which causes sensitivity to UV light and neurodevelopmental defects. It is the result of mutations in the SNF2 like protein CSB (Cockayne Syndrome B protein), which is required for DNA excision repair (Troelstra *et al* 1992). Chromatin remodelling defects have also been implicated in cancer. Examples include the NuRD complex component and tumour suppressor CHD5 and the SNF2 chromatin remodeler BRG1, which has been shown to cause a predisposition towards tumours in heterozygous mice (Bultman *et al* 2000) and is mutated in various cancer cell lines (Reisman *et al* 2003, Wong *et al* 2000).

1.3 Chromatin remodelling in the DNA damage response

DNA repair covers a wide variety of processes ranging from removal of DNA crosslinks to mismatch repair. These require the cellular repair machinery to access to the DNA. For repair of DNA damage within euchromatic DNA this may not pose a problem. However in the context of heterochromatin, modification of chromatin structure is required to allow the bulky repair machinery to access DNA. This has been shown in DSB repair, where euchromatic breaks repair faster than heterochromatic breaks, which require additional ATP-dependent relaxation of the chromatin by chromatin remodelling proteins (Table 1.1) (Kruhlak *et al* 2006, Ziv *et al* 2006). Histone modifications also occur at sites of DNA repair, either as recruitment factors or to alter DNA:histone interactions. Here I focus on the involvement of chromatin modification in two of the most well characterised DNA damage response pathways, NER and DSB repair.

Family	Complex	ATPase	Species
SWI/SNF	SWI/SNF	Snf2	Yeast
	RSC	Sth1	Yeast
	BAF	BRG1, BRM	Mammal
	INO80	Ino80	Yeast
INO80	SWR1	Swr1	Yeast
	INO80	INO80	Mammal
	TRRAP/Tip601	EP400/p400	Mammal
	NuRD	CHD3, CHD4	Mammal
CHD	CHD22		Mammal
	ISWIa	Isw1	Yeast
ISWI	ISWIb	Isw1	Yeast
	ISW2	Isw2	Yeast
	ACF	SMARCA5/hSNF2H	Mammal
	CHRAC	SMARCA5/hSNF2H	Mammal
	WICH	SMARCA5/hSNF2H	Human
	NURF	SMARCA1/hSNF2L	Mammal
	Rad16		Yeast
Uncategorized	Rad26		Yeast
	Rad5		Yeast
	Rdh54		Yeast
	CHD1L/ALC1		Mammal
	ERCC6/CSB		Mammal
	HLTF		Mammal
	RAD54L		Mammal
	RAD54B		Mammal
	SHPRH		Mammal
	SMARCAL1		Mammal

Table 1.1: Yeast and mammalian ATP-dependent chromatin remodelling proteins implicated in DNA damage response (Lans *et al* 2012).

1.3.1 Chromatin remodelling in nucleotide excision repair

NER removes DNA adducts that distort the DNA double helix, including those induced by UV. NER is more efficient on naked DNA than in chromatin and is inhibited by heterochromatin (Gong *et al* 2005, Osley *et al* 2007). This suggests that chromatin remodelling is important for NER to allow repair proteins to access the DNA. Several chromatin-remodelling complexes have been implicated in NER response to UV irradiation (Table 1.1). CSB is an SNF2 like chromatin remodelling enzyme required for TC-NER, which can remodel chromatin *in vitro* in an ATP-dependent fashion (Selzer *et al* 2002). When mutated it leads to Cockayne Syndrome B, which causes sensitivity to UV light and neurodevelopmental defects. Rad16 is another SWI/SNF chromatin-remodelling enzyme that is also a NER factor required for GG-NER in yeast. It does not slide or evict nucleosomes, but alters chromatin structure through its DNA translocase activity (Yu *et al* 2004). Activation of NER through UV induced damage also results in histone modifications. For example acetylation of histone H3 by the histone acetyltransferase GCN5 results in a more permissive chromatin state and promotes chromatin remodelling. It is necessary for efficient repair of DNA damage (Yu *et al* 2011).

1.3.2. Chromatin remodelling in DNA double strand break repair

DSBs present a major challenge to cells as they can lead to chromosomal instability and loss of chromosome arms. DSBs are repaired by HR (San Filippo *et al* 2008) or NHEJ (Lieber 2010), which begin with DSB detection followed by processing of the broken DNA ends. This is associated with extensive histone modifications such as phosphorylation and ubiquitination (Bekker-Jensen *et al* 2010). Histone H2AX is phosphorylated by kinases ATM and ATR and recruits mediator factors like MDC1 and 53BP1 required for cell cycle checkpoint signalling (Jackson & Bartek 2009, Kinner *et al* 2008). Mediator factors also recruit further histone modifying enzymes such as Ubc13, which polyubiquitinates H2AX and is required for a single stranded DNA overhang for repair by HR (Kobayashi *et al* 2008). A reduction in either histone modifying enzyme leads to hypersensitivity to DNA damage.

Chromatin structure can also affect the efficiency of DSB signalling and repair. As previously mentioned DSBs that occur within heterochromatic DNA repair slower and require relaxation of the local chromatin state for efficient DSB signalling and repair. ATM dependent phosphorylation of the heterochromatin protein KAP1 has been shown to promote a more permissive chromatin state surrounding DSBs (Goodarzi *et al* 2011). Phosphorylated KAP1 promotes disassociation of heterochromatic factors such as HP1 and the ATP dependent chromatin remodelling protein CHD3, which normally function to promote chromatin compaction (Goodarzi *et al* 2008). Other ATP dependent chromatin remodelling proteins are actively recruited to DSBs, such as members of the RSC complex in yeast and BRG1 in mammals. RSC cause nucleosome displacement, which increases DNA accessibility at the site of damage (Kent *et al* 2007). BRG1 is recruited to DSBs in a γH2AX dependent manner by binding acetylated lysine residues of histone H3 in γH2AX containing nucleosome (Lee *et al* 2010). This stimulates further phosphorylation of H2AX, which reinforces DSB signalling (Park *et al* 2006). Mutation of either the RSC complex in yeast or BRG1 in mammals sensitise cells to DNA damage.

1.4 Functions of Lymphoid specific helicase and its homologs

LSH (Lymphoid specific helicase) has been identified as a SWI/SNF ATPase with SNF2 and helicase domains homologous to the SNF2 family (Figure 1.10). LSH was initially characterised as being predominantly expressed in proliferating cells such as lymphoid tissue (Geiman *et al* 1998) and was shown to be required for proliferation of mature T-lymphocytes (Geiman & Muegge 2000). LSH has since been shown to be ubiquitously expressed, with particularly high expression levels recorded during embryogenesis (Geiman *et al* 2001).

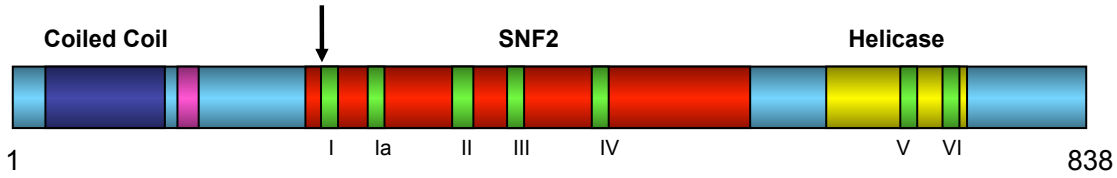

Figure 1.10: Lsh protein structure. The SNF2 and helicase domains are shown in red and yellow respectively. The helicase motifs are in green, coiled coiled in dark blue and the nuclear localisation signal in pink, the arrow shows position of the ATP binding site.

LSH is an important DNA methyltransferase (DNMT) accessory factor, required for correct DNA methylation (Dennis *et al* 2001). However, it has also been shown to be required for other process, such as HDAC dependent transcriptional repression and meiotic recombination between sister chromosomes (Myant & Stancheva 2008, De La Fuente *et al* 2006). Homologs of LSH have been identified in a wide range of species such *Arabidopsis thaliana* and *Saccharomyces cerevisiae* (Figure 1.11). Some functions are conserved between LSH and it homologues, such the requirement of the *A. thaliana* homolog DDM1, for DNA methylation in plants (Jeddeloh *et al* 1999). However, an additional role in the DNA damage response has been shown in plants and yeast (Alvaro *et al* 2007, Shaked *et al* 2006) that has yet to be demonstrated for mammalian LSH.

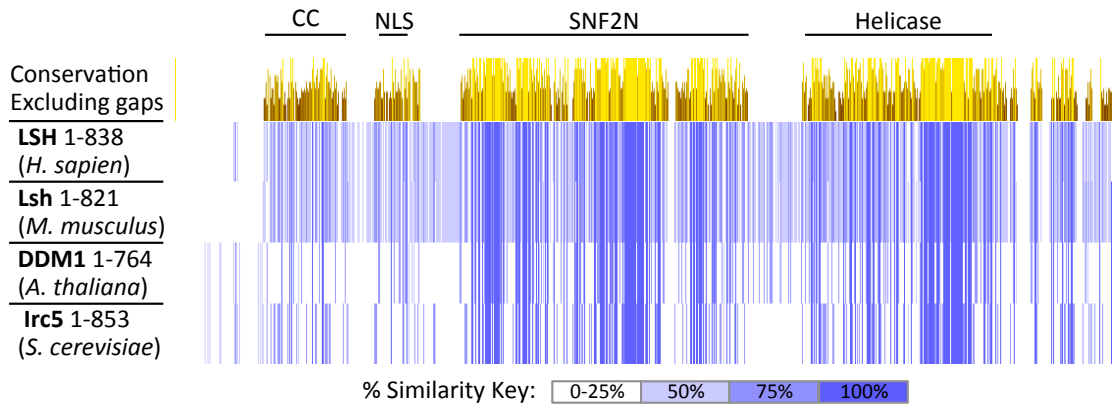

Figure 1.11: T-COFFEE (Di Tommaso *et al* 2011) protein sequence alignments of LSH and its homologues showing amino acid similarity and sequence conservation.

1.4.1 Functions of DDM1, the *A. thaliana* homolog of LSH

DDM1 (Decreased DNA Methylation 1) was the first of the LSH homologues to be identified by screening *A. thaliana* mutants for defects in DNA methylation (Jeddeloh *et al* 1999, Vongs *et al* 1993). The main defect observed in DDM1 mutant plants was a 70% reduction in global DNA methylation levels. This was associated with a range of morphological defects that increased in severity with each subsequent generation, due to the activation of retrotransposons through loss of DNA methylation (Kakutani 1997, Kakutani *et al* 1995). Levels of DNMTs and their associated activities were shown to be unaffected in DDM1 mutants, suggesting that DDM1 directly affects DNA methylation (Kakutani *et al* 1995).

DDM1 was identified as a member of the SWI/SNF family of ATPases. Biochemical studies confirmed chromatin-remodelling activity *in vitro* by demonstrating the ability of DDM1 to reposition nucleosomes (Brusk & Jermanowski 2003). This suggested a mechanism that could account for the link between DDM1 and DNA methylation, where by DDM1 is able to regulate DNMT activity by creating an open chromatin environment that would allow DNMTs to gain access to the DNA.

DDM1 mutants also show increased sensitivity to DNA damage when exposed to ionising radiation (Shaked *et al* 2006). This phenotype was shown to be independent of DNA methylation, as it was not reproduced in *met1* mutants lacking maintenance DNA methyltransferase MET1 and DNA methylation. This sensitivity to ionising radiation may reflect the nucleosome repositioning activity of DDM1 since chromatin remodelling is known to play an important role in regulating the function of various aspects of the DNA damage response pathway (Lans *et al* 2012).

1.4.2 Functions of IRC5, the *S. cerevisiae* homolog of LSH

Little is known about *irc5* (Increased Recombination Centres 5), the yeast homologue of LSH. It has been shown to encode a putative SWI/SNF family helicase with sequence similarities that identify IRC5 as a LSH homologue (Alvaro *et al* 2007, Shiraton *et al* 1999). It has also been shown that mutation of IRC5 causes an increase in the number of spontaneous RAD52 foci in *S. cerevisiae* (Alvaro *et al* 2007). RAD52 foci form during homologous recombination and are often used as markers of DNA damage as they can indicate sites of double strand break repair. An increase in the number of RAD52 foci in IRC5 mutant *S. cerevisiae* supports the hypersensitivity to DNA damage seen in DDM1 mutant plants and implicates a second LSH homologue in DNA damage response.

Genetic interaction studies identified enhanced growth defects in double mutant *S. cerevisiae* when IRC5 was mutated in combination with other proteins involved in the DNA damage response. These include, proteins of the MRX complex involved in DSB recognition (homologous to the human MRN complex), RAD proteins required for DSB HR repair and members of the RSC chromatin remodelling complex, which are also involved in the DNA damage response (Table 1.2) (Collins *et al* 2007). These associations give an indication that IRC5 may be involved in DNA damage response.

GENE	SCREENING METHOD
MRE11	Phenotypic Enhancement
RAD50	Phenotypic Enhancement
RAD51	Phenotypic Enhancement
RAD52	Phenotypic Enhancement
RAD52	Synthetic Growth Defect
RAD54	Phenotypic Enhancement
RSC58	Phenotypic Enhancement
RSC6	Phenotypic Suppression

Table 1.2: Table showing selected IRC5 genetic interaction data (Collins *et al* 2007), highlighting interactions with known repair proteins. Red are DSB recognition proteins, Blue are members of the RAD52 epistasis group involved in homologous recombination and DSB repair and Green are chromatin remodelling proteins of the RSC complex also required for DSB repair.

1.4.3 LSH is required for DNA methylation

In mice, LSH has been shown to be essential for development. Mice containing a deletion within the *Lsh* gene where a part of the helicase domain and the ATP binding site were removed die soon after birth, although embryonic development appears normal (Geiman *et al* 2001). More detailed analysis revealed widespread DNA hypomethylation throughout the genome. Remaining methylation levels were estimated to be between 30-40% of wild type (Dennis *et al* 2001). A second study, in which the latter half of the helicase domain was deleted and a C-terminal truncated protein produced, also showed that genomic DNA methylation was approximately 30-40% of wild type levels (Sun *et al* 2004). However, in this study 40% of the mice survived and displayed a phenotype of reduced birth weight, slow growth and premature ageing (Sun *et al* 2004).

The difference in survival between the complete knockout mice produced by Geiman *et al* and the mice from Sun *et al* expressing a C-terminal truncation of LSH may be due to an additional role for LSH connected to its C-terminal region or variation in the genetic background between the 2 mice strains. Since similar levels of loss of DNA methylation occur in both mice strains, the survival of 40% of the Sun *et al* $Lsh^{-/-}$ mice suggests the possibility of an additional function of LSH. The premature ageing displayed in these mice also hints at the possibility of a DNA repair defect as a more rapid accumulation of unrepaired DNA damage may lead to senescence, which can cause this phenotype (Weirich-Schwaiger *et al* 1994, De Boer *et al* 2002). This is consistent with observations in IRC5 mutant yeast and DDM1 mutant plants.

These two studies independently confirm the involvement of LSH in establishing DNA methylation within the embryo. The mouse produced by Sun *et al* also shows that the N-terminal predicted coiled coil of LSH cannot establish DNA methylation alone and that the SNF2 domain may also be required, suggesting that LSH chromatin remodelling is required for DNA methylation. Experiments using embryonic fibroblast cells in culture have confirmed the findings of *in vivo* studies and shown that LSH is required for *de novo* methylation (Myant *et al* 2011, Zhu *et al* 2006).

It was shown in embryonic fibroblasts that, although the presence of LSH is required to *de novo* methylate an episomal vector, it is not required to maintain existing DNA methylation, suggesting that LSH does not play a role in methylation maintenance (Zhu *et al* 2006). However, observations in the human cell line TIG-7, in which LSH levels were reduced to approximately 20% of normal levels by shRNA knockdown, contradicts the findings from mouse embryonic fibroblasts by demonstrating that LSH is required for DNA methylation maintenance. After 34 population doublings, methylation of α-satellite DNA was shown to be gradually decreased to 60% of normal levels (Suzuki *et al* 2008), suggesting that in somatic cells LSH does play a role in maintaining DNA methylation.

1.4.4 LSH is an HDAC dependent transcriptional repressor

Study of DNMT 1, 3a & b knockout human cancer cells showed that both DNMT1 & 3b are required for effective LSH mediated transcription silencing (Myant & Stancheva 2008). LSH tethered to a luciferase reporter by a GAL4 binding domain was insufficient to repress transcription in either DNMT1 or 3b knockout cells. However, re-introduction of DNMTs into DNMT knockout cells in combination with LSH-GAL4 was able to repress luciferase expression (Myant & Stancheva 2008). Furthermore, a truncated form of LSH in which the ATP binding site and SNF2 and helicase domains were removed was also able to induce transcriptional repression when co-transfected with DNMTs (Myant & Stancheva 2008), which suggests that the ATPase activity of LSH is not required for transcriptional repression in this system.

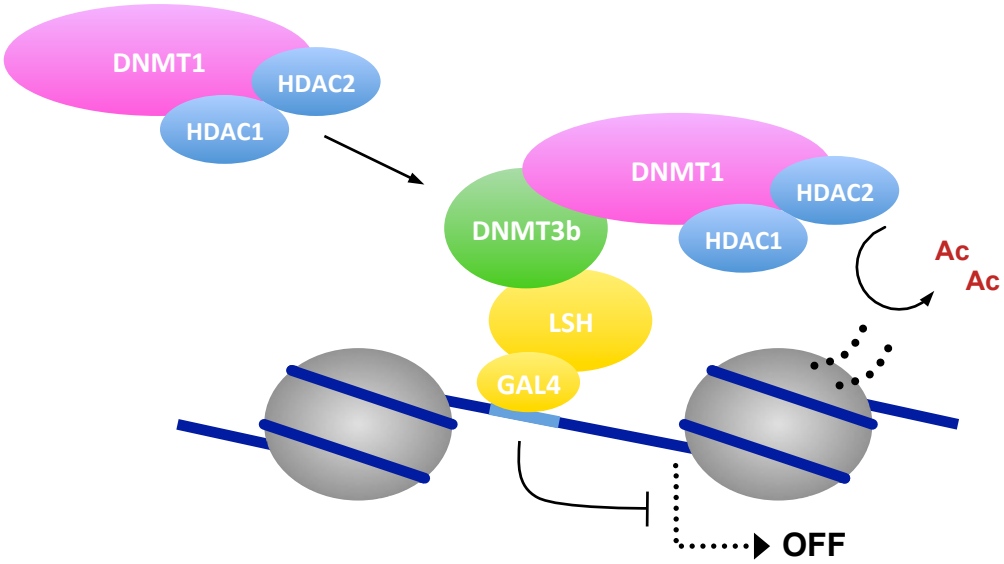

Figure 1.12: Model of how LSH may interact with DNMT3B, DNMT1, HDAC1, and HDAC2 to repress transcription (Myant & Stancheva 2008).

A LSH containing multisubunit complex has not been detected, however co-immunoprecipitation experiments have demonstrated interactions between LSH and DNMTs1&3b and HDACs1&2 (Myant & Stancheva 2008). Furthermore DNMT3b was shown to be required for interaction between LSH and DNMT1 and DNMTs1&3b for interactions between LSH and HDACs 1&2. This suggests an order of binding to a theoretical LSH-DNMT-HDAC transcriptional repression complex (Figure 1.12). Interactions with both DNMT1 & 3b are consistent with LSH having a role in both *de novo* and maintenance methylation.

1.4.5 LSH is required to resolve synapsed chromosomes during meiosis

LSH has also been implicated in correct recombination occurring during meiosis. Meiosis is accompanied by dynamic changes in global DNA methylation and the generation of double-strand DNA breaks for recombination between homologous paternal and maternal chromosomes (Reik *et al* 2001, Mahadevaiah *et al* 2001). It was initially thought that LSH might have a function during meiosis due its role in the regulation of DNA methylation (Dennis *et al* 2001, Muegge 2005).

Prophase I of meiosis starts during foetal development and continues until homologous chromosomes align and undergo recombination (Hassold & Hunt 2001). *Lsh*$^{-/-}$ mice created by Geiman *et al* 2001 die soon after birth, preventing study of the completion of meiosis. However germ cells were seen in the gonads of female *Lsh*$^{-/-}$ mice at 18 days gestation indicating that LSH is not required for primordial germ cell formation. When these were cultured no mature oocytes developed, suggesting that LSH is essential for post-natal oocyte growth and differentiation (De La Fuente *et al* 2006).

Closer investigation of WT mouse oocytes revealed that LSH co-localises with condensed chromosomes during the pachytene stage of Prophase I. However in *Lsh*$^{-/-}$ oocytes asynapsed chromosomes can be seen in the pachytene stage, accompanied with persistence in γH2AX staining indicating unrepaired DSBs and incomplete recombination (De La Fuente *et al* 2006). This shows that LSH is essential for completion of recombination during meiosis, possibly by helping resolve synapsed chromosomes or aiding in repair of DSBs. The phenotype is consistent with observations in *A. thaliana* and *S. cerevisiae* linking LSH homologues to roles in DNA damage repair. This raises the question of whether mammalian LSH is limited to aid in repair of DSBs induced for recombination during meiosis or has a wider role to play in DNA damage repair.

1.4.6 LSH summary

The major phenotype associated with mutation of LSH or its plant homolog is loss of DNA methylation. However, further analysis of *ddm1 A. thaliana* has also implicated DDM1 in the DNA damage response pathway (Shaked *et al* 2006). *S. cerevisiae* deficient for IRC5 also have a phenotype that implicates the yeast homolog of LSH in DNA damage response (Collins *et al* 2007). LSH has not been shown to be involved in the mammalian DNA damage response. However premature aging in surviving *Lsh*$^{-/-}$ mice (Sun *et al* 2004) and chromosomal defects in *Lsh*$^{-/-}$ primordial germ cells (De La Fuente *et al* 2006), suggests a conserved role for LSH in the mammalian DNA damage response.

1.5 Project Aims

This study aims to investigate whether LSH has a role in the mammalian DNA damage response. Initial investigations were to determine if LSH is involved in the DNA damage response. These are shown in chapter three, where the effects of various DNA damaging agents on LSH deficient cells demonstrated that LSH is required for repair of DSBs. The DSB repair defects of LSH deficient cells are characterised in chapter four, which provide a more detailed understanding of how LSH is in involved in DSB repair. We show correct recognition of DSBs in LSH deficient cells, but weaker phosphorylation of variant histone H2AX at a proportion of DSBs. This leads to impaired recruitment of mediator proteins to DSBs and compromised cell cycle arrest. In chapter five we explored the function and response of LSH to the induction of DSB repair. We show that LSH ATPase activity is vital for its role in DSB repair. We also show that the majority of LSH is normally bound to chromatin and is not recruited to broken DNA ends.

Our data implies that LSH has a conserved function in DSB repair. Interestingly LSH is not recruited to broken DNA ends but is required for repair at a proportion of DSBs. Although the exact role of LSH in the DSB response is unclear, we suggest two possible hypotheses to explain our observations and demonstrate a model system to further investigate these in chapter six.

Materials and Methods - Chapter Two

2.1 Materials

2.1.1 Common Reagents

Phosphate-buffered saline (PBS): 140 mM NaCl, 3 mM KCl, 2 mM KH_2PO_4, 10 mM Na_2HPO_4

SDS running buffer: 25 mM Tris, 250 mM Glycine, 0.1% SDS

Transfer buffer: 25 mM Tris, 250 mM Glycine (for transfers using PVDF membrane this was supplemented with 20% methanol)

Tris-buffered saline (TBS): 50 mM Tris-HCl pH 8.0, 150 mM NaCl

Tris-acetate EDTA (TAE): 40 mM Tris, 20 mM glacial acetic acid, 1 mM EDTA and adjusted to pH 8.0

Tris-EDTA (TE): 10 mM Tris-HCl pH 7.5, 1 mM EDTA pH 8.0

DNA isolation buffer: 10 mM Tris HCl pH8.0, 10 mM EDTA pH 8.0

2.1.2 Reagents for manipulation of proteins

NE1: 20 mM Hepes pH 7.0, 10 mM KCl, 1 mM $MgCl_2$, 0.1% (v/v) Triton X-100, 20% (v/v) glycerol, 0.5 mM DTT and complete protease inhibitors (Sigma).

PonceauS staining solution: 1% (v/v) glacial acetic acid, 0.5% (w/v) PonceauS

SDS PAGE loading buffer (5×): 225 mM Tris-HCl pH 6.8, 50% glycerol, 5% SDS, 0.05% bromophenol blue, 250 mM DTT. Stored at room temperature, DTT added just prior to use.

SDS PAGE separating gel: 7-15% (w/v) 29:1 acrylamide:bis-acrylamide, 0.1% (w/v) SDS, 390 mM Tris HCl pH 8.8, 0.08% (v/v) TEMED, 0.1% (w/v) APS.

SDS PAGE stacking gel: 5% (w/v) 29:1 acrylamide:bis-acrylamide, 0.1% (w/v) SDS, 129 mM Tris HCl pH 6.8, 0.1% (v/v) TEMED, 0.1% (w/v) APS.

2.1.3 Primary Antibodies

Name	Source, catalogue no.	Type	Western blot dilution	Immunofluorescence dilution
anti-LSH	Santa Cruz, sc-46665	Mouse, monoclonal	1:1000	
anti-gH2AX	Millipore, 05-636	Mouse, monoclonal	1:500	1:8000
anti-H2AX	Active Motif, 39690	Rabbit, polyclonal	1:1000	
anti-H4	Millipore, 07-108	Rabbit, polyclonal	1:500	
anti-ATM^{pS1981}	Millipore, 05-740	Mouse, monoclonal	1:500	1:1000
anti-MRE11	Calbiochem, PC388	Rabbit, polyclonal	1:2000	
anti-CHK2	Cell Signalling, 2662	Rabbit, polyclonal	1:500	
anti-p53	Santa Cruz, sc-126	Mouse, monoclonal	1:1000	
	Cell Signalling, 2524	Mouse, monoclonal	1:1000	
anti-p53^{pS15}	Cell Signalling, 9284	Rabbit, polyclonal	1:1000	
anit-53BP1	Cell Signalling, 4987	Rabbit, polyclonal		1:100
anti-MDC1	Abcam, ab11171	Rabbit, polyclonal		1: 500
anti-FLAG	Sigma Aldrich, F3165	Mouse, monoclonal		1:500

Table 2.1: Primary antibodies and conditions used for Western Blots and immunofluorescence.

2.1.4 Secondary Antibodies

Name	Source, catalogue no.	Western blot dilution	Immunofluorescence dilution
anti-rabbit IR680	LiCOR Biosciences	1:1000	
anti-mouse IR800	LiCOR Biosciences	1:500	
anti-rabbit Alexa 488	Invitrogen, Alexa Fluor®		1:1000
anti-mouse Alexa 565	Invitrogen, Alexa Fluor®		1:1000

Table 2.2: Secondary antibodies and conditions used for Western Blots and immunofluorescence.

2.2 Tissue culture

2.2.1 Cell lines

Wild type and *Lsh*$^{-/-}$ MEFs: Mouse embryonic fibroblasts obtained from the Muegge lab (Dennis *et al* 2001). Grown in Dulbecco modified Eagle medium (Sigma) supplemented with 10% (v/v) FBS, 100 u/mL penicillin, 100 μg/ml of a streptomycin and 2 mM L-glutamine (Sigma).

WT and mutant rescued *Lsh*$^{-/-}$ MEFs: *Lsh*$^{-/-}$ MEFs (Dennis *et al* 2001) that have been infected with synthetic cDNAs (GeneArt) of 3xFLAG C-terminally-tagged LSH and K254Q mutant LSH cloned into pMSCV-puro plasmids and packaged into lentiviral particles. Infected cells were selected with 2.5 μg/ml of puromycin for 2 weeks and stable colonies derived from single infected cells. Grown in Dulbecco modified Eagle medium (Sigma) supplemented with 10% (v/v) FBS, 100 u/mL penicillin, 100 μg/ml of a streptomycin and 2 mM L-glutamine (Sigma)

MRC5^{hT}: Human, primary embryonic lung fibroblasts immortalised with human Telomerase by retroviral infection with pBabe-hTERT-Neo plasmid (laboratory stock from Katrina Gordon). Grown in DMEM medium containing 10% (v/v) FBS, supplemented with 100 u/mL penicillin, 100 μg/ml of a streptomycin and 2 mM L-glutamine (Sigma).

shLSH and non-silencing MRC5^{hT}: LSH was stably knocked down in MRC5^{hT} cells by introducing two independent pGIPZ-shRNAmir plasmids V2LHS_ 155499 and V2LHS_155497 packaged into lentiviral particles (Open Biosystems). Control cells were infected under the same conditions with non-silencing pGIPZ-shRNAmir particles RHS4348 (Open Biosystems). The infected cells were selected with 2.5 mg/ml of puromycin for 7 days and LSH knockdown assessed by Western blots. Grown in DMEM medium containing 10% (v/v) FBS, supplemented with 100 u/mL penicillin, 100 μg/ml of a streptomycin and 2 mM L-glutamine (Sigma).

MRC5$^{hT\ ER\text{-}AsiSI\text{-}HA}$: pBABE ER–AsiSI–HA plasmid (from Gaëlle Legube) was packaged into lentiviral particles in amphotropic Phoenix cells and used to infect MRC5^{hT} cells. The infected cells were selected with 200 μg/ml of hygromycin for 14 days and stable colonies derived from single infected cells. Grown in DMEM medium containing 10% (v/v) FBS, supplemented with 100 u/mL penicillin, 100 mg/ml of a streptomycin and 2 mM L-glutamine (Sigma).

VA13$^{LSH\text{-}GFP}$: Foetal human diploid fibroblast cell line WI-38 transformed with simian virus 40 and stably expressing LSH-GFP (laboratory stock). Grown in DMEM medium containing 10% (v/v) FBS, supplemented with a mix of 100 u/mL penicillin, 100 μg/ml of a streptomycin and 2 mM L-glutamine (Sigma).

2.2.2 Viability screening

For short-term analyses of cell proliferation and viability, human fibroblasts were plated on 6-well plates (1x10^5 cells/well) and treated with a range of different DNA damaging agents. These included irradiation with 5 Gy of ionising radiation or 20 J/M^2 of UV, a 1h treatment with either 0.02% methyl methanesulfonate, 80mM bleomycin or 0.3% H_2O_2 or a 24 h treatment with 2 mM hydroxyurea. Cells were collected at the indicated time point after treatment and live and dead cells distinguished by staining with Trypan Blue solution. Counting was carried out in triplicate using a Countess Cell Counter (Invitrogen).

2.2.3 Survival studies

To investigate cell survival after DNA damage, wild-type and LSH-deficient mouse or human fibroblasts were plated on 10 cm dishes in triplicate at a density of 200 cell/plate and irradiated with indicated doses of IR in a Torrex X-ray cabinet (Faxitron Ltd). The irradiated cells were left to recover and form colonies for 10-14 days, stained with Giemsa and counted.

2.2.4 Laser micro-irradiation

VA13 cells expressing GFP-tagged LSH, were seeded at $1x10^5$ over cover slips in a 35 mm dish. Cells were pre-sensitised to UV-A irradiation with 10 μM of 5-bromo-2'-deoxyuridine (BrdU, Sigma Aldrich) in Dulbecco modified Eagle medium for 24 h. Laser micro-irradiations were carried out using a Lieca SP5 confocal microscope (Lieca) equipped with a 37°C heating stage and a 405 nm laser diode (20 mW) focused through a 40x HCX PL APO CS/1.25 oil objective. Laser settings (0.40 mW output, 50 scans) were chosen to generate a detectable damage response in a BrdU presensitised, dependent manner. Data was analysed using ImagePro 9.0 software (Media Cybernetics).

2.3 DNA manipulation and analysis

2.3.1 Genomic DNA extraction

Cells were resuspended in DNA isolation buffer, and treated with 100 μg/ml RNase A for 15 minutes at 37°C. Following RNase treatment, SDS and Proteinase K were added to 1% (w/v) and 200 μg/ml respectively and incubated overnight at 65°C. Digested peptides were removed by two extractions with phenol:chloroform:isoamyl alcohol and a single extraction with chloroform. DNA was precipitated by addition of 0.7 volumes isopropanol and centrifuged at 13000 rpm for 15 minutes at 4°C. The DNA was washed twice with 70% ethanol, allowed to dry and resuspended in 500 μl of TE.

2.3.2 5-methylcytosine ELISA assay

The global levels of 5-methyl cytosine in the genome of $MRC5^{hT}$, shLSH and non-silencing control cells were investigated by ELISA assays using Imprint™ kit (Sigma Aldrich) according to manufacturer's instructions.

2.3.3 Comet assays

Cells were plated on 10 cm dishes at ~60% confluency and cultured overnight. Cells were subjected to 10 Gy of ionising radiation and either collected immediately or left to recover for 8 hours. Cells were diluted to $6x10^5$ cells/ml with PBS, then mixed 1:10 with 0.6% low melting point agarose. 55 μL of sample were pipette onto glass slides pre-coated with 1% agarose and left to set for 10 minutes. Slides were placed in lysis buffer (2.5 M NaCl, 10 mM Tris, 1% Triton-X, pH 10) overnight at 4°C. Lysis buffer was removed, the slides washed twice with dH_2O and electrophoresis was carried out in a cold alkaline buffer (300 mM NaCl, 1 mM EDTA, pH 13) at 100 A, 12 V for 20 mins. Slides were neutralised with three 5 minute washes with cold 0.4 M Tris, pH 7.5 followed by 10 minutes washing with cold dH_2O. Staining was carried out with a 20 μg/ml propidium iodide solution followed by two, 5 minute washes in cold dH_2O. Images were collected by Olympus BX61 microscope equipped with 20X objectives and AnalySIS software (Soft Imaging Systems). Comet tail lengths were quantified using customised macro in ImagePro 9.0 software (Media Cybernetics).

2.4 Protein manipulation and analysis

2.4.1 Nuclear protein extraction

Nuclei were prepared by disrupting the cells in hypotonic buffer (NE1). Nuclei were released by 10 plunges of a dounce homogeniser. Nuclei were recovered by centrifugation at 3000 rpm for 5 min at 4°C. Nuclei were re-suspended in NE1 buffer supplemented with 25 U of Benzonase nuclease (Merck). Following 1 hour incubation on ice, NaCl was added to a final concentration of 500 mM and incubated at 4°C for 1 hour. After centrifugation, supernatant containing the nuclear proteins was collected. All buffers were supplemented with phosphatase (Pierce) and protease inhibitors (Sigma Aldrich).

2.4.2 Chromatin retention assays

Cells were plated on 20 cm dishes at ~60% confluency, subjected to the indicated dose of IR and collected at the indicated time point after irradiation. Nuclei were prepared by disrupting the cells in hypotonic buffer (NE1) as previously described (section 2.4.1). Soluble nuclear proteins and those loosely associated with chromatin were extracted using NE1 supplemented with 100 mM NaCl. After centrifugation, pellets containing chromatin bound proteins were resuspended in NE1 buffer supplemented with 25 U of Benzonase nuclease (Merck). Following 1 hour incubation on ice, NaCl was added to a final concentration of 500mM and incubated at 4°C for 1 hour. After centrifugation, supernatant containing the chromatin-associated proteins was collected. All buffers were supplemented with phosphatase (Pierce) and protease inhibitors (Sigma Aldrich).

2.4.3 Measuring protein concentration

Protein concentration was measured using a BCA Protein Assay (Pierce Biotechnology). Stock reagents A and B were mixed together at a 50:1 ratio and 1 μL protein sample added to 1 mL of the mixture. The reagent was incubated at 65°C for 15 minutes after which absorbance at 562 nm was measured. Protein concentration was calculated using an absorbance ratio of 0.04 = 1 μg/mL protein concentration.

2.4.4 SDS-PAGE

70 μg of each nuclear extract were diluted in SDS-PAGE loading buffer and heated for 5 min at 100°C to denature proteins. 0.75 mm thick gels were assembled in a Bio-Rad Mini-Protean 3 apparatus. All gels used an acrylamide to bis-acrylamide ratio of 29:1 with 0.1% SDS. The acrylamide was polymerised by the addition of ammonium persulfate and TEMED as a catalyst. Gels consisted of a stacking gel buffered at pH 6.8 and a separating gel at pH 8.8. Gels were run at 270V.

2.4.5 Wet transfer to nitrocellulose membrane

Wet transfer was carried out on a Bio-Rad Mini Trans-Blot Electrophoretic Transfer Cell according to the manufacturer's recommendations. A layer of 0.3 mm Whatman paper was placed on the SDS-PAGE gel and soaked in transfer buffer. A Trans-Blot transfer membrane (BioRad) was pre-wetted in dH_20 and placed on top of the gel. For the transfer of histones, Immuno-Blot PVDF Membrane (BioRad) membrane pre-wetted in methanol was used. An additional layer of 0.3 mm Whatman paper pre-soaked in transfer buffer was placed on top on the gel. The construct was assembled into the gel holder cassette between two fibre pads also pre-soaked in transfer buffer. The assembled cassette was inserted into the electrode module and transferred with 270 V for 1 hour. After transfer the gel sandwich was disassembled and the membrane stained with PonceauS stain to ensure efficient transfer.

2.4.6 Western Blots

Membranes were blocked in TBS supplemented with 2% milk and 0.1% Tween, for 1 hour. Fresh blocking solution containing a 1:1000 dilution of the primary antibody was applied and incubated overnight at 4°C. Unbound primary antibody was removed by three consecutive 15 minute washes with PBS / 0.1% Tween. Membranes were blocked again, for 1 hour at room temperature. The secondary antibody was applied at a dilution of 1:2000 in fresh blocking solution for 3 hours at room temperature. Unbound secondary antibody was removed by three consecutive 15 minute washes with PBS / 0.1% Tween. Membranes were imaged on an Odyssey Imager (LiCOR Biosciences) and quantified where indicated with the aid of Odyssey V3.0 software.

2.4.7 Immunofluorescence

Cells were seeded over cover slips in a 35 mm dish and cultured overnight. Cells were fixed either with 4% paraformaldehyde for 5 minutes or with cold 100% methanol for 1 minute. After fixation cell and cover slips were washed twice with PBS and before incubating in PBS with 0.1% Triton (Sigma) at 37°C for 15 minutes to permeablise the cell membranes. Fixed cells were blocked in PBS with 4% (w/v) immunofluorescence grade BSA (Fisher Scientific) for 1 hour. Fresh blocking solution containing a dilution of primary antibody was applied for 1 hour at room temperature. Fixed cells were washed three times in PBS for 10 minutes before blocked again for 30 minutes at room temperature. The secondary antibody was applied at a dilution of 1:1000 in fresh blocking solution for 1 hour at room temperature. Fixed cells were washed three times in PBS for 10 minutes and counterstained with DAP. Fixed, stained cells were washed in PBS before mounting in Vectashield (Vector Laboratories). Images were collected by Olympus BX61 microscope equipped with 20x and 40x PlanApo objectives (Olympus), ColorViewII camera and AnalySIS software (Soft Imaging Systems). Where indicated, fluorescent images were quantified using a customised macro in ImagePro 9.0 software (Media Cybernetics).

Results - Chapter Three

3.0 Identification of a sensitised DNA damage phenotype in LSH depleted mammalian cells

3.1 Introduction

Initial identification and characterisation of the LSH homolog, DDM1 in *A. thaliana* showed a loss in DNA methylation by up to 70% to be a major phenotype associated with deletion of this protein (Shaked *et al* 2006). Further studies of the homologous mammalian protein, LSH, have also shown a conserved role in DNA methylation in mammals (Geiman *et al* 2001, Sun *et al* 2004). However the initial characterisation of DDM1 also indicated that *ddm1 A. thaliana* have an increased sensitivity to the DNA damaging agents, UV and gamma irradiation, which was found to be independent of the loss of DNA methylation (Shaked *et al* 2006). This increased sensitivity to DNA damage has not been further characterised since it's preliminary description.

Conservation of the LSH homolog, IRC5 in *S. cerevisiae*, despite a lack of DNA methylation in this species indicated an additional function of IRC5. Synthetic growth defects of IRC5 double mutants highlighted interactions with members of the homologous recombination pathway (Collins *et al* 2007), which suggested a role for IRC5 in the DNA damage response. The premature ageing phenotype of surviving *Lsh*$^{-/-}$ mice produced by Sun *et al* 2004 and meiotic defects in oocytes derived from *Lsh*$^{-/-}$ embryos (De La Fuente *et al* 2006) could both be the result of defects in DNA repair. Defects caused by the mutation of LSH homologs in *A. thaliana* and *S. cerevisiae*, coupled with observations from *Lsh*$^{-/-}$ mice, suggested that in addition to a role in DNA methylation, LSH may have a conserved function in the mammalian DNA damage response.

3.2 LSH KD MRC5^{hT} cells show a higher degree of cell death following treatment with DSB inducing agents but not with other forms of DNA damaging agents

To test whether LSH has a conserved function in the mammalian DNA damage response, we wished to perform a screen of various DNA damaging agents in order to determine if LSH depleted cells have enhanced sensitivity. LSH was depleted by shRNA knockdown in human lung fibroblast (Figure 3.1), which had been previously immortalised by the introduction of human telomerase (MRC5^{hT}) (produced by Kat Gordon, unpublished). These provided a suitable comparison for screening as both shLSH and non-silencing controls were derived from the same genetic background and following knockdown of LSH, MRC5^{hT} cells had similar global levels of DNA methylation (Burrage *et al* 2012).

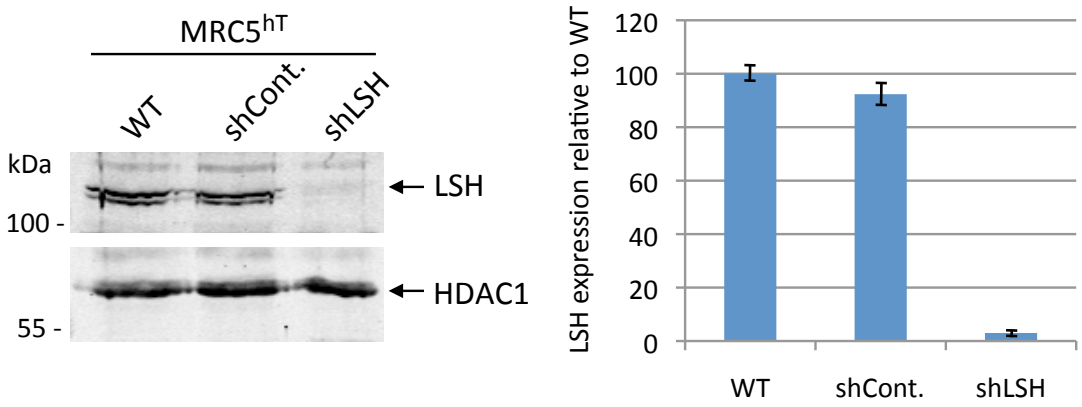

Figure 3.1: Nuclear extracts examined by Western blotting using an anti-LSH primary antibody to examine shLSH knockdown efficiency in MRC5^{hT} cells. An anti-HDAC1 antibody was as a loading control. The graph shows LSH expression relative to HDAC1 as a percentage of WT LSH expression (Quantified using Odyssey V3.0).

Sensitivity to DNA damaging agents was determined by counting cell viability 48 hours and 96 hours after treatment. Viability was established by staining cells with a negatively charged chromopore, Trypan Blue, which can only enter a cell if the membrane is damaged. Viable cells exclude Trypan Blue and appear bright. Various DNA damaging agents were used to create a range of DNA lesions.

- UV was used to create pyrimidine dimers, which are repaired by the nucleotide excision repair pathway. This was of particular interest since *ddm1 A. thaliana* have an increased sensitivity to UV.
- MMS treatment was used to induce mainly double strand breaks (DSBs), although MMS is known to methylate DNA at N^7-deoxyguanine and N^3-deoxyadenine. Its mechanism of DSB formation is still unclear.
- H_2O_2 and ionising radiation where used to induce oxidative damage, which creates double and single strand breaks.
- Hydroxyurea was used to deplete the nucleotide pool and induce replication fork collapse, generating both double and single strand breaks although through a different mechanism to H_2O_2 and ionising radiation.
- Bleomycin is an intercalating agent with several actions, able to create both single and double strand breaks. However treatment is used to induce mainly single strand breaks (SSBs) at a ratio approximately 7 fold higher than DSB induction (Stubbe *et al* 2008).

The results of the viability study showed that 20 J/m^2 UV reduced the viability of both shLSH and non-silencing control $MRC5^{hT}$ cells by approximately 40%, 96 h post treatment (Figure 3.2). Interestingly shLSH $MRC5^{hT}$ cells do not have an increased sensitivity to UV unlike *ddm1 A. thaliana*. 96 h after H_2O_2 or ionising radiation treatment, shLSH $MRC5^{hT}$ had reduced viability compared to non-silencing control cells. 0.03% H_2O_2 only caused reduced viability in shLSH $MRC5^{hT}$ cells, but a 5 Gy dose of ionising radiation was more damaging and reduced the viability of non-silencing and shLSH $MRC5^{hT}$ cells by 29% and 48% respectively (Figure 3.2). This indicated that LSH depleted cells are sensitised to oxidative damage, consistent with findings from γ-irradiation of *ddm1 A. thaliana*.

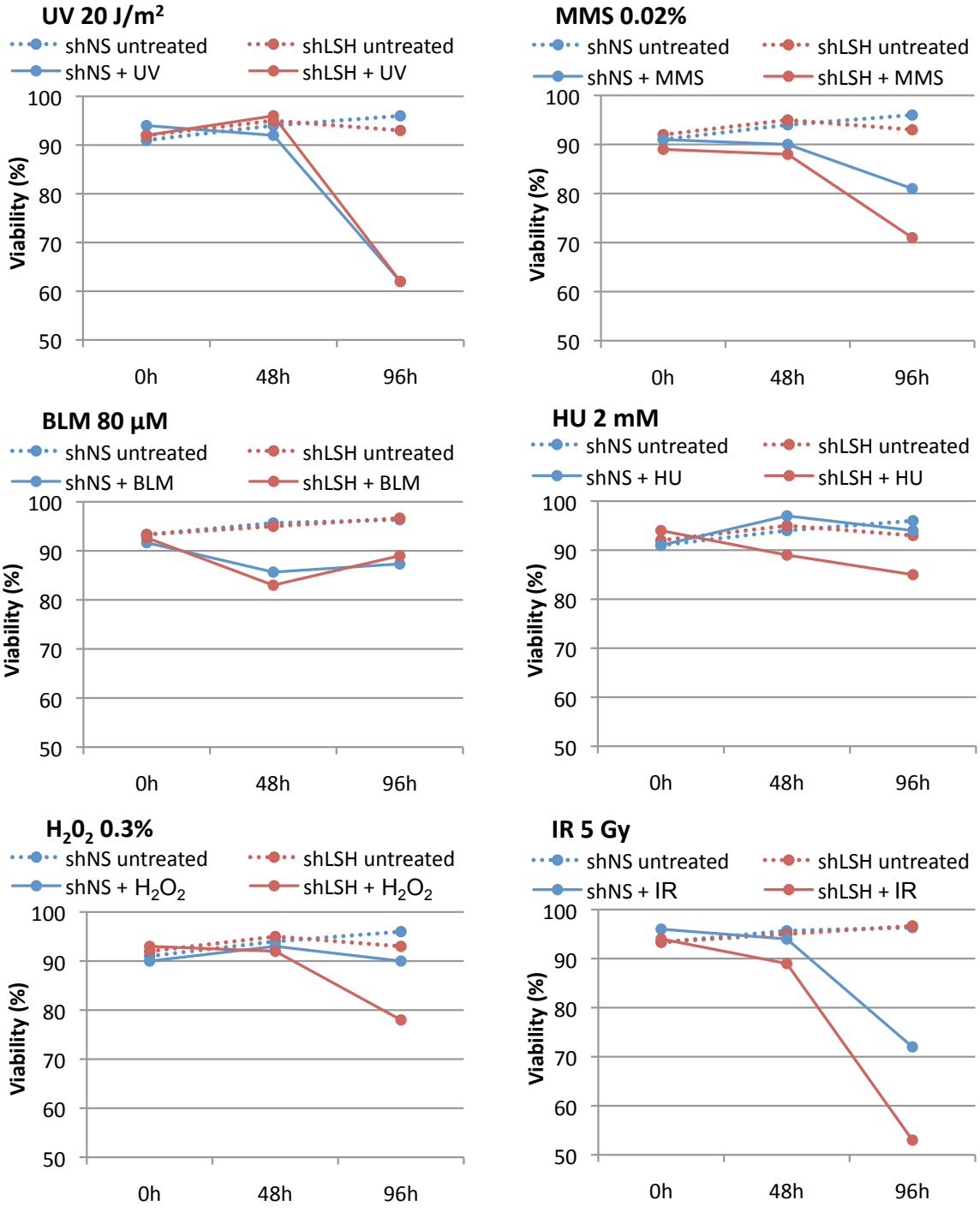

Figure 3.2: Graphs comparing viability of untreated and treated shLSH and non-silencing control MRC5^{hT} cells as determined by Trypan Blue staining, 48 h and 96 h after treatment with the indicated DNA damaging agent.

2 mM Hydroxyurea treatment also caused a decrease in the viability of shLSH MRC5^{hT} over non-silencing controls (Figure 3.2). Hydroxyurea induces a mixture of single and double strand break. However MMS treatment exclusively causes DSBs, and showed reduced viability of shLSH MRC5^{hT} cells compared to non-silencing controls 96 h after treatment. Bleomycin treatment only caused a modest decrease in viability and did not have a sensitising effect on shLSH MRC5^{hT} cells.

These preliminary viability screening data suggest that mammalian cells depleted of LSH are sensitive to DSB inducing agents, consistent with a conserved function of LSH in DNA repair. However the function of LSH has not been completely conserved, as depletion of LSH does not sensitise cells to UV unlike DDM1 knockout in *A. thaliana*.

3.3 LSH KD MRC5^{hT} and *Lsh*$^{-/-}$ MEFs are sensitised to ionising radiation

To further investigate the function of LSH in the DNA damage response we performed survival studies on both shLSH MRC5^{hT} and *Lsh*$^{-/-}$ MEFs. These studies involved seeding cells at a low, single cell density just prior to treatment. Each colony represents a single cell that survived. Examining the MEFs provided the opportunity to study the function of LSH in a mammalian DNA damage response other than *H. sapiens*. Survival studies were carried out using ionising radiation, as this produced the most significant difference in viability between non-silencing and shLSH MRC5^{hT} cells. The effects of x-rays also closely mirror those of gamma irradiation, to which *ddm1 A. thaliana* have an increased sensitivity.

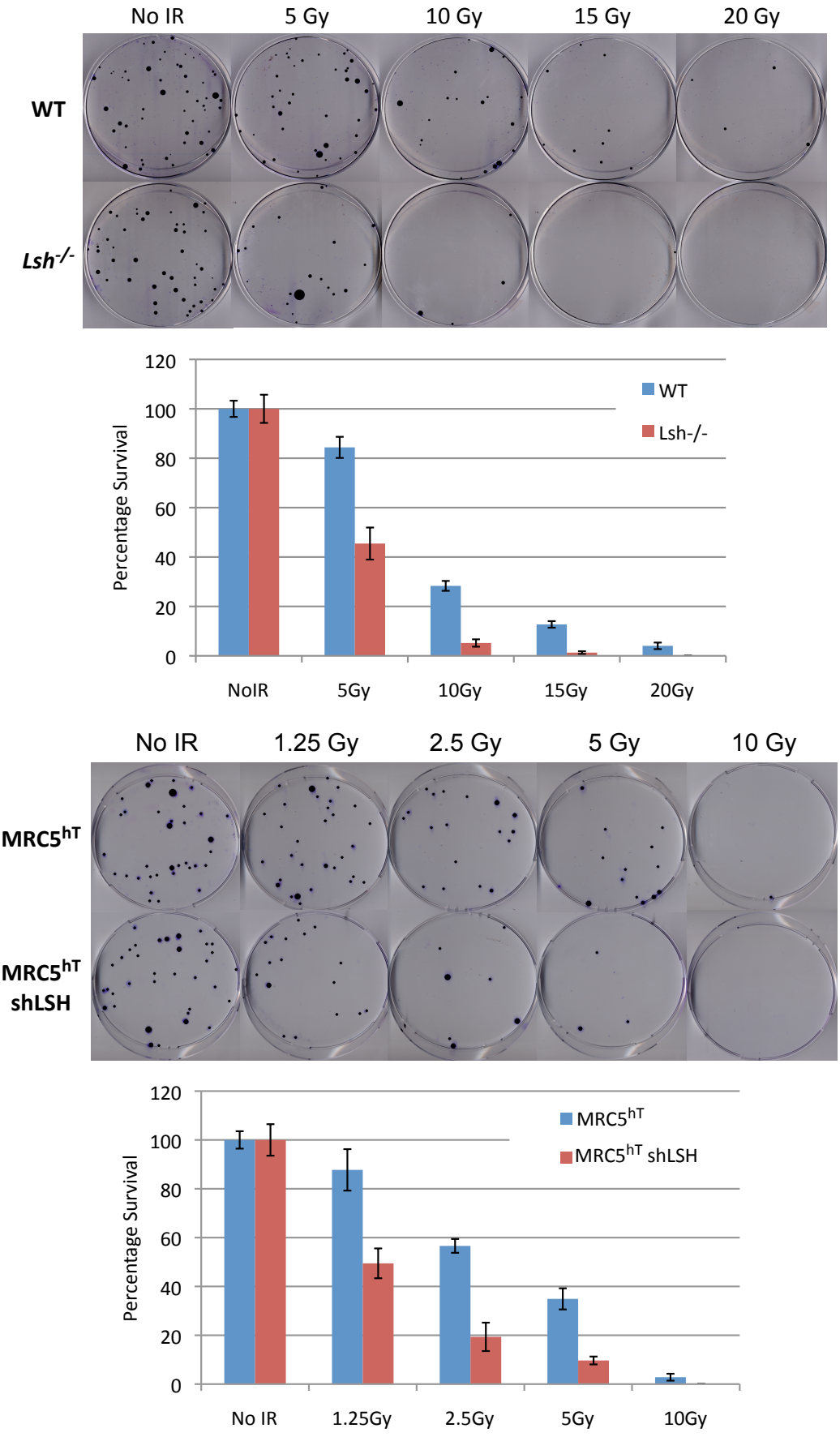

Figure 3.3: Giemsa stained plates and colony counts of WT and *Lsh*$^{-/-}$ MEFs and shLSH and non-silencing control MRC5^{hT} cells plated at 100 cells per dish and irradiated with the indicated dose of ionising radiation.

The results show that the survival of shLSH MRC5^{hT} cells following ionising radiation treatment was decreased compared to the non-silencing controls (Figure 3.3). This agrees with the reduced viability of shLSH MRC5^{hT} cells, 96 h after a 5 Gy dose of ionising radiation. *Lsh*$^{-/-}$ MEFs also show decreased survival following ionising radiation treatment compared WT cells from a matched littermate (Figure 3.3). However the MEFs have a much greater tolerance and can withstand higher doses of ionising radiation than MRC5^{hT} cells. Although these data show that LSH deficient cells have a reduced tolerance to DSB inducing agents leading to decreased survival, it is unclear whether this is due to a failure to repair breaks or the result of a larger number of breaks being induced in LSH depleted cells.

3.4 *Lsh*$^{-/-}$ MEFs repair DSBs less efficiently

The increased sensitivity of LSH deficient cells to DSB inducing agents could be due to defects in DSB repair or from an increase in the number of breaks induced in LSH deficient cells. To further investigate why LSH deficient cells are more sensitive to ionizing radiation a neutral comet assay was performed to establish if the same number of DSBs were induced in *Lsh*$^{-/-}$ and WT MEFs Following 10 Gy ionizing radiation, cells were immobilised in agarose on a glass slide and lysed in situ. Electrophoresis was carried out in a neutral buffer followed by propidium iodide staining. The greater the number of DSBs induced, the more fragmented the DNA, leading to a proportional increase in the distance the DNA travels away from the nucleus. A measure of this distance away from the nucleus or 'tail' gives a relative indication of the number of DSBs induced.

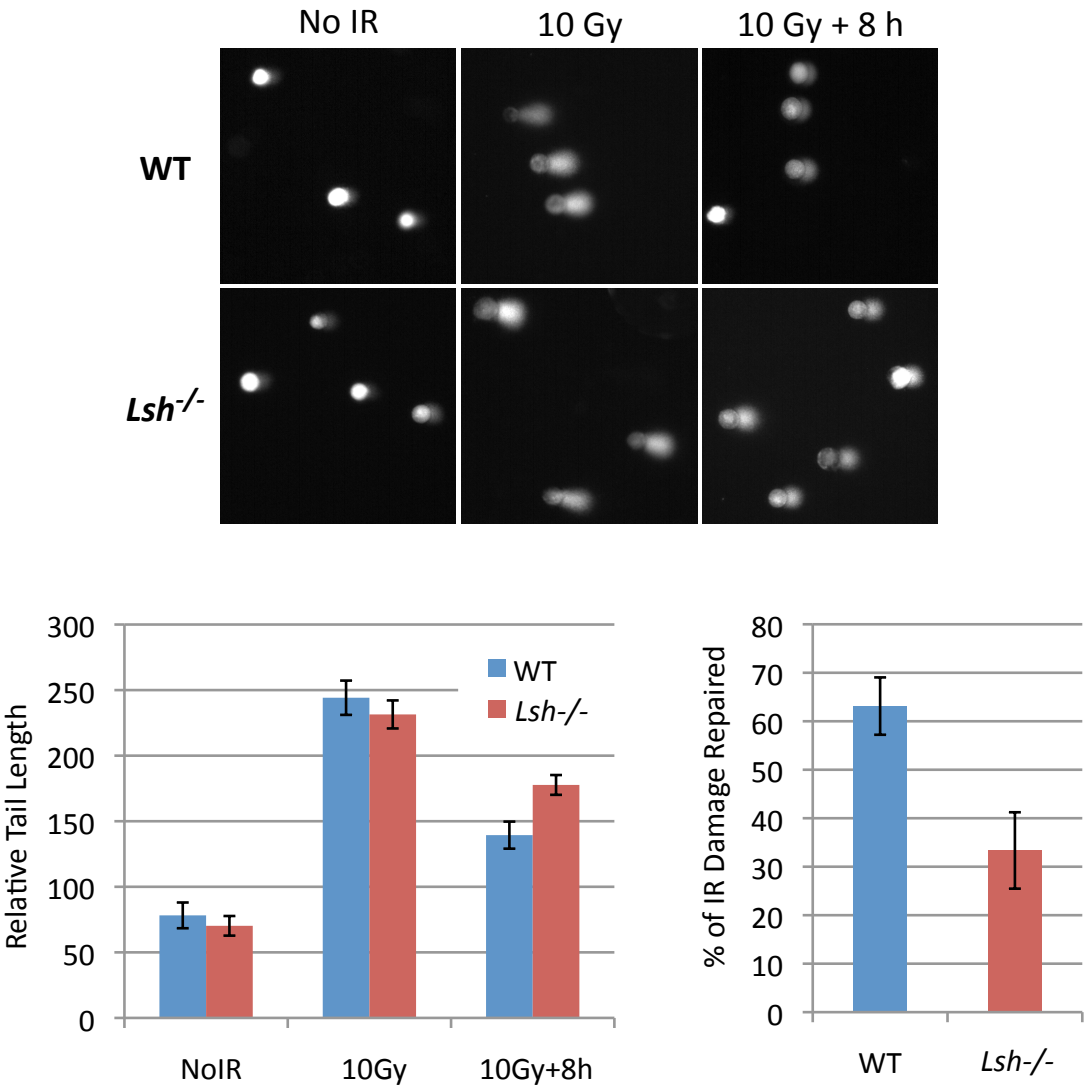

Figure 3.4: Representative images of comet assays performed on WT and *Lsh*$^{-/-}$ MEFs. Graphs show average tail lengths of n=35 cells measured from the centre of the nucleus and percentage of damage repaired by plotting tail length at 8 h as a proportion of tail length after irradiation minus NoIR background tail length.

Prior to treatment both WT and *Lsh*$^{-/-}$ MEFs had little or no tail, indicating intact, unbroken DNA (Figure 3.4). However immediately after a 10 Gy dose of ionising radiation both WT and *Lsh*$^{-/-}$ MEFs had longer tails as a result of DSBs induced by the ionising radiation treatment. There was no significant difference in the tail length between WT and *Lsh*$^{-/-}$ MEFs (Figure 3.4), which indicates that the same number of DSBs have been generated in both cell lines. From this we can conclude that LSH does not play a role in protecting cells from the formation of DSBs.

In addition to examining the tail length immediately post treatment we also left cells to recover for 8 h before carrying out comet assays. Since a 10 Gy dose of ionising radiation induced the same number of DSBs in both WT and *Lsh*$^{-/-}$ MEFs, the tail length 8 h post treatment gives an indication of the relative efficiency of DSB repair. In this case WT MEFs had significantly shorter tails than *Lsh*$^{-/-}$ MEFs (Figure 3.4), suggesting that lack of LSH results in less efficient repair of DSBs. When the tail length at 8 h is plotted as a function of the tail length immediately post treatment, it appears that *Lsh*$^{-/-}$ MEFs repair DSBs with half the efficiency of WT MEFs.

3.5 Summary

Depletion of LSH in mammalian cells increases their sensitivity to DSB inducing agents (Figures 3.2). These cells repair DSBs less efficiently (Figure 3.4), leading to a decrease in viability post treatment and reduced survival compared to control cells (Figure 3.3). These data confirm a conserved requirement for LSH in mammalian DNA repair, specifically in the repair of DSBs. However its homologous protein in *A. thaliana*, DDM1, is also required for repair of UV induced pyrimidine dimers, a function which does not appear to be conserved in mammalian cells. Although these data show that LSH is required for efficient DSB repair they do not give any indication of how LSH functions to aid in repair. To further characterise why LSH is required for DSB repair we compared the DSB repair response of WT and LSH deficient cells in greater detail. We also examined the other effects of LSH depletion for any indirect causes of the DSB repair phenotype, such as the loss of DNA methylation or changes in the expression of known DSB repair proteins.

Results - Chapter Four

4.0 Analysis of the effects of LSH depletion on mammalian DSB repair

4.1 Introduction

Although we had identified a DSB repair phenotype in LSH deficient cells, it was unclear how LSH functions to aid DSB repair. Repair of DSBs is a complex process involving several stages and many interacting proteins. The cells have to first correctly detect the presence of DSBs and signal checkpoints to arrest the cell cycle while the breaks are repaired. Mediator proteins bind at the break to aid in the recruitment of repair proteins, which prepare the broken end for repair by either HR or NHEJ and maintain signalling to cell cycle checkpoints. Finally the break has to be repaired and native epigenetic marks and chromatin state restored. By identifying which parts of the DSB response are affected in LSH depleted cells we hoped to be able to hypothesise how LSH may be involved in repair.

We also needed to consider other indirect ways in which LSH may affect DSB repair. LSH deficient cells are known to lose a large proportion of their DNA methylation. This could effect chromatin compaction and alter how efficiently the repair machinery can assemble at broken DNA ends. Alternative, LSH may affect the distribution of variant histone H2AX, which is normally found at approximately every fifth nucleosome and required as a major recruitment factor for DSB repair and signalling proteins. LSH is also a HDAC dependent transcriptional repressor and LSH deficient cells may have changes in expression of DSB repair proteins, which could be causing the DSB repair phenotype in LSH deficient cells.

4.2 *Lsh*$^{-/-}$ MEFs have no significant changes in expression of known DSB response proteins

Firstly, we examined if the increased sensitivity to DSB causing agents could be caused by changes in expression of known components of the DSB response. Previous work carried out in the lab used expression arrays to compare *Lsh*$^{-/-}$ MEFs with WT MEFS from matched littermates (Myant *et al* 2011). From this expression data known components of the DSB repair pathway were extracted and found to not have any changes in expression greater than a 1.5 fold difference between WT and *Lsh*$^{-/-}$ MEFs (Table 4.1). This suggested that the DSB phenotype of *Lsh*$^{-/-}$ MEFs was not the result of changes in expression of know components of the DSB response.

Name	Gene ID	Description	Fold change
H2AX	15270	H2A histone family, member X	**0.9**
Mre11	17535	Meiotic recombination 11	**0.7**
Rad50	19360	RAD50 homolog (*S. cerevisiae*)	**0.9**
Nbs	27354	Nibrin, Cell cycle regulatory protein p95	**0.9**
Ku70	14375	X-ray repair complementing defective repair	**0.6**
Ku80	22596	X-ray repair complementing defective repair	**0.9**
Atm	11920	Ataxia telangiectasia mutated homolog (*H. sapien*)	**0.8**
DNA-PK	19090	Protein kinase, DNA activated, catalytic polypeptide	**1.5**
CtIP	225182	Retinoblastoma binding protein 8	**0.7**
Xrcc2, Rad51	57434	X-ray repair complementing defective repair	**0.5**
Rad51l3	19364	RAD51-like 3 (*S. cerevisiae*)	**0.9**
Rad51c	114714	Rad51 homolog c (*S. cerevisiae*)	**0.8**
Rad51l1	19363	RAD51-like 1 (*S. cerevisiae*)	**0.9**
Rad51l3	19364	RAD51-like 3 (*S. cerevisiae*)	**0.9**
Rpa1	68275	Replication protein A1	**0.7**
Rad52	19365	RAD52 homolog (*S. cerevisiae*)	**0.8**
Rad54l2	81000	Rad54 like 2 (*S. cerevisiae*)	**1.3**
Rad54l	19366	RAD54 like (*S. cerevisiae*)	**0.6**
Mdc1	240087	Mediator of DNA damage checkpoint 1	**0.6**
p53BP1	19367	RAD9 homolog (*S. pombe*)	**0.7**
Dclre1c	227525	DNA cross-link repair 1C, PSO2 homolog (*S. cerevisiae*)	**1**
Xrcc4 (lig3)	108138	X-ray repair complementing defective repair	**1**
Xrcc1 (lig3)	22594	X-ray repair complementing defective repair	**0.7**
Xrcc3	74335	X-ray repair complementing defective repair	**1.3**

Rad1	19355	RAD1 homolog (*S. pombe*)	**1**
Rad21	19357	RAD21 homolog (*S. pombe*)	**1**
Rad17	19356	RAD17 homolog (*S. pombe*)	**0.9**
Rad23a	19358	RAD23a homolog (*S. cerevisiae*)	**1.5**
Rad18	58186	RAD18 homolog (*S. cerevisiae*)	**0.6**
Rad9b	231724	RAD9 homolog B (*S. cerevisiae*)	**1.5**
Rad23b	19359	RAD23b homolog (*S. cerevisiae*)	**0.8**
Rad52	19365	RAD52 homolog (*S. cerevisiae*)	**0.8**
Brca1	12189	Breast cancer 1	**0.9**
Brca2	12190	Breast cancer 2	**0.8**
Chk1	12649	Checkpoint kinase 1 homolog (*S. pombe*)	**0.9**
Chk2	50883	Checkpoint kinase 2 homolog (*S. pombe*)	**0.6**
p53	22059	Transformation related protein 53	**1.5**
Tip60	81601	HIV-1 tat interactive protein, homolog (*H. sapien*)	**1**
Htatip2	53415	HIV-1 tat interactive protein 2, homolog (*H. sapien*)	**1.4**
Ddb1	13194	Damage specific DNA binding protein 1	**0.9**
Ddb2	107986	Damage specific DNA binding protein 2	**1.4**
Cul4a	99375	Cullin 4A	**0.7**
Cul4b	72584	Cullin 4B	**0.8**
Rnf8	58230	Ring finger protein 8	**0.6**
Rnf168	70238	Ring finger protein 168	**1**
Smarcal1	54380	Swi/SNF related, actin dependent chromatin regulator	**1.4**
Ino80	68142	INO80 complex homolog 1 (*S. cerevisiae*)	**1**
Smarca3	20585	SWI/SNF related, actin dependent chromatin regulator	**0.4**
Smarca3	20585	SWI/SNF related, actin dependent chromatin regulator	**0.5**
Chd1l	68058	Chromodomain helicase DNA binding protein 1-like	**0.3**
Smarcad1	13990	SWI/SNF related, actin-dependent chromatin regulator	**0.7**
Snf2h	93762	SWI/SNF related, actin dependent chromatin regulator	**0.7**
Brg1	20586	SWI/SNF related, actin dependent chromatin regulator	**0.9**
Brm	67155	SWI/SNF related, actin dependent chromatin regulator	**1**
Snf2L	93761	SWI/SNF related, actin dependent chromatin regulator	**0.2**
Chd4	107932	Chromodomain helicase DNA binding protein 4	**1.1**
Ppp1ca	19045	Protein phosphatase 1, catalytic subunit, alpha isoform	**0.8**
Ppp2ca	19052	Protein phosphatase 2, catalytic subunit, alpha isoform	**1**
Ppp4c	56420	Protein phosphatase 4, catalytic subunit	**1.1**
Ppp6c	67857	Protein phosphatase 6, catalytic subunit	**1.4**
Ppm1d (Wip1)	53892	Protein phosphatase 1D magnesium-dependent	**1**

Table 4.1: Selective expression array data, highlighting genes encoding proteins that have been shown to be involved the DSB response. The data shows the fold change in expression between *Lsh*$^{-/-}$ and WT MEFs.

4.3 *Lsh*$^{-/-}$ MEF correctly recognise broken DNA ends

To explore the DSB repair pathway in greater detail we began by examining if *Lsh*$^{-/-}$ MEFs could correctly recognise the breaks induced following treatment with 10 Gy of ionising radiation. Initial recognition is carried out by the proteins of the MRN complex, which bind to the broken DNA ends. In the nucleoplasm, inactive dimers of ATM kinase are signalled by an, as yet unknown, mechanism and auto-phosphorylates serine residue 1981 to form ATM monomers (Bakkenist & Kastan 2003). These are recruited to the MRN complex at the broken end and help to establish the mediator complex through phosphorylation of a range of key recruitment proteins such as the variant histone H2AX.

We examined the localisation of the MRN complex following ionising radiation treatment to determine if DSB are correctly recognised in the *Lsh*$^{-/-}$ MEFs. Initial investigations were made using immunofluorescence imaging to visualise the localisation of RAD50, NBS1 or MRE11 following a 10 Gy dose of ionising radiation. Unfortunately, antibodies against all 3 members of the MRN complex proved unsuitable for immunofluorescence in our hands. We therefore performed chromatin retention studies of MRE11 which utilised a low salt nuclear extraction followed by Benzonase endonuclease treatment and high salt extraction of the remaining proteins to examine the strength of protein / chromatin interaction pre and post ionising radiation treatment. Free nuclear proteins and those with weak chromatin interaction will be extracted under low salt conditions, proteins more tightly associated with chromatin will be extracted following Benzonase treatment and high salt conditions. MRE11 is expected to be more tightly associated with chromatin following ionising radiation treatment, as it binds to the broken DNA ends. Since the same number of DSB are induced in WT and *Lsh*$^{-/-}$ MEFs, correct recognition of the broken end by the MRN complex should result in similar chromatin association following treatment.

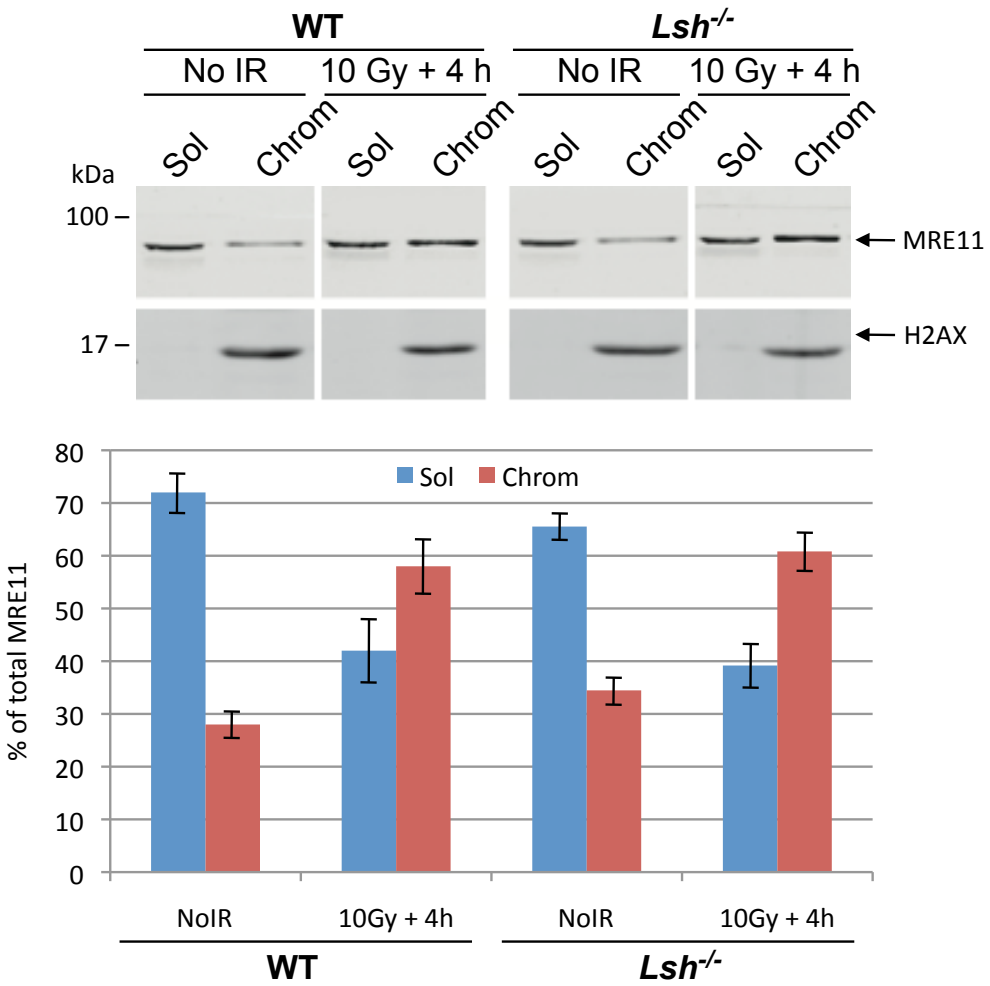

Figure 4.1: Chromatin retention assay followed by Western blot analysis of WT and *Lsh*$^{-/-}$ MEFs using anti-MRE11 and antI-H2AX primary antibodies to highlight soluble and chromatin bound fractions before and 4 h post treatment with 10 Gy of ionising radiation. Quantification of MRE11 is plotted as a percentage of soluble and chromatin bound signals combined, (Quantified using Odyssey V3.0).

Western Blot analysis shows that approximately 70% of MRE11 can be extracted under soluble extraction conditions, in both WT and *Lsh*$^{-/-}$ untreated MEFs (Figure 4.1). This shifts to approximately 60% of MRE11 becoming chromatin-bound following ionising radiation treatment (Figure 4.1). This demonstrates that MRE11 binds DNA more tightly in response to induction of DSBs. The results also show no difference in the amount of MRE11 bound to chromatin in WT and *Lsh*$^{-/-}$ MEFs post treatment, suggesting loss of LSH does not cause a reduction in MRN complex binding to DSBs.

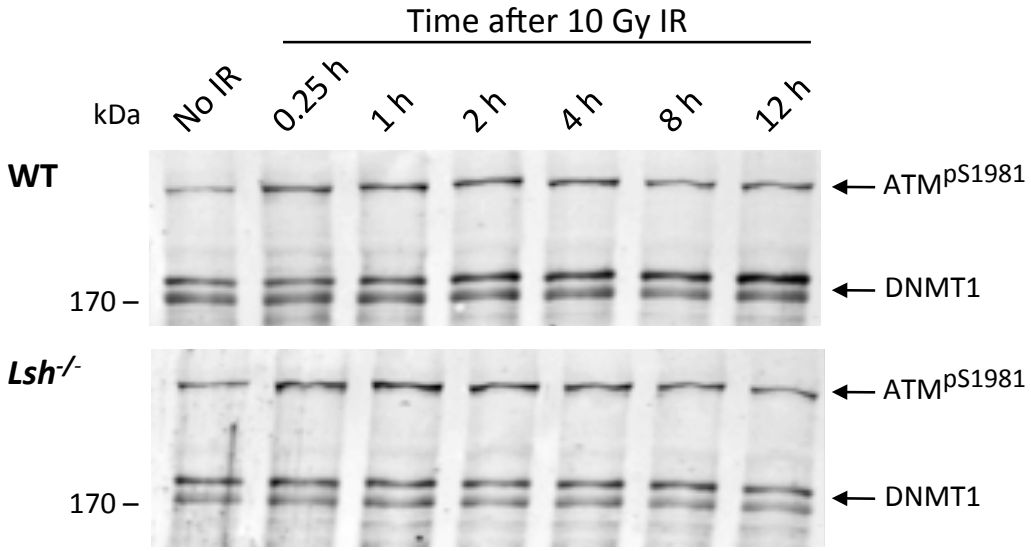

Figure 4.2: Nuclear extracts examined by Western blotting using an anti-ATM^{pS1981} primary antibody to examine phosphorylated ATM levels in WT and *Lsh*$^{-/-}$ MEFs at a range of time points following 10 Gy of ionising radiation. An anti-DNMT1 antibody was also used to show the level of DNMT1 to act as a loading control.

We further investigated DSB recognition by comparing the levels of phosphorylated ATM in the nucleus of WT and *Lsh*$^{-/-}$ MEFs. This was carried out by Western Blot analysis of nuclear extracts from *Lsh*$^{-/-}$ and WT MEFs over a range of time points post ionising radiation treatment. The results show similar kinetics and levels of phosphorylated ATM at serine residue 1981 in both *Lsh*$^{-/-}$ and WT MEFs (Figure 4.2). Although this shows that activation of ATM functions correctly in *Lsh*$^{-/-}$ MEFs, it does not indicate that DSB are recognised correctly and bound by phosphorylated ATM.

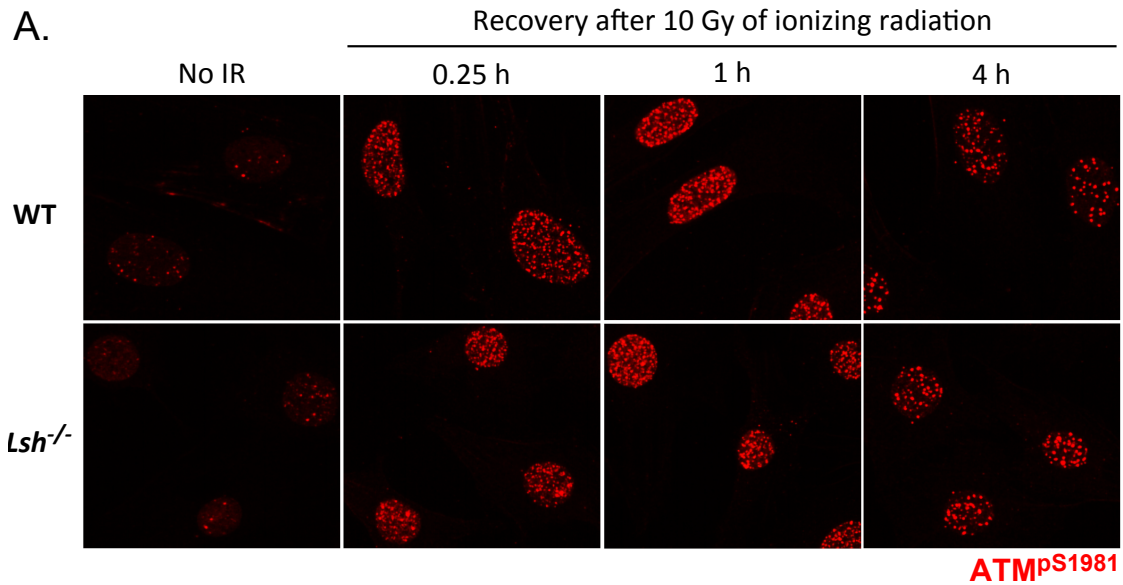

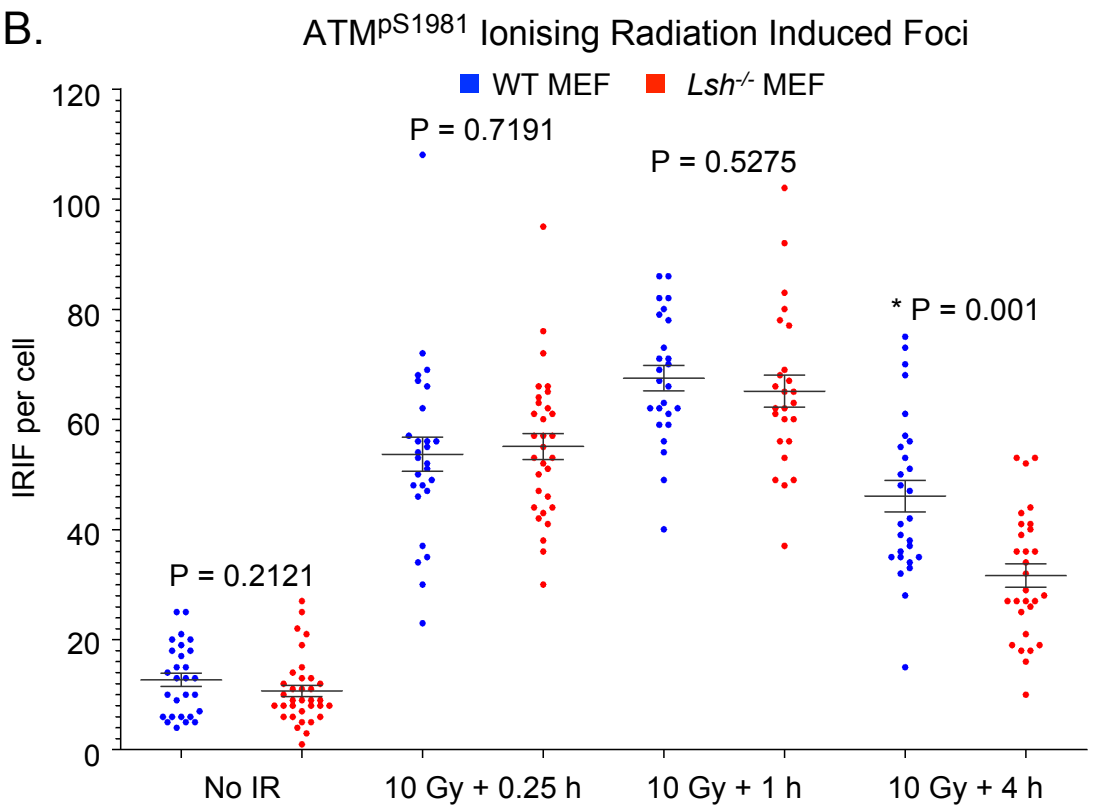

Figure 4.3: (A.) Representative immunofluorescence images showing localisation of phosphorylated ATM in WT and *Lsh*$^{-/-}$ MEFs at the indicated time points after 10 Gy of ionising radiation. (B.) The graph shows the number of IRIF per cell, n=35 cells. Lines indicate the mean and SEM.

To examine phosphorylated ATM recruitment in addition to activation, immunofluorescence imaging was performed on *Lsh*$^{-/-}$ and WT MEFs at various time points after ionising radiation treatment. Ionising radiation induced foci (IRIF) can clearly be seen following treatment, consistent with recruitment of phosphorylated ATM to the broken DNA ends (Figure 4.3). When the number of IRIF per cell were counted and plotted as column scatter plots the data indicates that the foci of phosphorylated ATM significantly increase following ionising radiation treatment, peaking at 1 h and falling in number again by 4 h (Figure 4.3). Theses plots are consistent with the induction of total phosphorylated ATM serine 1981 seen by Western Blots.

Furthermore there was no significant difference between the number of IRIF in Lsh$^{-/-}$ and WT MEFs at 0.25h or 1 h, suggesting that phosphorylated ATM is correctly recruited to DSBs. However, 4 h after treatment fewer IRIF were observed in *Lsh*$^{-/-}$ cells compared to WT (Figure 4.3). As well its initial recruitment to the broken DNA end via the MRN complex, phosphorylated ATM can also aid in mediator complex formation later in repair (Riches *et al* 2008). It is unlikely that 4 h post ionising radiation treatment the reduced number of IRIF in *Lsh*$^{-/-}$ cells represents a defect in DSB recognition, especially since no difference can be observed at the earlier time points 0.25 h or 1 h. Therefore we hypothesised that the inefficient recruitment of ATM phosphorylated at serine 1981 to IRIF 4 h post treatment could be result of defects in mediator complex assembly.

4.4 H2AX is phosphorylated less efficiently in LSH depleted cells

We have shown that the increased sensitivity of LSH depleted cells to DSB inducing agents is the result of a deficiency in repair, but not because of inefficient DSB detection. However, a reduction in the number phosphorylated ATM IRIF after initial break recognition, without an accompanying decrease in phosphorylated ATM levels, has led us to hypothesise that the inefficient repair of DSBs in LSH depleted cells may be caused by defects in mediator complex assembly / recruitment.

The fist step in mediator complex assembly is phosphorylation of H2AX by phosphorylated ATM. Phosphorylated H2AX (γH2AX) acts as the initial recruitment factor which either directly or indirectly recruits the remaining components of the mediator complex such as MDC1 and 53BP1. These help to bringing about other histone modifications, recruit repair proteins and maintain cell cycle checkpoint signalling (Fernandez-Capetillo et al 2004). γH2AX foci are widely regarded as one of the major diagnostic markers of DSBs. We therefore wished to examine whether H2AX is efficiently phosphorylated in Lsh$^{-/-}$ MEFs. Initially γH2AX immunofluorescence imaging was performed on WT and *Lsh*$^{-/-}$ MEFs at a range of time points following 10 Gy of ionising radiation.

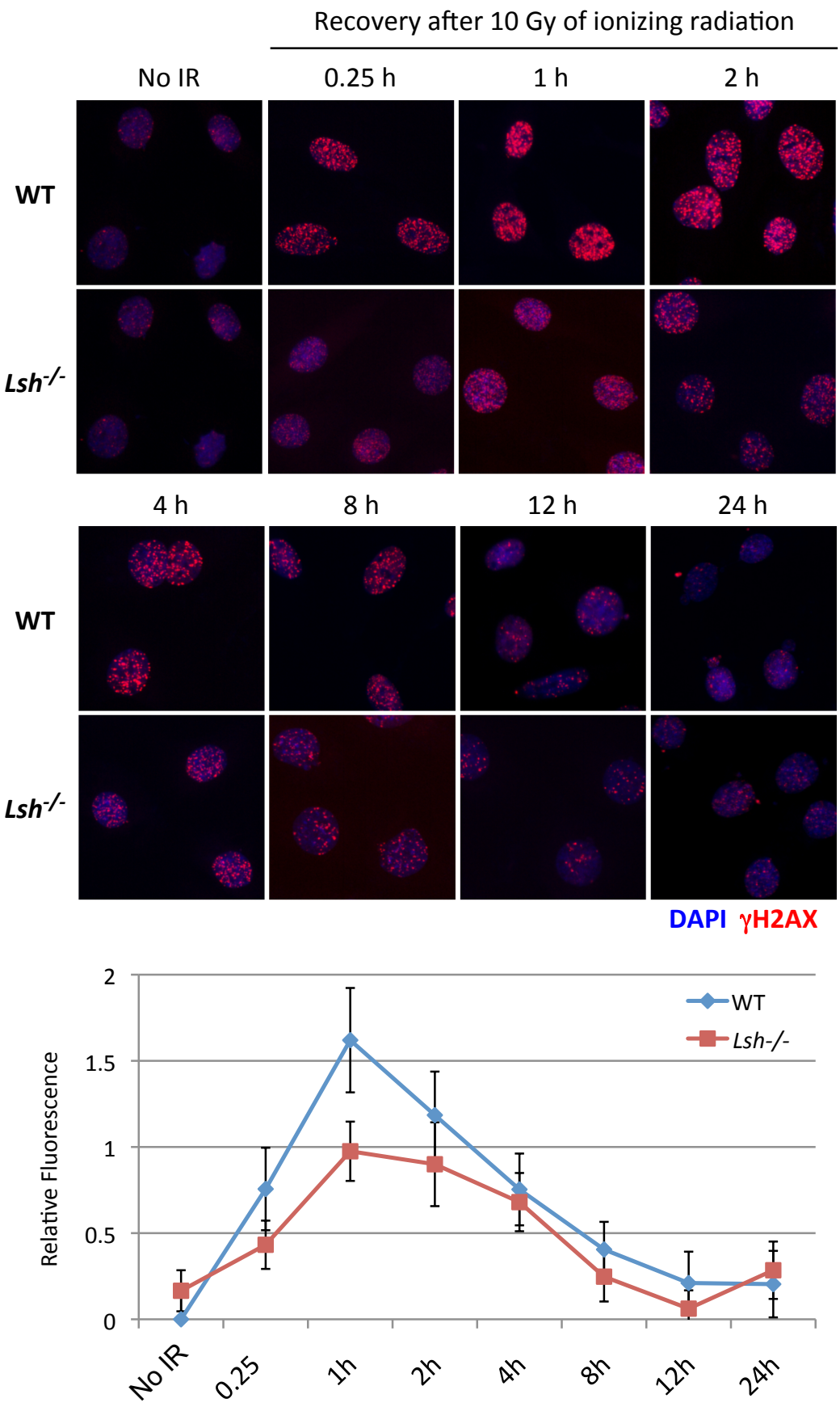

Figure 4.4: Representative immunofluorescence images showing γH2AX in WT and *Lsh*$^{-/-}$ MEFs at the indicated time points after 10 Gy of ionising radiation. The graph shows total nuclear fluorescence of n=35 cells.

It was not possible to count the γH2AX IRIF following a 10 Gy dose of ionising radiation due to the high number of IRIF making individual foci undistinguishable. However, since the antibody used is specific for phosphorylated H2AX, the total fluoresce per cell was taken as a measure of H2AX phosphorylation. In WT MEFs a clear increase in γH2AX could be seen, peaking at 1 h, which fell back to approximately basal levels after 12 h (Figure 4.4). *Lsh*$^{-/-}$ MEFs displayed similar kinetics, with the peak signal occurring after 1h. However the levels of H2AX phosphorylation in *Lsh*$^{-/-}$ MEFs never achieved those reached in the WT cells. The quantification of total fluorescence indicated a decrease in H2AX phosphorylation at 1h by approximately a third (Figure 4.4).

The observed reduction in H2AX phosphorylation in the *Lsh*$^{-/-}$ MEFs could be the result of a reduction in the amount of H2AX phosphorylation at DSBs, the failure to phosphorylated H2AX at a proportion of breaks or mis-localisation of H2AX throughout the chromatin. It is also possible that the reduced H2AX phosphorylation in LSH deficient cells is due to the 70% decrease in DNA methylation in *Lsh*$^{-/-}$ MEFs.

4.4.1 H2AX is phosphorylated at fewer broken DNA ends in *Lsh*$^{-/-}$ MEFs

To test whether the reduction in H2AX phosphorylation was caused by a failure to phosphorylated H2AX at a proportion of breaks, we counted the number of IRIF per cell. A failure to phosphorylate H2AX at a proportion of breaks was expected to result in fewer IRIF. Since a 10 Gy dose of ionising radiation resulted in too many IRIF to count, DSBs were induced using a 5 Gy dose of ionising radiation and the number of IRIF per cell plotted as a column scatted plot.

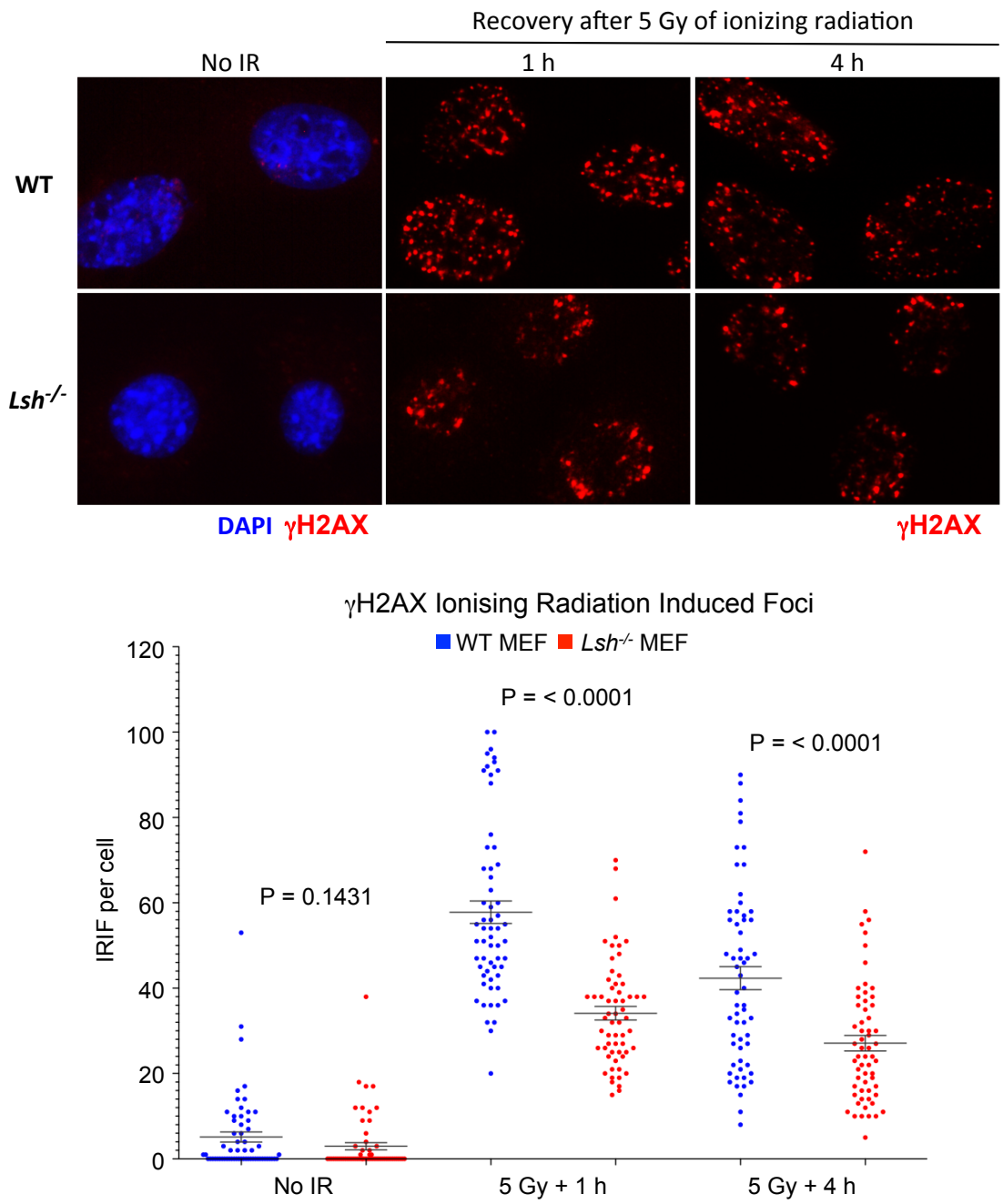

Figure 4.5: Representative immunofluorescence images showing localisation of γH2AX in WT and *Lsh*$^{-/-}$ MEFs at the indicated time points after 5 Gy of ionising radiation. The graph shows the number of IRIF per cell, n=35 cells. Lines indicate the mean and SEM.

The results showed significantly fewer γH2AX IRIF in *Lsh*$^{-/-}$ MEF both 1h and 4h post ionising radiation treatment (Figure 4.5). Since DSB are detected equally well in both WT and *Lsh*$^{-/-}$ MEF, as shown by no significant difference in the number of phosphorylated ATM IRIF 1 h post treatment (Figure 4.3), the significant difference in γH2AX IRIF suggests that a proportion of DSB in *Lsh*$^{-/-}$ MEFs do not have phosphorylated H2AX.

The amount of H2AX and its association with the chromatin remains unchanged between WT and *Lsh*$^{-/-}$ MEFs, as shown by the chromatin retention assays (Figure 4.1). Although we were are unable to conclude that the reduced number of γH2AX IRIF is not a result of mis-localisation of H2AX containing nucleosomes, we have shown that it is not as a result of a reduction in the amount of total H2AX contained within the chromatin. Another hypothesis of why *Lsh*$^{-/-}$ MEFs have reduced γH2AX IRIF could be linked to the loss of DNA methylation detected in *Lsh*$^{-/-}$ cells. We hypothesised that substantial loss of DNA methylation might affect chromatin compaction and may result in mis-localisation of H2AX containing nucleosomes, which could cause the described reduction in H2AX phosphorylation.

4.4.2 Loss of DNA methylation does not affect H2AX phosphorylation

To control for the effects of DNA methylation loss on H2AX phosphorylation we examined γH2AX levels following ionising radiation treatment in *Dnmt1*$^{-/-}$ MEFs. *Dnmt1*$^{-/-}$ MEFs lack the maintenance DNA methyltransferase DNMT1 and reportedly lose 90% of their DNA methylation (Jackson-Grusby *et al* 2001). Since this degree of methylation loss triggers activation of the p53 apoptotic pathway, *Dnmt1*$^{-/-}$ cells are by necessity also *p53*$^{-/-}$. We therefore also examined *p53*$^{-/-}$ MEFs as a control. γH2AX levels were investigated by Western Blots of nuclear extracts made from cells at a range of time points after ionising radiation treatment.

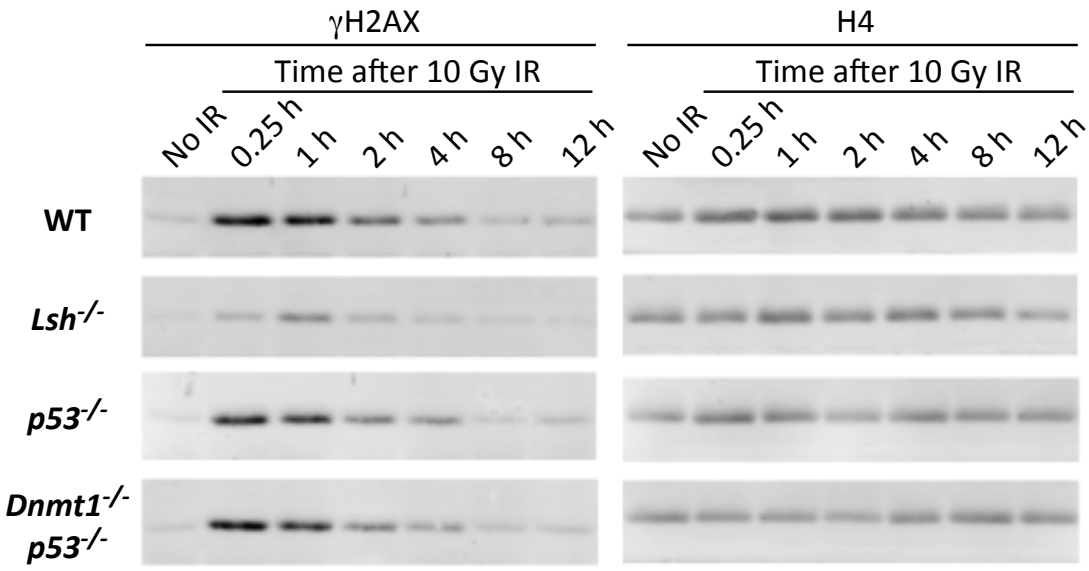

Figure 4.6: Nuclear extracts examined by Western blotting using an anti-γH2AX primary antibody to examine γH2AX levels in WT, *Lsh*$^{-/-}$, *p53*$^{-/-}$ and *DNMT1*, *p53*$^{-/-}$ MEFs at a range time points following 10 Gy of ionising radiation. An anti-H4 antibody was also used to show the level of H4 to act as a loading control.

These experiments showed that the *Lsh*$^{-/-}$ MEFs clearly display a reduction in γH2AX when compared to WT MEFs (Figure 4.6), as previously described by immunofluorescence imaging. However, we detected no difference in γH2AX when we compared the WT, *p53*$^{-/-}$ and *Dnmt1*$^{-/-}$, *p53*$^{-/-}$ MEFs. This suggests that the reduction in H2AX phosphorylation seen in the *Lsh*$^{-/-}$ MEFs (Figure 4.4, 4.5 and 4.6) is independent of the loss of DNA methylation. Interestingly, this is in agreement with data from *ddm1 A. thaliana*, where the increased sensitivity of *ddm1* plants to γ-radiation was independent of the loss of DNA methylation.

We further investigated whether reduction in H2AX phosphorylation can be observed by Western blot in LSH knockdown MRC5^{hT} cells to ensure that the phenomenon was not an artefact of *Lsh*$^{-/-}$ MEFs. We again saw a substantial reduction in γH2AX in the knockdown cells when compared to the control knockdown MRC5^{hT} cells (Figure 4.7).

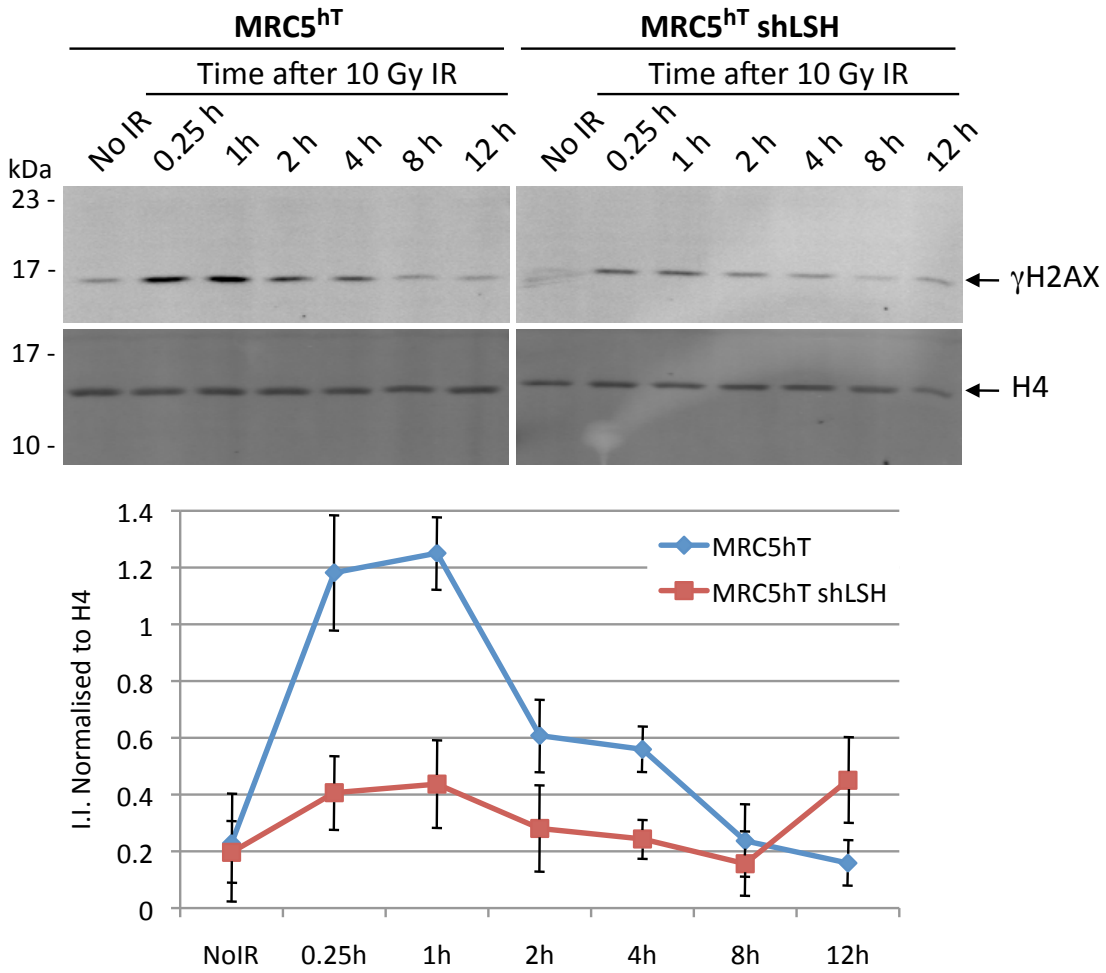

Figure 4.7: Nuclear extracts examined by Western blotting using an anti-γH2AX primary antibody to examine γH2AX levels in shLSH and non-silencing control MRC5^{hT} cells at a range time points following 10 Gy of ionising radiation. An anti-H4 antibody was also used to show the level of H4 to act as a loading control, (Quantified by Odyssey V3.0 using Integrated Intensity values).

These results indicate that the initial establishment of the mediator complex is impaired in LSH depleted cells at, at least a proportion, of DSBs. This is most likely the contributing factor to the increased sensitivity of LSH depleted cells to DSB inducing agents. Although our data shows that the reduced phosphorylation of H2AX in response to DNA damage in *Lsh*$^{-/-}$ MEFs is not a result of reduced H2AX incorporation into the chromatin, we cannot yet determine the mechanistic defect by which lack of LSH causes fewer IRIF in the *Lsh*$^{-/-}$ MEFs. Although the likely contributing factor, it is also unclear how reduced H2AX phosphorylation results in decreased viability and increased sensitivity to DSB inducing agents seen in LSH depleted cells.

4.5 The formation of DSB repair mediator complex is impaired in *Lsh*$^{-/-}$ MEFs

To further investigate the impact of reduced H2AX phosphorylation on downstream mediator complex assembly in the *Lsh*$^{-/-}$ MEFs, we examined the recruitment of downstream mediator complex components MDC1 and 53BP1 to IRIF by immunofluorescence imaging. MDC1 was chosen as it binds directly to γH2AX and is responsible for the recruitment of checkpoint kinase CHK2, which is important for cell cycle arrest. We also examined 53BP1 as it is recruited further downstream in mediator complex assembly and relies on both γH2AX (Ward *et al* 2003) and MDC1 (Eliezer *et al* 2008) for recruitment to breaks as well as additional histone modifications such as H4K20 methylation (Pei *et al* 2011), which are established indirectly as a result of H2AX phosphorylation.

53BP1 recruitment to IRIF in WT and *Lsh*$^{-/-}$ MEFs was examined by immunofluorescence imaging. 53BP1 is located throughout the nucleoplasm and appears as diffuse nuclear staining in un-irradiated cells. Upon irradiation 53BP1 is recruited to DSBs as a downstream component of the mediator complex, relying on γH2AX dependent recruitment of ubiquitinases and methylases to alter local histone modifications for efficient 53BP1 binding, which can be seen as IRIF. The immunofluorescence imaging revealed cells could be classified into two groups, those with IRIF and cells that displayed diffuse nuclear staining (Figure 4.8).

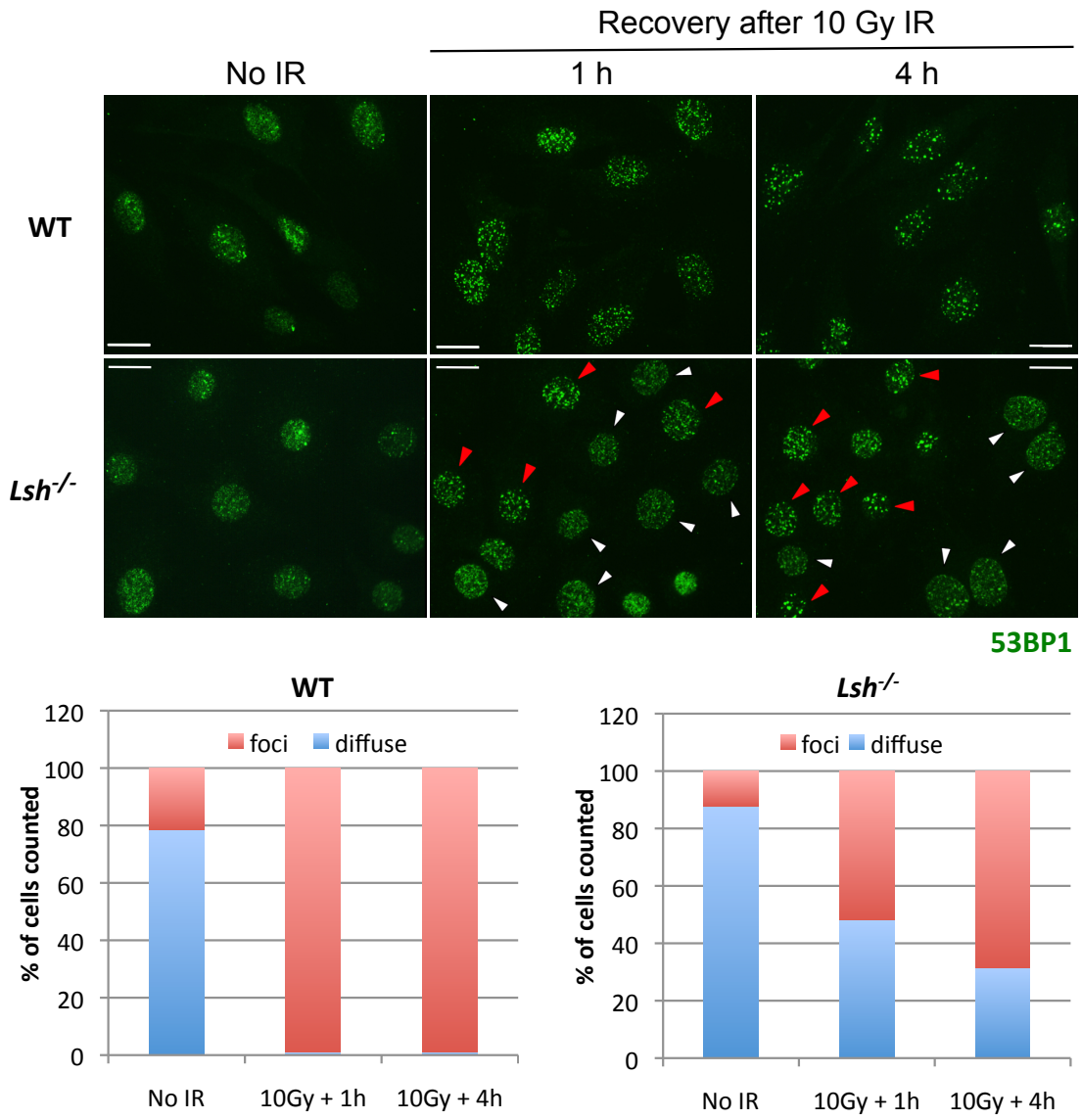

Figure 4.8: Representative immunofluorescence images showing 53BP1 localisation in WT and *Lsh*$^{-/-}$ MEFs at the indicated time points after 10 Gy of ionising radiation. The graphs show percentage of fociated (red arrows) or diffuse nuclear stained (white arrows) nuclei of n=35 cells.

WT and *Lsh*$^{-/-}$ MEFs were counted and classified as either containing foci or having diffuse nuclear staining at 1 h and 4 h post irradiation and the results plotted as a percentage of cells counted. As expected, prior to treatment the majority of cells show diffuse nuclear staining. Upon induction of DSBs, the proportion of fociated cells shifts to nearly 100% of the population both 1 h and 4 h post treatment in WT MEFs (Figure 4.8). However, a more heterogeneous response was observed in *Lsh*$^{-/-}$ MEFs, with approximately 30-50% of cells showing diffuse staining (Figure 4.8). This is in agreement with the γH2AX data as it also suggests impaired mediator complex assembly in the *Lsh*$^{-/-}$ MEFs. We may have expected to see 53BP1 IRIF in all *Lsh*$^{-/-}$ MEFs but at a lower frequency

than in the WT cells, similar to what was observed in γH2AX immunofluorescence. However, unlike the γH2AX antibody, which is specific to the protein when phosphorylated in response to damage, the antibody against 53BP1 detects all 53BP1 in a cell pre and post ionising radiation treatment. By observing translocation of the protein rather than activation, reduced mediator complex assembly will result in an increase in un-localised 53BP1. This will result in a higher background signal throughout the nucleoplasm, obscuring the fewer IRIF that remain and making 53BP1 localisation appear diffuse, as observed.

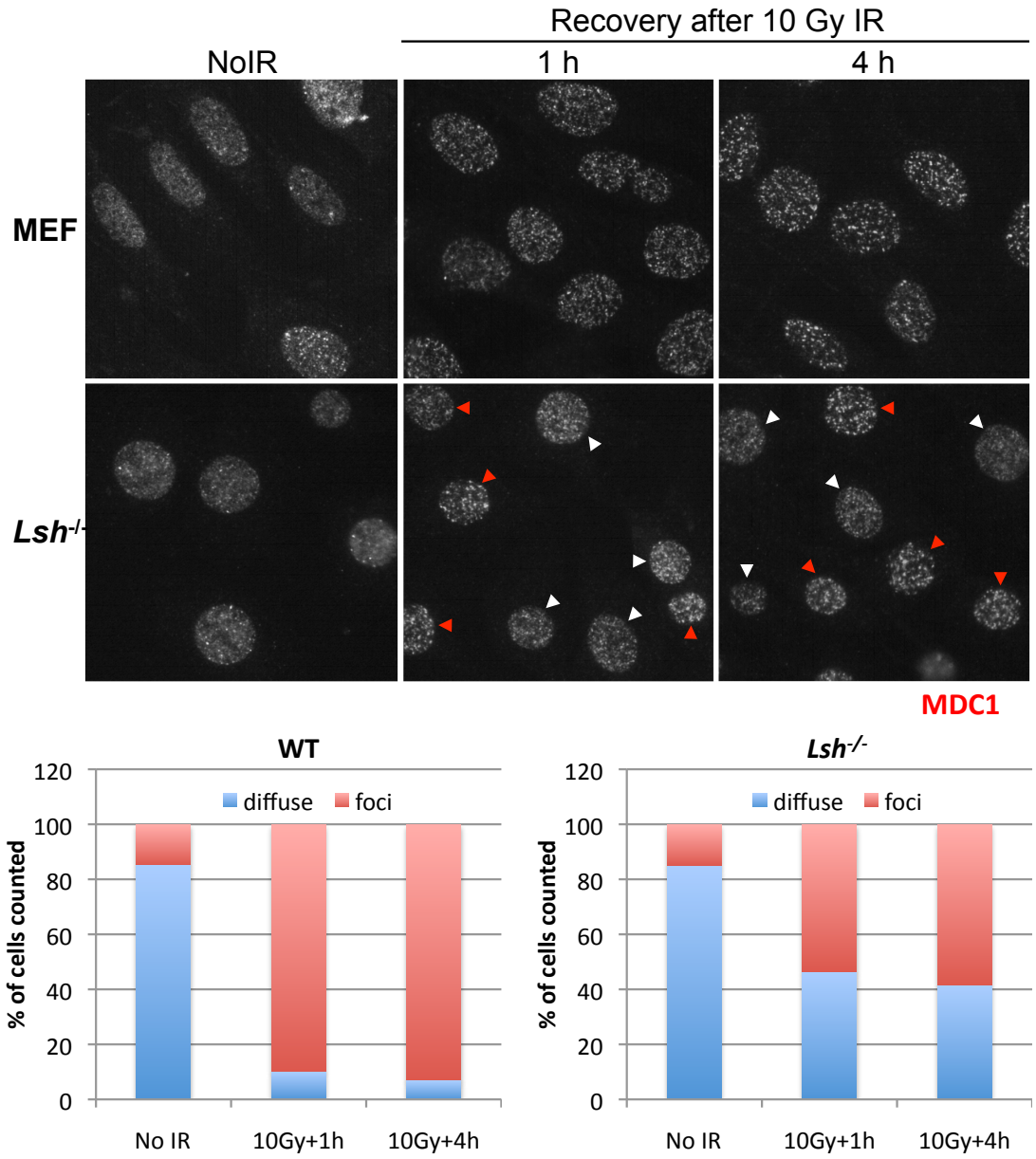

Figure 4.9: Representative immunofluorescence images showing MDC1 localisation in WT and *Lsh*$^{-/-}$ MEFs at the indicated time points after 10 Gy of ionising radiation. The graphs show percentage of fociated (red arrows) or diffuse nuclear stained (white arrows) nuclei of n=35 cells.

We also examined MDC1 recruitment to IRIF, as this protein is upstream of 53BP1 and recruited directly by γH2AX. Translocation from an un-localised nucleoplasmic protein to IRIF was observed in response to ionising radiation (Figure 4.9), similar to the localisation of 53BP1, and cells were again classified as either fociated or diffuse at 1 h and 4 h post irradiation. The results showed a similar pattern to that observed for 53BP1. WT MEFs displayed a shift from 85% diffuse MDC1 staining prior to treatment to approximately 90% fociated both 1 h and 4 h after ionising radiation, where as in *Lsh*$^{-/-}$ MEFs only 40-50% of the population showed IRIF (Figure 4.9).

These data clearly show that the formation of the mediator complex is impaired in the *Lsh*$^{-/-}$ MEFs, as predicted by the reduced H2AX phosphorylation observed in these cells. Furthermore the reduction in MDC1 recruitment to IRIF suggests that reduced or lack of H2AX phosphorylation at some DSBs is the cause of inefficient mediator complex assembly in the *Lsh*$^{-/-}$ MEFs as MDC1 is directly recruited to γH2AX.

4.6 Cell cycle checkpoint signalling is impaired in LSH depleted cells

It was still unclear how impaired mediator complex assembly caused decreased viability and increased sensitivity to DSB inducing agents in LSH depleted cells. Since components of the mediator complex, such as MDC1 and 53BP1, are required for recruitment of checkpoint proteins to DSBs and efficient cell cycle arrest, we hypothesised that activation of cell cycle checkpoints may be less efficient in LSH depleted cells with impaired mediator complex assembly. Impaired activation of checkpoint proteins and cell cycle arrest can lead to cells continuing though mitosis before DSBs are repaired. Cell division with unrepaired DSBs can result in chromosomal abnormalities, such as chromosome fusions and loss of entire chromosome arms. This in turn triggers the apoptotic pathway, which may explain the higher rate of apoptosis observed in LSH depleted cells following induction of DSBs. We attempted to examine the activation of the checkpoint proteins CHK2 and p53 in response to ionising radiation in the *Lsh*$^{-/-}$ and WT MEFs. However the *Lsh*$^{-/-}$ and WT MEFs had been maintained in culture through spontaneous immortalisation, which often

results in defects in p53 and apoptotic signalling. Unfortunately we found the WT MEFs did not express p53, which made them unsuitable for examining checkpoint signalling. In order to test this hypothesis we examined the activation CHK2 and p53 in response to ionising radiation in shLSH and non-silencing control MRC5^{hT} cells.

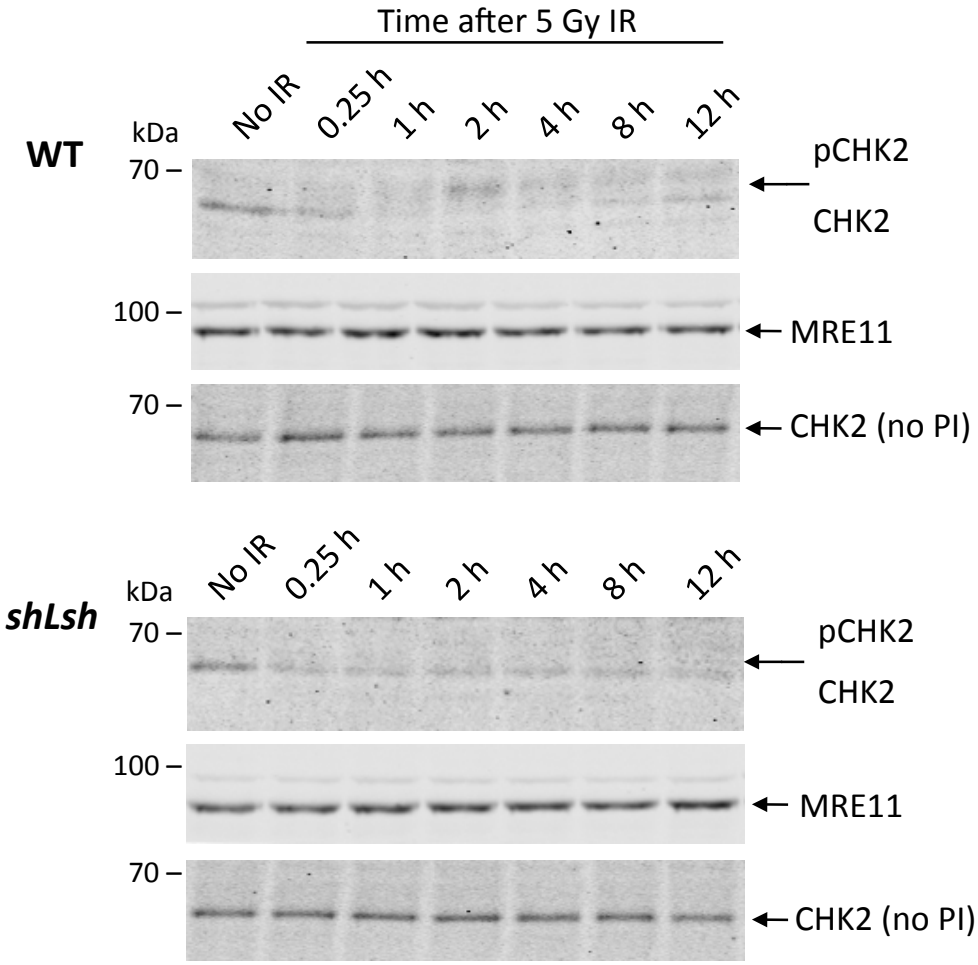

Figure 4.10: Nuclear extracts examined by Western blotting using an anti-CHK2 primary antibody to examine CHK2 levels in shLSH and non-silencing MRC5^{hT} cells at various time points after 5 Gy of ionising radiation. An anti-MRE11 antibody was also used to show the level of MRE11 protein to act as a loading control.

To investigate CHK2 activation, we examined the phosphorylation of CHK2 in response to DNA damage by Western blotting. Unfortunately the phosphorylated CHK2 antibody did not work in our hands. However, we could separate the phosphorylated and un-phosphorylated CHK2 by size and identified the bands using a general anti-CHK2 antibody. In nuclear extracts made without phosphatase inhibitors the top band could not be identified, confirming that the top band is the phosphorylated form of CHK2 (Figure 4.10).

In non-silencing control MRC5^{hT} cells a band of phosphorylated CHK2 appeared following ionising radiation, peaking 2 h after treatment and fell back toward basal levels after 8 to 12 h (Figure 4.8). An inverse correlation in the un-phosphorylated band was seen, which decreased following ionising radiation, reaching its lowest levels 1 to 2 h post treatment. This indicates that the majority of CHK2 becomes phosphorylated in the non-silencing control MRC5^{hT} cells 2 h post treatment. However, in shLSH MRC5^{hT} cells a phosphorylated CHK2 band cannot be detected after ionising radiation. Un-phosphorylated CHK2 does decrease after treatment, but to a lesser extent than in the non-silencing control cells (Figure 4.8), suggesting that a smaller proportion of CHK2 becomes phosphorylated in shLSH MRC5^{hT} cells, which is below the threshold of detection of the antibody.

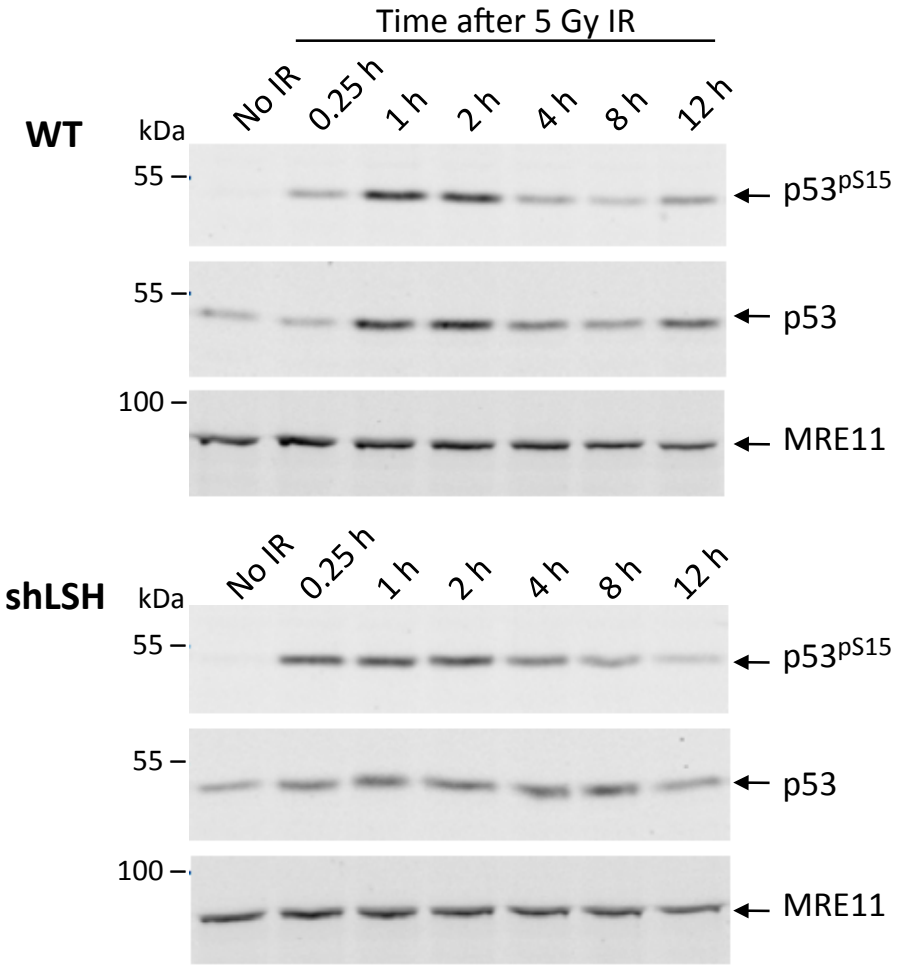

Figure 4.11: Nuclear extracts examined by Western blotting using an anti-p53 and anti-p53^{pS15} primary antibodies to examine un-phosphorylated and phosphorylated p53 levels in shLSH and non-silencing MRC5^{hT} cells at various time points after 5 Gy of ionising radiation. An anti-MRE11 antibody was also used to show the level of MRE11 protein to act as a loading control.

We also examined p53 activation by Western blotting. Normally p53 has a rapid turnover rate, which becomes stabilised upon phosphorylation by ATM / ATR kinases, we therefore examined total p53 levels in shLSH and non-silencing MRC5^{hT} cells following ionising radiation treatment. In addition to total p53 we examined active p53, using an antibody specific to p53 phosphorylated at serine 15, the site of activation by phosphorylated ATM. In non-silencing control cells the total p53 levels increase following ionising radiation treatment, specifically 1 and 2 h post treatment, this is accompanied by a similar increase in p53^{pS15} levels (Figure 4.11). Although p53^{pS15} levels also increase in shLSH MRC5^{hT} cells post treatment, it is only accompanied by a modest increase in total p53, which does not reflect the p53^{pS15} signal (Figure 4.11). These results show that, unlike CHK2, p53 can be phosphorylated in both shLSH and non-silencing MRC5^{hT} cells. The reduced levels of total p53 in shLSH cells suggests that stabilisation of p53 in response to ionising radiation is impaired, probably due to deficient p53 phosphorylation at other sites. Serine 20 phosphorylation by CHK2 blocks the interaction between p53 and MDM2, required for nuclear export and subsequent proteolytic degradation of p53 and we have shown that activation of CHK2 in response to ionising radiation treatment is reduced in LSH deficient cells (Figure 4.10).

Since loss of LSH results in significantly slower DSB repair we would have expected cell cycle checkpoint signalling to be extended in LSH depleted cells, in order to produce a longer arrest period for damage to be repaired. However, consistent with our hypothesis phosphorylation of CHK2 is less efficient in LSH depleted cells. p53 is also stabilised less efficiently in response to ionising radiation, also suggesting impaired cell cycle checkpoint signalling. The amount of p53 phosphorylated specifically by ATM at serine 15 does not appear reduced in shLSH MRC5^{hT} cells, however it also does not appear to be extended compared to non-silencing controls. These data suggest that a proportion of breaks in LSH depleted cells do not correctly activate cell cycle check points, consistent with the observed impaired mediator complex assembly. This could result in cells undergoing mitosis with unrepaired DSB still present, which can be lethal to the cells and would explain the increased cell death 96 h after treatment in shLSH MRC5^{hT} cells in which DSB have been induced (Figure 3.2).

4.7 Summary

Detailed investigation of DSBs recognition and repair in LSH deficient cells showed that broken DNA ends are correctly recognised in *Lsh*$^{-/-}$ MEFs. Although we were unable to show localisation of the MRN complex to broken DNA we did show that MRE11, a component of the MRN complex has an increased affinity for chromatin following ionising radiation treatment (Figure 4.1). We also demonstrated similar activation of ATM in *Lsh*$^{-/-}$ and WT MEFs after ionising radiation and showed no difference in the localisation of phosphorylated ATM to IRIF 15minutes and 1hour after treatment (Figure 4.2 and 4.3). Fewer phosphorylated ATM IRIF were seen in the *Lsh*$^{-/-}$ MEFs 4hours after treatment, however localisation of phosphorylated ATM to broken DNA ends later in repair involves additional interaction with components of the DSB mediator complex. Investigation of H2AX phosphorylation, the initial step in mediator complex assembly showed that γH2AX is reduced in LSH deficient cells (Figure 4.4). Further investigation revealed fewer γH2AX IRIF in *Lsh*$^{-/-}$ MEFs, which suggested only a proportion of DSBs were effected (Figure 4.6). Expression array data revealed no expression changes in *Lsh*$^{-/-}$ MEFs that could account for this (Table 4.1) and chromatin retention assays showed no difference in the amount of H2AX associated with the chromatin in *Lsh*$^{-/-}$ MEF (Figure 4.1).

We show that reduced γH2AX resulted in less robust recruitment of downstream mediator components, MDC1 and 53BP1 (Figures 4.8 and 4.9). Mediator complex facilitates the recruitment of proteins required for DSB repair by HR. This may explain why some DSBs are repaired slower in *Lsh*$^{-/-}$ MEFs. The mediator complex also facilitates correct cell cycle checkpoint signalling by recruiting checkpoint proteins to broken DNA ends. Analysis of checkpoint activation showed similar activation of p53 in shLSH and non-silencing control MRC5^{hT} cells but reduced phosphorylation of CHK2 (Figures 4.10 and 4.11). This showed that cell cycle checkpoint signalling is not extended to accommodate the slower DSB repair of LSH deficient cells. This indicates that DSB, which require LSH for H2AX phosphorylation and repair, do not activate cell cycle arrest in LSH deficient cells. This would allow mitosis to occur which unrepaired DSBs, which could result in chromosomal defects and explains reduced survival of LSH deficient cells following ionising radiation treatment.

Results - Chapter Five

5.0 Rescue of DNA DSB repair defects in *Lsh*$^{-/-}$ MEFs

5.1 Introduction

We have identified a phenotype of increased sensitivity to DSB inducing agents in LSH deficient cells and have shown that a proportion of DSBs are repaired slower in these cells. We have also demonstrated that mediator complex assembly and cell cycle checkpoint signalling are impaired in the absence of LSH and that these are most likely the cause for the observed increase in cell death and sensitivity to DSB inducing agents. Although microarray data did not reveal any obvious expression changes that could be responsible for the observed phenotype, a direct involvement of LSH in DSB repair is yet to be demonstrated. We therefore followed two lines of enquiry to identify if LSH is actively involved in repair of DSBs. Firstly, we characterised *Lsh*$^{-/-}$ MEFs that had been infected with lentiviruses expressing either WT LSH or a catalytically inactive LSH which contained a lysine to glutamine mutation in the conserved ATPase domain. This mutation has previously been shown to abolish the ATP hydrolysing ability of LSH. This allowed us to test if the defective DSB repair phenotype of the *Lsh*$^{-/-}$ MEFs can be complemented. It also allowed us to investigate whether the ATPase activity of LSH is required for its function in DSB repair, which could suggest chromatin remodelling by LSH. Secondly, we examined LSH localisation pre and post ionising radiation treatment to determine if LSH is recruited to DSB as part of the recognition or mediator complexes.

5.2 WT but not catalytic null LSH improves survival of Lsh$^{-/-}$ MEFs following IR

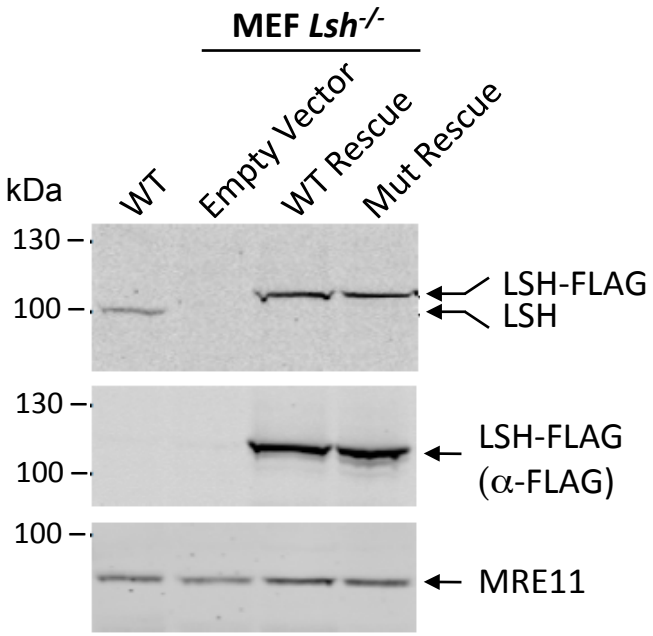

Figure 5.1: Nuclear extracts examined by Western blotting using anti-Lsh and anti-FLAG primary antibodies to examine LSH levels in *Lsh*$^{-/-}$ and rescue MEF cells. An anti-MRE11 antibody was also used to show the level of MRE11 protein to act as a loading control.

Expression levels of LSH in *Lsh*$^{-/-}$ MEFs, which had been infected with either an empty vector control, LSH-3xFLAG (WT rescue) or catalytically inactive LSH-3xFLAG (mutant rescue) were examined by Western blotting and compared to WT MEFs using both an anti-LSH antibody and anti-FLAG antibody specific for the rescue construct. The results of the anti-FLAG Western blot showed that both WT and mutant constructs were expressed at similar levels (Figure 5.1). This was confirmed by Western blot probed with an anti-LSH antibody, which also showed LSH expression in WT and mutant rescues to be slightly higher than LSH expression in WT MEFs (Figure 5.1).

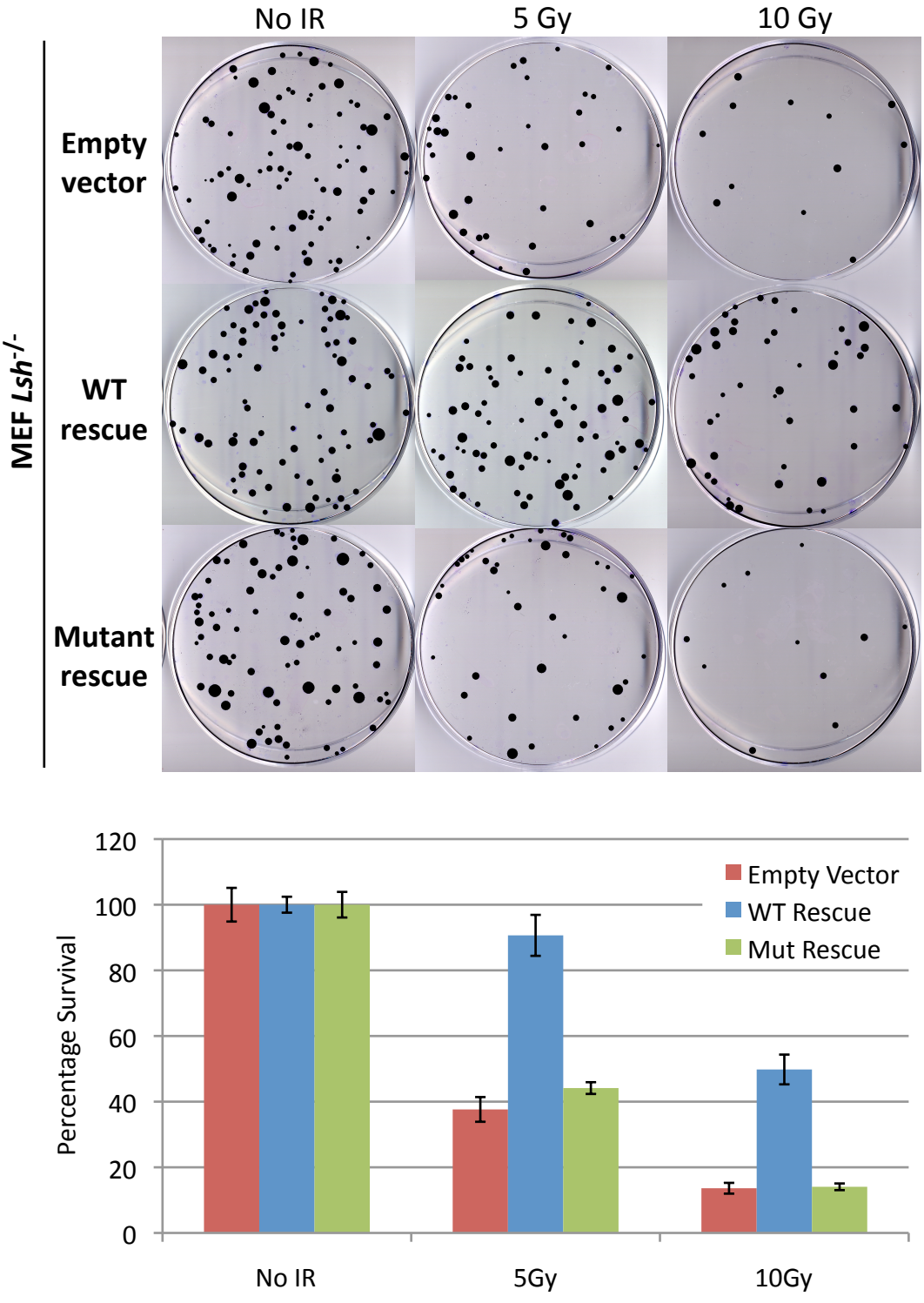

Figure 5.2: Giemsa stained plates and colony counts of empty vector control and rescue *Lsh*$^{-/-}$ MEFs plated at 100 cells per dish and irradiated with the indicated dose of ionising radiation.

To establish whether the increased sensitivity of *Lsh*$^{-/-}$ MEFs to ionising radiation can be rescued, survival studies were performed as previously described comparing *Lsh*$^{-/-}$ cells expressing WT and mutant LSH with empty vector controls. The results showed no difference between the survival of both empty vector controls and mutant rescued cells, with approximately 40% and 10% survival after either a 5 Gy or 10 Gy dose of ionising radiation, respectively (Figure 5.2). Furthermore, the results are comparable to the sensitivity of *Lsh*$^{-/-}$ MEFs that was observed previously (Figure 3.3). However, WT rescued cells were much less sensitive to ionising radiation and even displayed an improvement on the survival of WT MEFs that was observed previously (Figures 5.2 and 3.3). The improved survival of the *Lsh*$^{-/-}$ cells expressing WT LSH indicates that LSH is able to reverse the increased sensitivity to ionising radiation seen in LSH deficient cells. Furthermore, the failure of the mutant LSH to improve the survival of *Lsh*$^{-/-}$ MEFs suggests that a functional ATPase domain is required for the function of LSH in DSB repair. The improvement in survival of *Lsh*$^{-/-}$ cells expressing WT LSH above the levels detected in the WT MEFs could be due to the over expression of LSH, raising the interesting possibility that excess LSH may improve the efficiency of DSB repair.

5.3 LSH ATPase activity is required to restore efficient mediator complex assembly in *Lsh*$^{-/-}$ MEFs

The improved survival of WT rescued cells to ionising radiation treatment suggests that DSBs are repaired more efficiently. To examine DSB repair in more detail we explored H2AX phosphorylation and 53BP1 localisation in WT and mutant rescued cells to determine whether we see improved mediator complex assembly, which would be consistent with the results of the survival study. γH2AX levels were investigated by Western Blots of nuclear extracts prepared from *Lsh*$^{-/-}$ cells carrying either empty vector control, WT rescued or mutant rescued constructs and WT MEFs at a range of time points after treatment with ionising radiation.

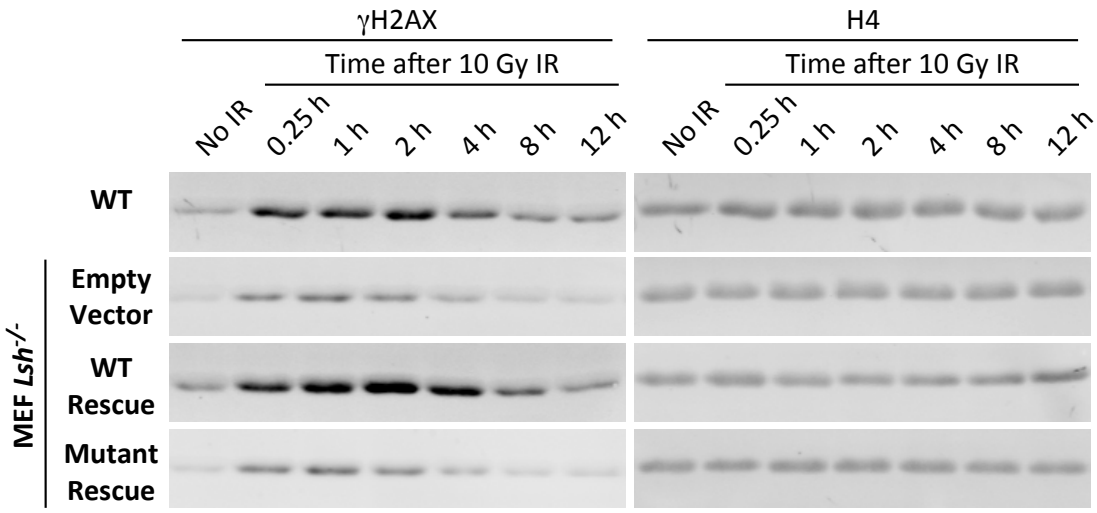

Figure 5.3: Nuclear extracts examined by Western blotting using an anti-γH2AX primary antibody to examine γH2AX levels in empty vector control and rescue *Lsh*$^{-/-}$ MEFs at a range of time points following 10 Gy of ionising radiation. An anti-H4 antibody was also used to show the level of H4 to act as a loading control.

As expected, empty vector control *Lsh*$^{-/-}$ MEFs showed reduced γH2AX when compared to the WT MEFs (Figure 5.3). Mutant rescue cells also had reduced γH2AX levels compared to the WT MEFs and displayed a similar amount of H2AX phosphorylation as empty vector control cells. This confirmed that LSH without a functional ATPase domain cannot promote efficient DSB repair. However in WT rescued cells the phosphorylation of H2AX was restored to WT levels (Figure 5.3), consistent with the results from the survival study (Figure 5.2).

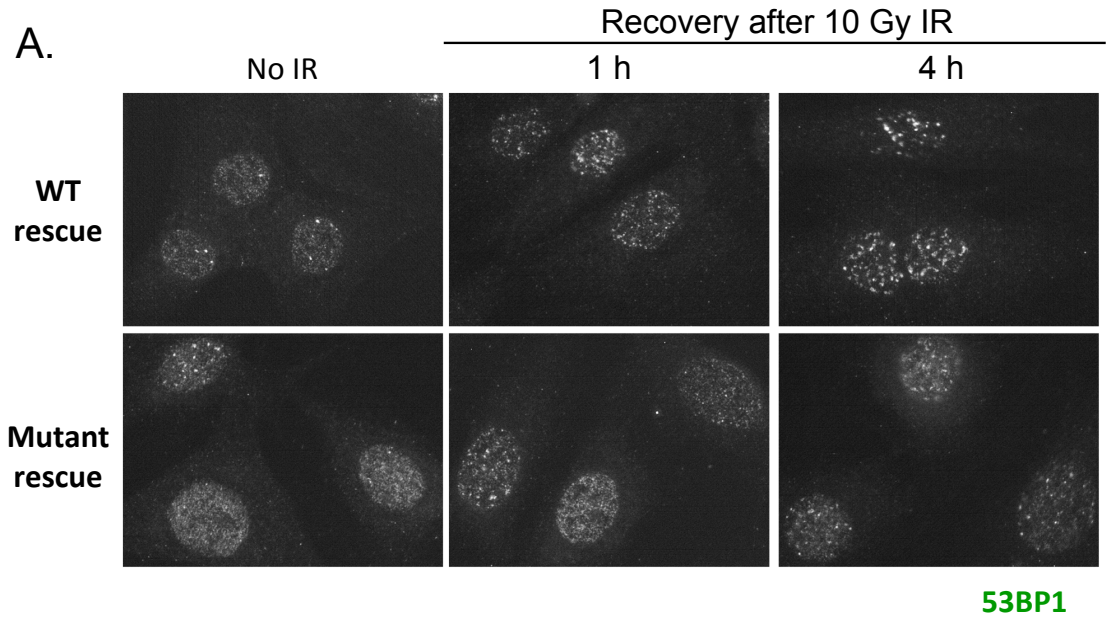

B.

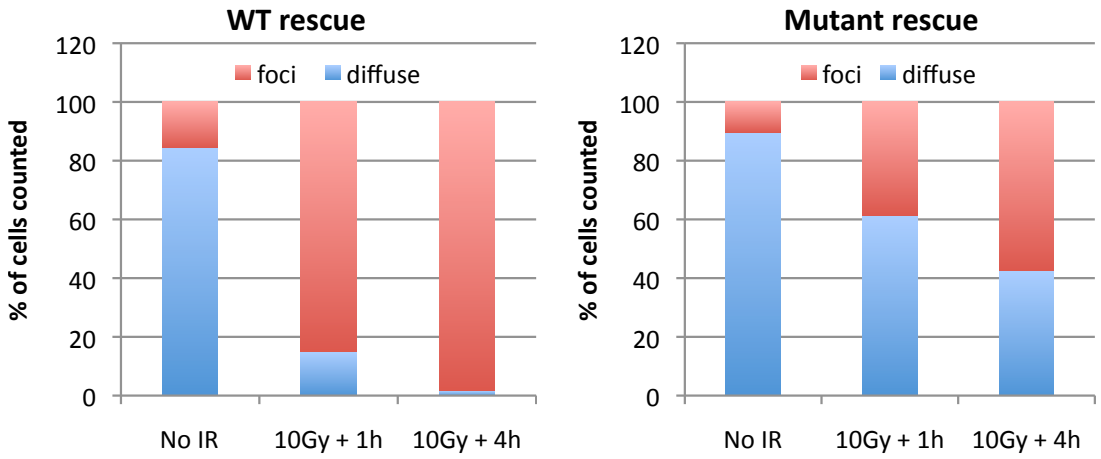

Figure 5.4: (A.) Representative immunofluorescence images showing 53BP1 localisation in WT and mutant rescued *Lsh*$^{-/-}$ MEFs at the indicated time points after 10 Gy of ionising radiation. (B.) The graphs show percentage of fociated or diffuse nuclear stained nuclei of n=35 cells.

To confirm that restored H2AX phosphorylation in WT rescued cells is functioning correctly we also examined 53BP1 recruitment to IRIF as a sign of correct mediator complex assembly. Immunofluorescence for 53BP1 was carried out as previously described and cells were again classified as either containing foci or having diffuse nuclear staining at 1 h and 4 h post 10 Gy of ionising radiation. The localisation of 53BP1 in mutant rescued cells was similar to what was previously observed in the *Lsh*$^{-/-}$ MEFs (Figure 4.8), with IRIF only identifiable in 40% and 60% of cells 1hour and 4hours after treatment (Figure 5.4). WT rescued cells exhibited a pattern of 53BP1 localisation that resembled WT MEFs, with 85% and 100% of cells having IRIF 1 h and 4 h after treatment.

In summary the expression of WT or catalytically inactive LSH in *Lsh*$^{-/-}$ MEFs clearly demonstrates that the inefficient DSB repair phenotype can be reversed and that the ATPase activity of LSH is required for its function in DSB repair. These data add further credibility to the hypothesis that LSH is required for efficient DSB repair and its function is connected to chromatin remodelling.

5.4 LSH does not accumulate at the sites of DNA damage

Another piece of evidence that would confirm that LSH is involved in DSB break repair would be to show that LSH is recruited to the site of DNA damage. The time of recruitment may also help to understand the function of LSH in DSB repair. Late recruitment would suggest a role in repair, possibly in relaxing the chromatin in preparation for strand invasion and homologous recombination. This may explain the inefficient DSB repair seen in *Lsh*$^{-/-}$ MEFs. Alternatively, early recruitment may suggest a role in DSB detection, possibly by remodelling the chromatin to allow space for mediator complex assembly. This could provide an explanation for the reduced H2AX phosphorylation and mediator complex assembly in LSH deficient cells.

To address these questions we performed immunofluorescence on WT MEFs to see if endogenous LSH localises to IRIF. Unfortunately, we could not obtain an anti-LSH antibody that was suitable for immunofluorescence in our hands. However, the WT and mutant rescued cell lines expressing LSH tagged with a triple FLAG peptide detectable by immunofluorescence using an anti-FLAG antibody were suitable for localisation studies. Since our investigation has shown that the WT rescued cells can restore DSB repair to normal, we surmised that LSH is functioning correctly in DNA repair in these cells. Therefore, the WT rescued cells are a suitable model in which to investigate LSH localisation following ionising radiation treatment. Mutant rescue cells were also examined to determine whether any localisation in response to ionising radiation treatment that could be seen in the WT rescue cells is dependent on ATP hydrolysis. We predicted that if LSH is recruited to DSBs through protein-protein interactions, these could still occur with a catalytically inactive ATPase domain so IRIF could still form. However if LSH translocates along the DNA to the site of a DSB, ATP hydrolysis would be required so IRIF would not be present in the mutant rescued cells.

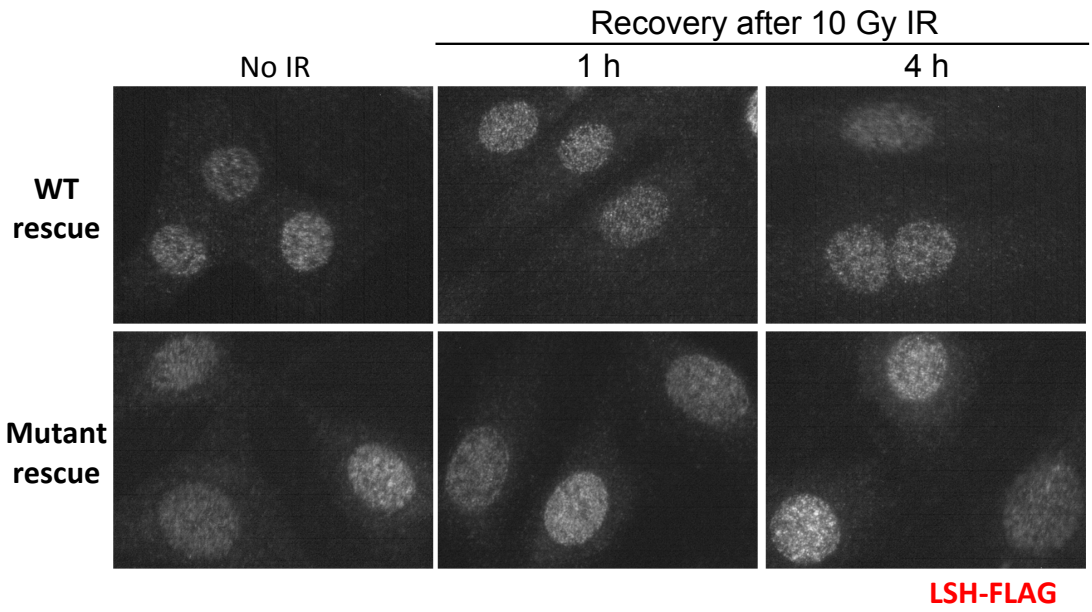

Figure 5.5: Representative immunofluorescence images using an anti-FLAG antibody to show LSH localisation in WT and mutant rescued *Lsh*$^{-/-}$ MEFs at the indicated time points after 10Gy of ionising radiation.

Although localisation of FLAG-tagged LSH to IRIF was not observed in the mutant rescued cells, we also did not detect recruitment of LSH to IRIF in the WT rescued cells post ionising radiation treatment (Figure 5.5). These results suggest that LSH is either not recruited to DSB or recruited at too low a level to be detected above background levels in the nucleoplasm. A third possibility is that LSH is not freely moving in the nucleoplasm but is associated with the chromatin and doesn't translocate far or accumulate at sites of DNA damage, but rather acts locally and only aids in repair of DSBs that occur close to where it is associated.

If LSH is normally recruited to DNA damage at levels too low to be detected above nucleoplasm background we can improve our chance of observing LSH recruitment by inducing a high frequency of DSBs within an defined area of the nucleus. A high number of DSB will result in a stronger signal, which should be seen over the nucleoplasmic background. To achieve this laser induced micro-irradiation was performed, whereby cells expressing GFP-tagged LSH were cultured with BrdU, which incorporates into the DNA making it more heat labile. This was followed by passing a laser across a cell to disrupt the heat labile DNA creating a high number of DNA lesions under the path of the laser.

We also wished to examine LSH localisation immediately after laser irradiation in case it is recruited very early to DSBs and dissociates rapidly, in which case LSH localisation to breaks could be missed in the time it took to fix the cells for immunofluorescence. To overcome this we performed live cell imaging and followed GFP-tagged LSH within a cell immediately after Laser micro irradiation. Fortunately VA13 cells (SV40 immortalised lung fibroblasts) expressing LSH-GFP were previously generated in the lab (Kevin Myant, unpublished) allowing visualisation of LSH *in vivo*. Laser micro-irradiation was therefore performed on VA13 LSH-GFP cells and images taken in real time to follow the localisation of LSH-GFP within the nucleus. After 4h cells were fixed and immunofluorescence carried out for γH2AX as a control for the induction of DSBs.

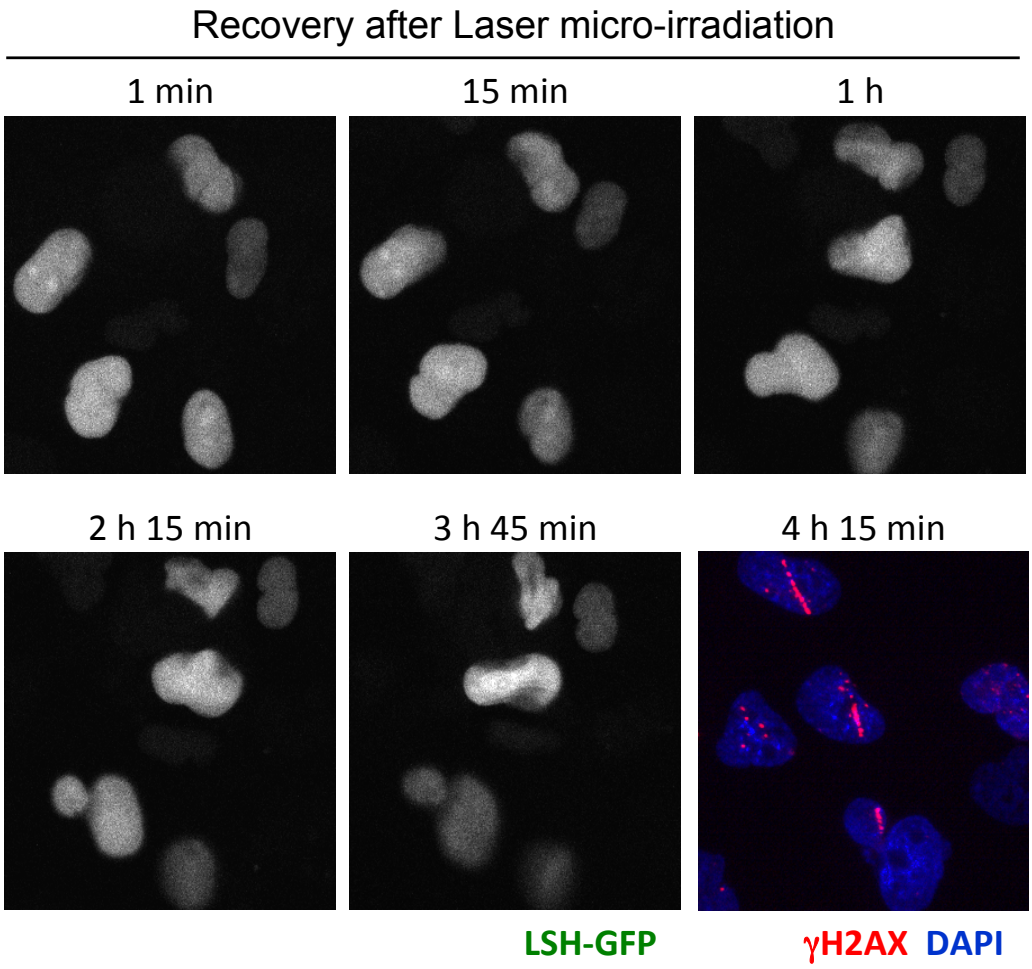

Figure 5.6: Confocal microscopy images showing LSH-GFP in VA13 cells at indicated time points after laser induced micro irradiation and immunofluorescence showing localisation of γH2AX.

The path of the laser could be seen by γH2AX immunofluorescence, which highlights a line of DSBs across the nucleus (Figure 5.6). However, LSH-GFP did not associate with the laser induced damage either later or immediately after irradiation (Figure 5.6). This maybe because native LSH is also produced in VA13 cells and is recruited to DSBs in preference to GFP tagged LSH or it may be that LSH is chromatin bound and acts to repair breaks locally and is not recruited to DSBs in general. It is also possible that LSH is not involved in the DNA damage response at sites of damage, but may facilitate the homogeneous distribution of H2AX throughout chromatin. In LSH deficient cells this could lead to regions of H2AX poor chromatin where there is insufficient H2AX, for phosphorylation in response to the formation of a DSB, to form γH2AX IRIF.

5.5 The LSH is mainly chromatin bound and not free in the nucleoplasm

To test the hypothesis that LSH is not recruited to breaks, but rather aids in repair of breaks close to where it is situated on the chromatin we investigated whether LSH accumulates on chromatin after IR. A chromatin retention assay was performed as previously described. If the hypothesis is correct we expect to find the majority of LSH in the chromatin bound fraction rather than the free nucleoplasmic fraction. The assay was carried out on WT MEFs pre and post treatment with a 10 Gy dose of ionising radiation to explore whether the chromatin affinity of LSH changed in response to the induction of DSBs.

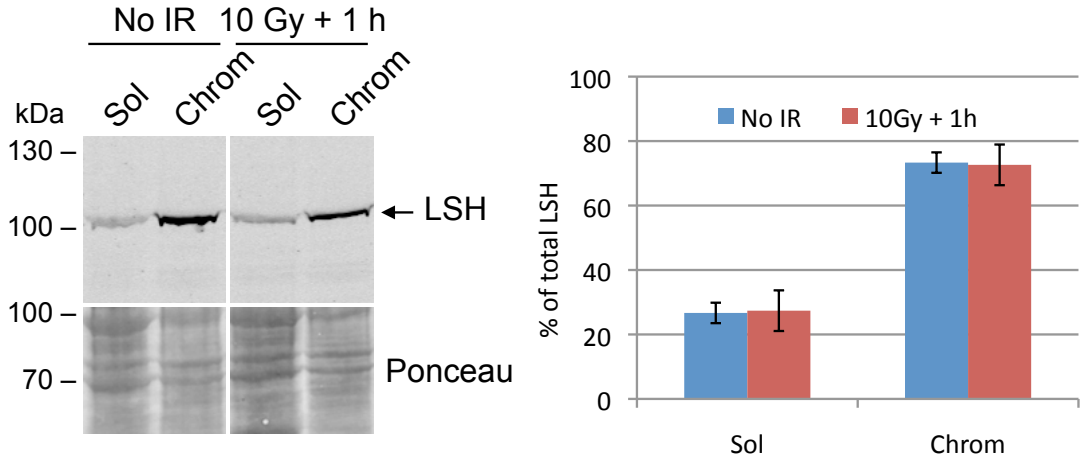

Figure 5.7: Chromatin retention assay shown by Western blot analysis of WT MEFs using an anti-LSH primary antibody to show soluble and chromatin bound fractions before and 1 h post 10 Gy of ionising radiation. Quantification of LSH is plotted as a percentage of soluble and chromatin bound signals combined (Quantified using Odyssey V3.0).

These experiments showed that a large proportion of LSH (75%) is chromatin bound (Figure 5.7). Furthermore there was no increase in the amount of chromatin bound LSH post irradiation suggesting that additional nucleoplasmic LSH is not recruited. These data, together with the lack of LSH accumulation at DSB are consistent with chromatin bound LSH acting locally to aid in DSB repair or LSH evenly distributing H2AX throughout chromatin. Either of these hypotheses may explain why in LSH depleted cells, H2AX phosphorylation occurs at some breaks but not others (Figures 4.3 and 4.5).

5.6 Summary

These results demonstrate that the DSB phenotype of the *Lsh*$^{-/-}$ MEFs can be fully reversed by the reintroduction of LSH into these cells, with both survival (Figure 5.2) and H2AX phosphorylation (Figure 5.3) returning to the level of WT MEFs. The results also showed that LSH ATPase activity is vital to its function in DSB repair, with catalytically inactive LSH having no restorative effect on DSB repair in the *Lsh*$^{-/-}$ MEFs. While this does not provide evidence of chromatin remodelling by LSH, the requirement of a functionally ATPase domain for effective DSB repair is consistent with the hypothesis that chromatin remodelling by LSH is what facilitates its role in DSB repair.

Unlike most DSB signalling and repair proteins, LSH does not accumulate at broken DNA ends. This was demonstrated by a lack of LSH IRIF in *Lsh*$^{-/-}$ MEFs expressing FLAG-tagged LSH (Figure 5.5) and the failure of GFP-tagged LSH to localise to sites of DNA damage in VA13 cells (Figure 5.6). We showed that a possible explanation for this is because the majority LSH is normally associated with the chromatin and that this does not change following ionising radiation treatment. This suggested two possible hypotheses, either LSH only aids in the repair of DSBs that occur close to where LSH is bound or the role of LSH in the DSB response is not at broken DNA ends. The first hypothesis implies that not all DSBs require LSH for repair and the second that LSH is not directly involved in DSB repair but has a related function such as ensuring the even distribution of H2AX. To test either of these we needed to compare the repair of individual DSBs, which require LSH for repair, in WT and LSH deficient cells.

Results - Chapter Six

6.0 Generation of an inducible DSB system for further investigation of LSH dependent repair

6.1 Introduction

The most identifiable DSB repair defect in LSH deficient cells is the reduced H2AX phosphorylation. To further investigate how LSH is involved in DSB repair we need to more closely examine in what way the γH2AX levels are reduced in LSH deficient cells. As previously stated inefficient H2AX phosphorylation in *Lsh*$^{-/-}$ MEFs could be the result of either a reduction in the amount of H2AX phosphorylation at all DSBs or the failure to phosphorylate H2AX at a proportion of breaks. The observation that fewer γH2AX IRIF can be seen in *Lsh*$^{-/-}$ compared to WT MEFs, despite the same number of breaks being induced indicates a failure to phosphorylate H2AX at a proportion of breaks. This is supported by the observations that LSH is mainly chromatin bound and does accumulate at breaks, which suggests that LSH is chromatin associated and only acts to aid in repair of breaks which occur close to where it is bound.

To further explore the role of LSH in DSB repair, individual breaks have to be examined rather than the cellular responses to DNA damage in general because only a proportion of DSBs seem to require LSH for efficient repair. We therefore need to compare DSBs in WT and LSH deficient cells to identify breaks that undergo LSH dependent repair. Since we do not yet know in which way LSH is mechanistically necessary for repair, we need to be able to characterise many breaks and perform statistical correlations. To achieve this a system is required that would allow DSBs to be induced at the same defined locations in the genomes of WT and LSH deficient cells for direct comparison of repair at individual DSBs. Multiple breaks are also needed to make any correlation statistically significant.

In order to achieve this, we employed the ER-AsiSI system developed by Lacovoni *et al* 2010, which uses the restriction enzyme AsiSI under the control of the estrogen receptor. Upon addition of 4-Hydroxytamoxifen (4OHT) ER-AsiSI translocates from the cytoplasm to the nucleus where it cleaves the DNA creating a DSB at a precise, known location within the genome. γH2AX ChIP-Chip could then be performed to compare H2AX phosphorylation at DSBs in the same location in both WT and LSH deficient cells, to identify DSBs that require LSH for efficient repair. AsiSI has approximately 1000 recognition sites within the human genome and has been reported to cut at approximately 25% of these providing a statistically significant number of sites to compare.

6.2 Generation of cells expressing ER-AsiSI

The AsiSI restriction enzyme employed in the ER-AsiSI inducible DSB system is methylation sensitive. Only 25% of potential AsiSI site are cut in cells with WT levels of DNA methylation, which induces a similar number of DSBs as a 10-15 Gy dose of ionising radiation (Lacovoni *et al* 2010, Rogakou *et al* 1999). *Lsh*$^{-/-}$ MEFs have a reduction in DNA methylation by approximately 70% compared to WT MEFs. This makes WT and *Lsh*$^{-/-}$ MEFs an unsuitable platform for the ER-AsiSI system as reduced methylation in *Lsh-/-* MEFs will make more restriction sites available to AsiSI, resulting in more DSBs being induced in the *Lsh-/-* MEFs than in the WT. We therefore opted to use non-silencing and shLSH MRC5^{hT} cells as the basis for the ER-AsiSI inducible DSB system. Although previous work has shown that knockdown of LSH results in loss of DNA methylation, it took over 15 population doublings for a significant difference in global methylation levels to occur.

Initially ER-AsiSI was introduced into MRC5^{hT} cells, prior to shLSH knockdown in order to base non-silencing and shLSH cells on the same ER-AsiSI MRC5^{hT} background. This was done to ensure the same level of ER-AsiSI expression in both non-silencing and shLSH cells so that variation in ER-AsiSI expression levels didn't affect efficiency of DSB induction. ER-AsiSI is also HA tagged, which allowed us to use an anti-HA antibody suitable for immunofluorescence to observe localisation of ER-AsiSI prior to and following Tamoxifen treatment.

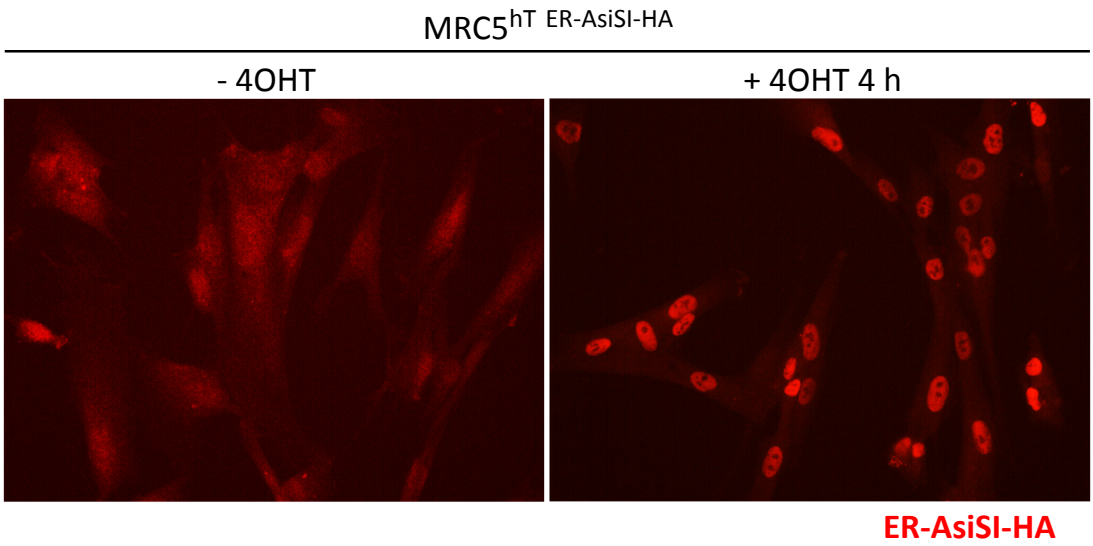

Figure 6.1: Representative immunofluorescence images using an anti-HA antibody to show ER-AsiSI-HA localisation in MRC5^{hT} cells before and after Tamoxifen treatment.

These experiments showed that ER-AsiSI was expressed in MRC5^{hT} cells and was distributed throughout the cytoplasm prior to 4OHT treatment (Figure 6.1). Upon induction with 4OHT clear nuclear staining is observered (Figure 6.1), indicating that the majority of ER-AsiSI translocates to the nucleus and the estrogen receptor is functioning correctly.

6.3 H2AX phosphorylation of AsiSI induced DSBs in non-silencing and shLSH MRC5$^{hT\ ER\text{-}AsiSI\text{-}HA}$ cells

shRNA knockdown of LSH in MRC5$^{hT\ ER\text{-}AsiSI}$ cells was performed as previously described and knockdown efficiency examined by Western blot. To ensure that AsiSI induced breaks behave similarly to previously observed ionising radiation induced DSBs we examined γH2AX levels following 4 h 4OHT treatment to induce AsiSI DSBs.

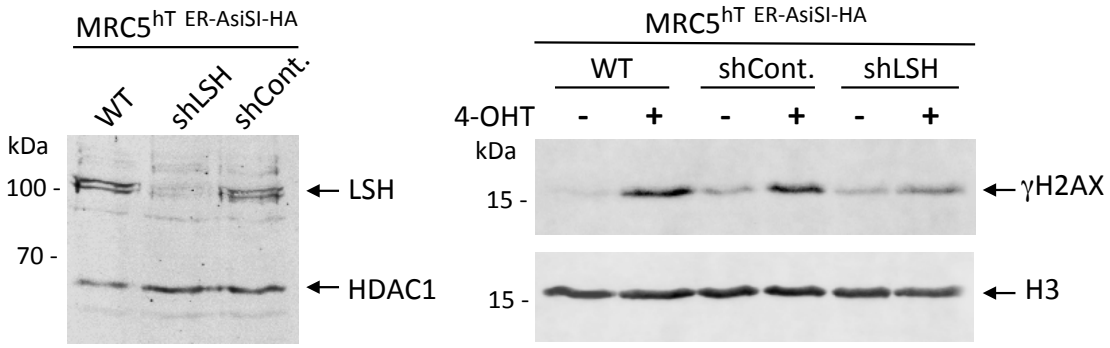

Figure 6.2: Nuclear extracts examined by Western blotting using either anti-LSH or anti-γH2AX primary antibody to examine shLSH knockdown efficiency and γH2AX response to AsiSI DSBs induced by 4h 4OHT treatment in WT, non-silencing and shLSH MRC5$^{hT\ ER\text{-}AsiSI\text{-}HA}$ cells. Anti-HDAC1 and anti-H3 antibodies were used as a loading control respectively.

The results showed shRNA knockdown reduced LSH to nearly undetectable levels in shLSH MRC5$^{hT\ ER\text{-}AsiSI}$ cells (Figure 6.2). γH2AX Western blots showed that H2AX phosphorylation occurred in response to 4OHT treatment in MRC5$^{hT\ ER\text{-}AsiSI}$ cells, indicating DSB induction and repair response. Furthermore levels of γH2AX were reduced in the shLSH MRC5$^{hT\ ER\text{-}AsiSI}$ cells have compared to WT or non-silencing controls (Figure 6.2), consistent with the previously observed defects in DSB repair in LSH deficient cells following ionising radiation treatment. This suggested that AsiSI induced DSBs in non-silencing and shLSH MRC5$^{hT\ ER\text{-}AsiSI}$ cells provide a suitable model system for comparing DSB repair at the same defined genomic locations in a WT or LSH deficient background in order to identify breaks that undergo LSH dependent repair.

6.4 Future characterisation of MRC5$^{hT\ ER\text{-}AsiSI}$ cells to investigate the role of LSH in DSB repair

To further investigate DSB repair at a variety of defined genomic locations in shLSH MRC5$^{hT\ ER\text{-}AsiSI}$ and non-silencing control cells, we suggest γH2AX ChIP-Chip be carried out on these cells. By using H2AX phosphorylation as an indicator of efficient DSB repair, breaks that undergo LSH dependent repair can identified as broken DNA ends with reduced H2AX phosphorylation in the shLSH MRC5$^{hT\ ER\text{-}AsiSI}$ cells compared to the non-silencing control cells. γH2AX ChIP-Chip may also indicate the reason for the reduced H2AX phosphorylation observed on a cellular level in LSH deficient cells. For example, γH2AX ChIP-Chip could indicate a reduction or lack of H2AX phosphorylation at a proportion of DSBs or a reduction in γH2AX spreading from the broken DNA end of some breaks or a combination of these, all of which would result in reduced cellular levels of γH2AX in response to the induction of DSBs

γH2AX ChIP-Chip may show that DSBs, which require LSH for efficient H2AX phosphorylation, occur sporadically or in clusters, which would suggest LSH either functions over large regions or at specific locations. Statistical comparisons between locations that require LSH for efficient DSB repair could indicate a correlation with other known features within the genome, such as repetitive elements or untranscribed regions. This may provide an insight into how LSH functions in DSB repair as it has previously been shown to act as a transcriptional repressor and be required at repetitive elements for maintenance of DNA methylation. Identifying DSBs, which repair less efficiently when LSH is depleted, will also indicate suitable regions for investigation in more detail. For example, a range of different ChIPs could be performed to examine heterochromatic or euchromatic marks or LSH occupancy in non-silencing control cells.

Discussion - Chapter Seven

DNA damage from both normal metabolic activities and environmental factors such as UV and radiation can cause as many as 1 million individual lesions to the DNA per cell per day. It is vital that these lesions are repaired or the cells enter senescence or undergo apoptosis to prevent the propagation of potentially harmful mutations. If DNA lesions are allowed to persist through mitosis they can affect transcript integrity and genome fidelity, leading to carcinogenesis. The repair of DNA lesions is a complex process involving many different mechanisms to cope with the variety of different DNA lesions that can occur. Despite their different functions, all DNA repair mechanisms require access to the DNA in order to facilitate its repair. However, DNA is found in a variety of different chromatin states throughout the nucleus depending on its sequence, chromosomal location, and transcriptional regulation. The DNA damage response has to cope with DNA in a variety of different states of compaction depending on the nucleosome occupancy, histone modifications and accessory factors associated with the chromatin. It is unsurprising that histone modifying enzymes and chromatin remodelling ATPases are associated with many of the DNA damage response pathways to relax the chromatin and facility access to the DNA for the repair machinery.

LSH is an ATP hydrolysing protein with functional domain and sequence similarities to SNF2 ATP dependent chromatin remodelling enzymes. To date the majority of published work regarding LSH focuses on its requirement for DNA methylation. However, unexplained phenotypes shown upon mutation of LSH or its homologues in *A. thaliana* and *S. cerevisiae* suggest that LSH is also involved in the DNA damage response. *DDM1*$^{-/-}$ *A. thaliana* have an increased sensitivity to ionising radiation and UV, which is independent of the reduced DNA methylation seen in these plants. These phenotypes indicate possible defects in the repair of DSBs and NER. A homolog of *Lsh*, *irc5* is also found in *S. cerevisiae*. Since *S. cerevisiae* lack DNA methylation, this suggests an additional role for IRC5 in yeast, which may be conserved in mammalian LSH. Synthetic growth defects indicate that IRC5 interacts with other known DSB repair proteins. IRC5 mutant *S. cerevisiae* also have increased numbers of RAD52 foci,

which are markers of DSB repair by HR. This suggests that, in addition to the *A. thaliana* homolog of LSH, the *S. cerevisiae* homolog of LSH is also involved in the DNA damage response.

Lsh$^{-/-}$ mice, which survive, have an unexplained premature aging phenotype in addition to loss of DNA methylation. This is caused by an increase in the number of senescent cells, often caused by DNA repair defects leading to a more rapid accumulation of DNA damage. Interestingly LSH has also been observed accumulating on meiotic chromosomes during the pachytene stage, prior to synapse formation. This observation is coupled with the occurrence of recombination defects in *Lsh*$^{-/-}$ oocytes, which suggests a role for LSH in homologous recombination between chromosomes during meiosis.

7.1 LSH is required for efficient DSB repair

Initially, viability screening was performed using a range of different DNA damaging agents to compare the DNA damage response of LSH deficient and WT cells to a variety of different DNA lesions. Viability screening indicates the sensitivity of a population of cells to DNA damage by identifying the proportion of cells still viable following treatment with a DNA damaging agent. The results showed that mammalian cells depleted of LSH are sensitive to DSB inducing agents but not other forms of DNA damage. Survival studies were also performed on both shLSH MRC5^{hT} and *Lsh*$^{-/-}$ MEFs compared to WT controls, using ionising radiation treatment to induce DSBs. These showed reduced survival in LSH deficient cells compared to WT controls, which is consistent with the reduced viability of LSH deficient cells following treatment with DSB inducing agents. These results are consistent with observations in *DDM1*$^{-/-}$ *A. thaliana*, which also have an increased sensitivity to ionising radiation treatment. However, *DDM1*$^{-/-}$ *A. thaliana* are also more sensitive to UV, which according to the viability screening data, does not appear to be a conserved function of LSH in mammalian species.

From the viability and survival data it was unclear whether the increased sensitivity of LSH deficient cells to ionising radiation was a result of a failure to repair DSBs or an increase in the number of DSBs induced. Neutral comet assays were preformed, immediately following ionising radiation treatment and after an 8 h recovery period, to examine the levels of DNA fragmentation. These showed that ionising radiation treatment induces a similar number of DSBs in both the *Lsh*$^{-/-}$ and WT MEFs, suggesting LSH does not play a role in protecting DNA from the formation of DSBs. After an 8 h recovery period 60% of the DSBs were repaired in the WT MEFs, however only half the amount were repaired in the *Lsh*$^{-/-}$ MEFs, which suggests that LSH aids repair of DSBs.

LSH has previously been reported to be an HDAC dependent transcriptional repressor and to aid in correct DNA methylation establishment and maintenance. Both of these functions could lead to changes in gene expression of previously identified DNA repair proteins, which could cause the inefficient DSB repair seen in LSH deficient cells. However, previous work carried out in the lab used expression arrays to compare the *Lsh*$^{-/-}$ MEFs with WT MEFs from matched littermates (Myant *et al* 2011). This data revealed no significant changes in the expression of known DSB repair proteins in the *Lsh*$^{-/-}$ MEFs, which suggested that LSH is involved in the DSB break response.

7.2 LSH deficient cells correctly recognise DSBs

When LSH is depleted DSBs repair less efficiently, which sensitises LSH deficient cells to DSB inducing agents. However it was unclear how the DSB response was affected or how LSH was involved. It was possible that LSH is involved in DSB detection and that DSBs are not recognised in LSH deficient cells. The MRN complex, comprised of MRE11, RAD50 and NBS1, binds broken DNA ends. Attempts to examine recognition of the broken DNA end were hampered by limitations of the available antibodies against the components of the MRN complex. However, we showed that MRE11 has an increased affinity for chromatin following ionising radiation treatment, which is similar in both the *Lsh*$^{-/-}$ and WT MEFs. We also investigated activation and localisation of ATM kinase, which is recruited to the broken DNA end by the MRN complex and is

required for cell cycle checkpoint signalling and establishing mediator complex assemble. Western blot analysis showed similar phosphorylation of ATM at serine residue 1981 in the *Lsh*$^{-/-}$ and WT MEFs in response to the induction of DSBs and immunofluorescence showed similar localisation of phosphorylated ATM to broken DNA ends immediately after DSB induction. This not only showed that ATM responds correctly to the induction of DSBs, but also suggests that the MRN complex correctly binds broken DNA ends, as MRN is responsible for initial recruitment of phosphorylated ATM. Further downstream in the DSB response phosphorylated ATM is recruited to DNA breaks by components of the DSB mediator complex such as MDC1. This is interesting as immunofluorescence also showed a reduction in phosphorylated ATM recruitment to broken DNA ends in the *Lsh*$^{-/-}$ MEFs 4h after induction of DSBs. This suggested that the *Lsh*$^{-/-}$ MEFs had defects in mediator complex assembly.

7.3 H2AX phosphorylation is reduced in LSH deficient cells

H2AX phosphorylation by ATM is a vital step in the establishment of the mediator complex at the broken DNA end, which reinforces DSB recognition and recruits proteins required for cell cycle checkpoint signalling and repair by homologous recombination. Since H2AX phosphorylation is the initial step in the formation of the mediator complex at broken DNA ends, we examined γH2AX by immunofluorescence. We showed that the amount of H2AX phosphorylation in the *Lsh*$^{-/-}$ MEFs was reduced compared to the WT MEFs following ionising radiation treatment. Upon counting the γH2AX IRIF we could see fewer foci in the *Lsh*$^{-/-}$ MEFs. Unfortunately we could not examine co-localisation of ATM and γH2AX as both were detected using monoclonal antibodies and we could not find polyclonal antibodies suitable for examining phosphorylated ATM or γH2AX IRIF in our hands. However, comet assays and ATM immunofluorescence suggested that in the *Lsh*$^{-/-}$ and WT MEFs the same number of DSBs were being induced and correctly recognised by binding of phosphorylated ATM. Therefore the reduced number of γH2AX IRIF in the *Lsh*$^{-/-}$ MEFs suggested that only a proportion of broken DNA ends required LSH for correctly phosphorylation of H2AX.

Expression arrays had revealed that a 70% reduction in DNA methylation and loss of LSH mediated HDAC dependent transcriptional silencing in the *Lsh*$^{-/-}$ MEFs causes no significant changes in the expression of known DSB repair proteins. However it was possible that reduced DNA methylation in the *Lsh*$^{-/-}$ MEFs was having an unknown affecting on DNA repair, which causes reduced H2AX phosphorylation at a proportion of broken DNA ends. However, Western blot analysis of H2AX phosphorylation following ionising radiation treatment showed no difference between the WT or *p53*$^{-/-}$ MEFs when compared to the *Dnmt1*$^{-/-}$, *p53*$^{-/-}$ MEFs, which have a 90% reduction in DNA methylation. The *Lsh*$^{-/-}$ MEFs have reduced levels of γH2AX compared to the WT MEFs, consistent with the reduced number of γH2AX observed by immunofluorescence. This indicated that the loss of DNA methylation in *Lsh*$^{-/-}$ MEFs is not causing a reduction in H2AX phosphorylation in response to the induction of DSBs.

We also performed Western blot analysis of H2AX phosphorylation following ionising radiation treatment in human MRC5^{hT} cells, in which LSH was depleted by shRNA knockdown and compared this non-silencing control cells. A similar reduction in the amount of γH2AX was observed in the MRC5^{hT} cells as was seen in the *Lsh*$^{-/-}$ MEFs, which demonstrates that the phenomenon is not an artefact of *Lsh*$^{-/-}$ MEFs. We also considered the possibility that LSH is involved in distributing H2AX throughout the chromatin and that the reduced H2AX phosphorylation in LSH deficient cells is due to a lack of H2AX on chromatin. However chromatin retention assays showed no difference in the amount of H2AX associated with the chromatin in the *Lsh*$^{-/-}$ and WT MEFs.

7.4 LSH deficient cells have impaired cell cycle checkpoint signalling

To determine how reduced H2AX phosphorylation leads to LSH deficient cells becoming sensitised to DSB inducing agents we examined mediator complex assembly and cell cycle checkpoint signalling. Immunofluorescence imaging of mediator complex proteins MDC1 and 53BP1 showed that the formation of IRIF is impaired in the *Lsh*$^{-/-}$ MEFs. This suggested that mediator complex formation at broken DNA ends is less robust in *Lsh*$^{-/-}$ MEFs. Less robust mediator complex formation can result in less efficient repair by homologous recombination as

failure to bind 53BP1 will reduced the amount of BRCA1 recruited to the broken DNA end, which will impair nucleoprotein filament formation and strand invasion of the homologous repair template. This hypothesis is supported by the comet assay data, which showed reduced DSB repair efficiency in *Lsh*$^{-/-}$ MEFs.

Recruitment of checkpoint proteins to broken DNA ends by components of the mediator complex is essential for activation of checkpoint proteins by ATM / ATR kinases and cell cycle arrest. LSH deficient cells have impaired assembly of mediator complex at broken DNA ends. These may recruit checkpoint proteins less efficient and fail to activate cell cycle arrest, which could result in LSH depleted cells continuing through mitosis with unrepaired DSBs. We wished to test this hypothesis in *Lsh*$^{-/-}$ MEFs, however the *Lsh*$^{-/-}$ and WT MEFs had been maintained in culture through spontaneous immortalisation, which often results in defects in p53 and apoptotic signalling. Unfortunately the MEFs obtained from the WT littermates of the *Lsh*$^{-/-}$ mice did not express p53, which made them unsuitable for examining checkpoint signalling. We therefore examined CHK2 and p53 phosphorylation in response to DSB induction using the MRC5^{hT} cells, which also displayed reduced H2AX phosphorylation when LSH is depleted by shRNA knockdown.

Western blot analysis showed that CHK2 is phosphorylated less efficiently in the shLSH MRC5^{hT} cells compared to the non-silencing controls following ionising radiation treatment. This is consistent with CHK2 activation being dependent on binding to MDC1 at broken DNA ends and the impaired mediator complex assembly observed in LSH deficient cells. Western blots also showed that p53 can be phosphorylated at the serine 15 residue equally well in both the shLSH and non-silencing MRC5^{hT} cells. This is interesting as 53BP1, which recruits p53 to broken DNA ends, is reduced in LSH deficient cells and suggested that activation of p53 by ATM does not require 53BP1 dependent localisation of p53 to broken DNA ends. However the total levels of p53 are reduced shLSH MRC5^{hT} cells, which showed that stabilisation of p53 in response to ionising radiation is decreased when mediator complex assembly is impaired. This could be due to a decrease in p53 phosphorylation at other sites that block MDM2 mediated nuclear export of p53 and subsequent degradation by the proteasome. This is consistent with reduced phosphorylation of CHK2 kinase in

response to DSBs in shLSH MRC5^{hT} cells, as phosphorylation of p53 at serine residue 20 by CHK2 blocks interactions with MDM2. The data suggested that despite reduced CHK2 phosphorylation and stabilisation of p53 in shLSH MRC5^{hT} cells, there is sufficient nuclear p53 for phosphorylation by ATM.

The comet assay data showed that LSH deficient cells repair DSBs less efficiently and have more unrepaired DSBs 8h after ionising radiation treatment. We would therefore expect cell cycle checkpoint signalling to be extended in LSH deficient cells to produce a longer arrest period for damage to be repaired. However, p53 serine 15 phosphorylation is not elevated above WT levels in LSH deficient cells 8 h after ionising radiation treatment and phosphorylation of CHK2 is less efficient. This suggested that a proportion of breaks do not correctly activate cell cycle checkpoints when LSH is depleted. This could result in cells undergoing mitosis with unrepaired DSB still present, which can be lethal to the cells and would explain the increased cell death 96 h after treatment of shLSH MRC5^{hT} cells with DSB inducing agents.

7.5 LSH ATPase activity is necessary for its function in DSB repair

To determine whether the DSB repair defects of Lsh deficient cells could be reversed, we examined the repair of DSBs in *Lsh*$^{-/-}$ MEFs that had been infected with lentiviruses expressing WT LSH. We also examined *Lsh*$^{-/-}$ MEFs expressing a catalytically inactive LSH to determine whether the ATPase activity of LSH is required for its function in DSB repair, which could suggest chromatin remodelling by LSH. Survival studies demonstrated that the efficient repair of DSB can be restored in the *Lsh*$^{-/-}$ MEFs by the reintroduction of LSH into these cells. We also showed that H2AX phosphorylation and efficient mediator complex assembly at broken DNA ends is restored in the *Lsh*$^{-/-}$ MEFs by the reintroduction of LSH. However catalytically inactive LSH could not improve the DSB response defects of the *Lsh*$^{-/-}$ MEFs. Although this does not demonstrate chromatin remodelling by LSH at sites of DNA damage, it showed that the ATPase activity of LSH is important for its function in DSB repair and adds credibility to the hypothesis that LSH is required for efficient DSB repair and suggests its function is connected to chromatin remodelling.

7.6 DSB repair doesn't involve recruitment of LSH to broken DNA ends

Although we have been able to demonstrate that LSH ATPase activity is required for H2AX phosphorylation at a proportion of broken DNA ends and efficient repair of DSBs, we have been unable to demonstrate a direct interaction between LSH and broken DNA ends during repair. The majority of DSB repair proteins accumulate at broken DNA ends following DSB induction and can be observed forming foci by immunofluorescence. However, anti-FLAG immunofluorescence imaging of WT rescue LSH in *Lsh*$^{-/-}$ MEFs after ionising radiation treatment showed that LSH does not form IRIF, which indicates that LSH is not recruited to broken DNA ends. Likewise, live cell imaging of LSH-GFP in VA13 cells in which DSBs were induced at a high frequency at defined nuclear locations by Laser micro irradiation also showed that LSH does not localise to site of DNA damage.

Interestingly, when we examined the general association between the LSH and chromatin we saw that the majority of LSH is chromatin bound, prior to ionising radiation treatment and that this doesn't alter after the induction of DSBs. This indicated that LSH might not have a high degree of mobility within the nucleus, which explains why LSH is not recruited to IRIF. The observation that LSH is chromatin bound prior to the induction of DSBs also suggested possible roles for LSH in DSB repair. One possibility is that LSH could be bound to the chromatin to evenly distribute variant histone H2AX throughout the chromatin via ATP dependent chromatin remodelling. Although we see no difference in the amount of H2AX bound to the DNA in LSH deficient cells, it could be unevenly distributed leaving H2AX low-density regions where there is insufficient H2AX for its phosphorylation to stimulate mediator complex assembly. This is one possible explanation for a lack of γH2AX at some DSBs. Alternatively LSH could be bound to the chromatin at specific DNA elements, such as repetitive elements at which LSH is known to be required for heterochromatin formation and silencing. LSH may only aid in the repair of DSBs that occur close to these regions by relaxing the heterochromatin through ATP dependent chromatin remodelling activity, allowing the DSB repair machinery access to the broken DNA end.

7.7 Concluding remarks

We have shown that LSH deficient cells have an increased sensitivity to DSB inducing agents and that LSH is required for efficient repair of a proportion of DSBs. This is consistent with observations that suggest LSH homologs in plants and yeast also have a role in the DNA damage response. We can therefore conclude that LSH has a role in the DNA damage response that is conserved in mammals.

We have further clarified the role of LSH in mammalian DSB repair by demonstrating that mediator complex assembly and cell cycle checkpoint signalling are impaired in the absence of LSH. Although microarray data did not reveal any obvious expression changes that could be responsible for this phenotype, we could not see an accumulation of LSH at broken DNA ends. Instead we showed that the majority of LSH is associated with the chromatin and suggest several possible mechanisms that could explain the requirement of LSH for DSB repair that does not involve LSH accumulating at broken DNA ends. We have created a model system for comparing DSB repair at many defined genomic location in WT and LSH deficient cells and suggest future experiments, which may reveal the mechanism behind the role of LSH in mammalian DSB repair.

References

Alarcon-Vargas D, Ronai Z. (2002). p53-Mdm2--the affair that never ends. Carcinogenesis. *23* 541-547.

Allard S, Masson JY, Cote J. (2004) Chromatin remodelling and the maintenance of genome integrity. Biochimica et biophysica acta. *1677* 158–164.

Alvaro D, Lisby M, Rothstein R. (2007). Genome-wide analysis of Rad52 foci reveals diverse mechanisms impacting recombination. PLoS Genet. *3* e228.

Bakkenist CJ, Kastan MB (2003). DNA damage activates ATM through intermolecular autophosphorylation and dimer dissociation. *421* 499–506.

Bannister AJ, Zegerman P, Partridge JF, Miska EA, Thomas JO, Allshire RC, Kouzarides T. (2001). Selective recognition of methylated lysine 9 on histone H3 by the HP1 chromo domain. Nature. *410* 120-124.

Bartek J, Shiloh Y. (2006). Chromatin relaxation in response to DNA double-strand breaks is modulated by a novel ATM- and KAP-1 dependent pathway. Nature Cell Biology. *8* 870-876.

Bartek J, Lukas J. (2001). Mammalian G1- and S-phase checkpoints in response to DNA damage. Curr Opin Cell Biol. *13* 738-747.

Batty DP, Wood RD. (2000). Damage recognition in nucleotide excision repair of DNA. Gene. *241* 193-204.

Bekker-Jensen S, Mailand N. (2010). Assembly and function of DNA double-strand break repair foci in mammalian cells. DNA Repair. *9* 1219-1228.

Blackwell LJ, Martik D, Bjornson KP, Bjornson ES, Modrich P. (1998). Nucleotide-promoted release of hMutS alpha from heteroduplex DNA is consistent with an ATP-dependent translocation mechanism. J Biol Chem. *273* 55-62.

Brzeski J, Jerzmanowski A. (2003). Deficient in DNA methylation 1 (DDM1) defines a novel family of chromatin-remodelling factors. The Journal of biological chemistry. *278* 823-828.

Buermeyer AB, Deschênes SM, Baker SM, Liskay RM. (1999). Mammalian DNA mismatch repair. Annu Rev Genet. *33* 533-564.

Bultman S, Gebuhr T, Yee D, La Mantia C, Nicholson J, Gilliam A, Randazzo F, Metzger D, Chambon P, Crabtree G. (2000). A Brg1 null mutation in the mouse reveals functional differences among mammalian SWI/SNF complexes. Molecular cell. *6* 1287-1295.

Burrage J, Termanis A, Geissner A, Myant K, Gordon K, Stancheva I. (2012). The SNF2 family ATPase LSH promotes phosphorylation of H2AX and efficient repair of DNA double-strand breaks in mammalian cells. J Cell Sci. *125* 5524-34.

Cairns BR. (2007). Chromatin remodeling: insights and intrigue from single-molecule studies. Nat Struct Mol Biol. *14* 989-96.

Chai B, Huang J, Cairns BR, Laurent BC. (2005). Distinct roles for the RSC and Swi/Snf ATP-dependent chromatin remodelers in DNA double-strand break repair. Genes & Development. *19* 1656–1661.

Chen J, Ghorai MK, Kenney G, Stubbe J. (2008). Mechanistic studies on bleomycin-mediated DNA damage: multiple binding modes can result in double-stranded DNA cleavage. Nucleic Acids Res. *36* 3781-3790.

Cheng Q, Cross B, Li B, Chen L, Li Z, Chen J. (2011). Regulation of MDM2 E3 ligase activity by phosphorylation after DNA damage. Mol Cell Biol. *31* 4951-4963.

Collins SR, Miller KM, Maas NL, Roguev A, Fillingham J, Chu CS, Schuldiner M, Gebbia M, Recht J, Shales M, Ding H, Xu H, Han J, Ingvarsdottir K, Cheng B, Andrews B, Boone C, Berger SL, Hieter P, Zhang Z, Brown GW, Ingles CJ, Emili A, Allis CD, Toczyski DP, Weissman JS, Greenblatt JF, Krogan NJ. (2007). Functional dissection of protein complexes involved in yeast chromosome biology using a genetic interaction map. Nature. *446*, 806-10.

Davey CA, Sargent DF, Luger K, Maeder AW, Richmond TJ. (2002). Solvent mediated interactions in the structure of the nucleosome core particle at 1.9 a resolution. J Mol Biol. *319* 1097-113.

De Boer J, Andressoo JO, de Wit J, Huijmans J, Beems RB, van Steeg H, Weeda G, van der Horst GT, van Leeuwen W, Themmen AP, Meradji M, Hoeijmakers JH. (2002). Premature aging in mice deficient in DNA repair and transcription. Science. *296* 1276-1279.

De La Fuente R, Baumann C, Fan T, Schmidtmann A, Dobrinski I, Muegge K. (2006). Lsh is required for meiotic chromosome synapsis and retrotransposon silencing in female germ cells. Nature Cell Biology. *8* 1448-1454.

Dechassa ML, Sabri A, Pondugula S, Kassabov SR, Chatterjee N, Kladde MP, Bartholomew B. (2010). SWI/SNF has intrinsic nucleosome disassembly activity that is dependent on adjacent nucleosomes. Molecular Cell. *38* 590–602.

Dennis K, Fan T, Geiman T, Yan Q, Muegge K. (2001). Lsh, a member of the SNF2 family, is required for genome-wide methylation. Genes & development. *15* 2940-2944.

Deuring R, Fanti L, Armstrong JA, Sarte M, Papoulas O, Prestel M, Daubresse G, Verardo M, Moseley SL, Berloco M. (2000). The ISWI chromatin-remodelling protein is required for gene expression and the maintenance of higher order chromatin structure in vivo. Molecular cell. *5* 355-365.

Di Tommaso P, Moretti S, Xenarios I, Orobitg M, Montanyola A, Chang JM, Taly JF, Notredame C. (2011).T-Coffee: a web server for the multiple sequence alignment of protein and RNA sequences using structural information and homology extension. Nucleic Acids Res. *39*

Dillon N. (2004). Heterochromatin structure and function. Biol Cell. *96* 631-7.

Dorigo B, Schalch T, Kulangara A, Duda S, Schroeder RR, Richmond TJ. (2004). Nucleosome arrays reveal the two-start organization of the chromatin fibre. Science New York, NY. *306* 1571-1573.

Durocher D, Jackson SP. (2001). DNA-PK, ATM and ATR as sensors of DNA damage: variations on a theme? Curr Opin Cell Biol. *13* 225-231.

Eisen JA, Sweder KS, Hanawalt PC (1995). Evolution of the SNF2 family of proteins: subfamilies with distinct sequences and functions. Nucleic acids research. *23* 2715-2723.

Eliezer Y, Argaman L, Rhie A, Doherty AJ, Goldberg M. (2009). The Direct Interaction between 53BP1 and MDC1 Is Required for the Recruitment of 53BP1 to Sites of Damage. J Biol Chem. *284* 426-35.

Featherstone C, Jackson SP. (1999). DNA double-strand break repair. Curr Biol. *9* 759-761.

Featherstone C, Jackson SP. (1999) Ku, a DNA repair protein with multiple cellular functions. Mut. Res. DNA Repair. *434* 3-15.

Fernandez-Capetillo O, Lee A, Nussenzweig M, Nussenzweig A. (2004). H2AX: the histone guardian of the genome. DNA Repair. *3* 959-967.

Flaus A, Martin DM, Barton GJ, Owen-Hughes T. (2006). Identification of multiple distinct Snf2 subfamilies with conserved structural motifs. Nucleic acids research. *34* 2887-2905.

Flaus A, Owen-Hughes T. (2004). Mechanisms for ATP-dependent chromatin remodelling: farewell to the tuna-can octamer? Current opinion in genetics & development. *14* 165-173.

Fuks F, Burgers WA, Godin N, Kasai M, Kouzarides T. (2001). Dnmt3a binds deacetylases and is recruited by a sequence-specific repressor to silence transcription. The EMBO journal. *20* 2536-2544.

Geiman TM, Tessarollo L, Anver MR, Kopp JB, Ward JM, Muegge K. (2001). Lsh, a SNF2 family member, is required for normal murine development. Biochimica et biophysica acta. *1526* 211-220.

Geiman TM, Muegge K. (2000). Lsh, an SNF2/helicase family member, is required for proliferation of mature T lymphocytes. Proc Natl Acad Sci USA. *97* 4772-4777.

Geiman TM, Durum SK, Muegge K. (1998). Characterization of gene expression, genomic structure, and chromosomal localization of Hells (Lsh). Genomics. *54* 477-483.

Gelato KA, Fischle W. (2008). Role of histone modifications in defining chromatin structure and function. Biol Chem. *389* 353-63.

Genschel J, Littman SJ, Drummond JT, Modrich P. (1998). Isolation of MutS beta from human cells and comparison of the mismatch repair specificities of MutS beta and MutS alpha. J Biol Chem. *273* 895-901.

Goodarzi AA, Kurka T, Jeggo PA. (2011). KAP-1 phosphorylation regulates CHD3 nucleosome remodelling during the DNA double-strand break response. Nat Struct Mol Biol. *18* 831-839.

Goodarzi AA, Noon AT, Deckbar D, Ziv Y, Shiloh Y, Löbrich M, Jeggo PA. (2008). ATM signalling facilitates repair of DNA double-strand breaks associated with heterochromatin. Mol Cell. *31* 167-177.

Gong F, Kwon Y, Smerdon MJ. (2005). Nucleotide excision repair in chromatin and the right of entry. DNA Repair. *4* 884-896.

Gradia S, Subramanian D, Wilson T, Acharya S, Makhov A, Griffith J, Fishel R. (1999). hMSH2-hMSH6 forms a hydrolysis-independent sliding clamp on mismatched DNA. Mol Cell. *3* 255-61.

Hark AT, Schoenherr CJ, Katz DJ, Ingram RS, Levorse JM, Tilghman SM. (2000). CTCF mediates methylation-sensitive enhancer-blocking activity at the H19/Igf2 locus. Nature. *405* 486-489.

Hassold, T, Hunt P. (2001). To err (meiotically) is human: The genesis of human aneuploidy. Nature Rev. Genet. *2* 280-291.

Havas, K., Flaus, A., Phelan, M., Kingston, R., Wade, P.A., Lilley, D.M., and Owen-Hughes, T. (2000). Generation of superhelical torsion by ATP-dependent chromatin remodelling activities. Cell. *103* 1133-1142.

Hess MT, Schwitter U, Petretta M, Giese B, Naegeli H. (1997). Bipartite substrate discrimination by human nucleotide excision repair. Proc Natl Acad Sci USA. *94* 6664-6669.

Hoeijmakers JHJ. (2001). review article Genome maintenance mechanisms for preventing cancer. Nature. *411* 366-374

Hogan C, Varga-Weisz P. (2007). The regulation of ATP-dependent nucleosome remodelling factors. Mutat Res. *618* 41-51.

Jackson SP. (2002). Sensing and repairing DNA double-strand breaks. Carcinogenesis. *23* 687-696.

Jackson SP, Bartek J. (2009). The DNA-damage response in human biology and disease. Nature. *461* 1071–1078.

Jackson-Grusby L, Beard C, Possemato R, Tudor M, Fambrough D, Csankovszki G, Dausman J, Lee P, Wilson C, Lander E, Jaenisch R. (2009). Loss of genomic methylation causes p53 dependent apoptosis and epigenetic deregulation. Nature Genetics. *27* 31-9.

Jeddeloh JA, Stokes TL, Richards EJ. (1999). Maintenance of genomic methylation requires a SWI2/SNF2-like protein. Nature genetics. *22* 94-97.

Kakutani T. (1997). Genetic characterization of late-flowering traits induced by DNA hypomethylation mutation in Arabidopsis thaliana. Plant J. *12* 1447-1451.

Kakutani T, Jeddeloh JA, Richards EJ. (1995). Characterization of an Arabidopsis thaliana DNA hypomethylation mutant. Nucleic acids research. *23* 130-137.

Khanna KK, Tibbetts RS. (2006). DNA Damage Response. eLS.

Kaidi A, Weinert BT, Choudhary C, Jackson SP. (2010). Human SIRT6 promotes DNA end resection through CtIP deacetylation. Science. *329* 1348-1353.

Kent NA, Chambers AL, Downs JA. (2007). Dual chromatin remodelling roles for RSC during DNA double strand break induction and repair at the yeast MAT locus. J Biol Chem. *282* 27693-701.

Kinner A, Wu W, Staudt C, Iliakis G. (2008) Gamma-H2AX in recognition and signalling of DNA double-strand breaks in the context of chromatin. Nucleic Acids Res. *36* 5678-5694.

Klimasauskas S., Kumar S., Roberts R.J., and Cheng X. (1994). HhaI methyltransferase flips its target base out of the DNA helix. Cell. *76* 357-369.

Kobayashi J, Iwabuchi K, Miyagawa K, Sonoda E, Suzuki K, Takata M, Tauchi H. (2008). Current topics in DNA double-strand break repair. J Radiation Research. *49* 93-103.

Kouzarides T. (2007). Chromatin Modifications and Their Function. Cell. *128* 693-705.

Kruhlak MJ, Celeste A, Dellaire G, Fernandez-Capetillo O, Muller WG, McNally JG, Bazett-Jones DP, Nussenzweig A. (2006). Changes in chromatin structure and mobility in living cells at sites of DNA double-strand breaks. J Cell Biol. *172* 823-834.

Kuzminov A, (2001). Single-strand interruptions in replicating chromosomes cause double-strand breaks. Proc Natl Acad Sci USA, *98* 8241–8246

Lacovoni JS, Caron P, Lassadi I, Nicolas E, Massip L, Trouche D, Legube G. (2010) High-resolution profiling of γH2AX around DNA double strand breaks in the mammalian genome. The EMBO journal, *29* 1446-1457.

Langst G, Becker PB. (2001). Nucleosome mobilization and positioning by ISWI-containing chromatin-remodelling factors. Journal of cell science, *114* 2561-2568.

Langst G, Bonte EJ, Corona DF, Becker PB. (1999). Nucleosome movement by CHRAC and ISWI without disruption or trans-displacement of the histone octamer. Cell. *97* 843-852.

Lans H, Marteijn JA, Vermeulen W. (2012). ATP-dependent chromatin remodelling in the DNA-damage response. Epigenetics Chromatin. 5-4.

Le Guezennec X, Vermeulen M, Brinkman AB, Hoeijmakers WA, Cohen A, Lasonder E, Stunnenberg, HG. (2006). MBD2/NuRD and MBD3/NuRD, two distinct complexes with different biochemical and functional properties. Molecular and cellular biology. *26* 843-851.

Lee HS, Park JH, Kim SJ, Kwon SJ, Kwon J. (2010). A cooperative activation loop among SWI/SNF, gamma-H2AX and H3 acetylation for DNA double-strand break repair. EMBO J. *29* 1434-1445.

Lieber MR. (2010). The mechanism of double-strand DNA break repair by the non-homologous DNA end-joining pathway. Annu Rev Biochem. *79* 181-211.

Liu Y, Masson JY, Shah R, O'Regan P, West SC. (2004). RAD51C is required for Holliday junction processing in mammalian cells. Science. *303* 243-246.

Lodish H, Berk A, Matsudaira P, Kaiser CA, Krieger M, Scott MP, Zipursky SL, Darnell J. (2004). Molecular Biology of the Cell, p963. WH Freeman: New York, NY. 5th ed.

Lou Z, Minter-Dykhouse K, Wu X, Chen J. (2003). MDC1 is coupled to activated CHK2 in mammalian DNA damage response pathways. Nature. *421* 957-961.

Mahadevaiah SK, Turner JM, Baudat F, Rogakou EP, de Boer P, Blanco-Rodríguez J, Jasin M, Keeney S, Bonner WM, Burgoyne PS. (2001). Recombinational DNA double-strand breaks in mice precede synapsis. Nature Genet. *27* 271–276.

Marti TM, Kunz C, Fleck O. (2002). DNA mismatch repair and mutation avoidance pathways. J Cell Physiol. *191* 28-41.

Martin A, Scharff MD. (2002). AID and mismatch repair in antibody diversification. Nature Reviews Immunology. *2* 605-614.

Matsumoto Y, Kim K. (1995). Excision of deoxyribose phosphate residues by DNA polymerase beta during DNA repair. Science. *269* 699-702.

Matsumoto Y, Kim K, Bogenhagen DF. (1994). Proliferating cell nuclear antigen-dependent abasic site repair in Xenopus laevis oocytes: an alternative pathway of base excision DNA repair. Mol Cell Biol. *14* 6187-6197.

Matsuoka S, Rotman G, Ogawa A, Shiloh Y, Tamai K, Elledge SJ. (2000). Ataxia telangiectasia-mutated phosphorylates Chk2 in vivo and in vitro. Proc Natl Acad Sci USA. *97* 10389-10394.

Memisoglu A, Samson L. (2000). Base excision repair in yeast and mammals. Mutation Res. *451* 39-51.

Mizuguchi G, Shen X, Landry J, Wu WH, Sen S, Wu C. (2004). ATP- driven exchange of histone H2AZ variant catalyzed by SWR1 chromatin remodelling complex. Science. *303* 343-348.

Moshous D, Callebaut I, de Chasseval R, Corneo B, Cavazzana-Calvo M, Le Deist F, Tezcan I, Sanal O, Bertrand Y, Philippe N, Fischer A, de Villartay JP. (2001). Artemis, a novel DNA double-strand break repair/V(D)J recombination protein, is mutated in human severe combined immune deficiency. Cell. *105* 177-86.

Muegge K. (2005). Lsh, a guardian of heterochromatin at repeat elements. Biochem. Cell Biology. *83* 548–554.

Myant K, Stancheva I, (2008). LSH cooperates with DNA methyltransferases to repress transcription. Mol Cell Biol. *28* 215-26.

Myant K, Termanis A, Sundaram AY, Boe T, Li C, Merusi C, Burrage J, de Las Heras JI, Stancheva I. (2011). LSH and G9a/GLP complex are required for developmentally programmed DNA methylation. Genome Res. *21* 83-94.

Nakayama J, Rice JC, Strahl BD, Allis CD, Grewal SIS. (2001). Role of Histone H3 Lysine 9 Methylation in Epigenetic Control of Heterochromatin Assembly. Science. *292* 110-113

Narlikar GJ, Fan HY, Kingston RE. (2002). Cooperation between complexes that regulate chromatin structure and transcription. Cell. *108* 475-487.

Ng HH, Johnson CA, Laherty CD, Turner BM, Eisenman RN, Bird A. (1998). Transcriptional repression by the methyl-CpG-binding protein MeCP2 involves a histone deacetylase complex. Nature. *393* 386-389.

Osley MA, Tsukuda T, Nickoloff JA. (2007). ATP-dependent chromatin remodelling factors and DNA damage repair. Mutation Research. *618* 65-80.

Park JH, Park EJ, Lee HS, Kim SJ, Hur SK, Imbalzano AN, Kwon J. (2006). Mammalian SWI/SNF complexes facilitate DNA double-strand break repair by promoting gamma-H2AX induction. EMBO Journal. *25* 3986-3997.

Pei H, Zhang L, Luo K, Qin Y, Chesi M, Fei F, Bergsagel PL, Wang L, You Z, Lou Z. (2011). MMSET regulates histone H4K20 methylation and 53BP1 accumulation at DNA damage sites. Nature. *470* 124-128.

Peltomäki P. (2001). DNA mismatch repair and cancer. Mutat Res. *488* 77-85.

Peng CY, Graves PR, Thoma RS, Wu Z, Shaw AS, Piwnica-Worms H. (1997). Mitotic and G2 checkpoint control: regulation of 14-3-3 protein binding by phosphorylation of Cdc25C on serine-216. Science. *277* 1501-1505.

Petrini JH. (2000). The Mre11 complex and ATM: collaborating to navigate S phase. Curr Opin Cell Biol.*12* 293-296.

Poot RA, Dellaire G, Hulsmann BB, Grimaldi MA, Corona DF, Becker PB, Bickmore WA, Varga-Weisz PD. (2000). HuCHRAC, a human ISWI chromatin-remodelling complex contains hACF1 and two novel histone-fold proteins. The EMBO journal. *19* 3377-3387.

R & D Systems. (2011). MiniReview DNA Damage Response. http://www.rndsystems.com/MiniReview_MR03_DNADamageResponse.aspx.

Reik W, Dean W, Walter J. (2001). Epigenetic reprogramming in mammalian development. Science. *293* 1089–1093.

Reisman DN, Sciarrotta J, Wang W, Funkhouser WK, Weissman BE. (2003). Loss of BRG1/BRM in human lung cancer cell lines and primary lung cancers: correlation with poor prognosis. Cancer research. *63* 560-566.

Riches LC, Lynch AM, Gooderham NJ. (2008). Early events in the mammalian response to DNA double-strand breaks. Mutagenesis. *23* 331-339.

Rogakou EP, Boon C, Redon C, Bonner WM. (1999). Megabase chromatin domains involved in DNA double-strand breaks in vivo. J Cell Biol. *146* 905-916.

San Filippo J, Sung P, Klein H. (2008). Mechanism of eukaryotic homologous recombination. Annu Rev Biochem. *77* 229-257.

Santoro R, Li J, Grummt I, (2002). The nucleolar remodelling complex NoRC mediates heterochromatin formation and silencing of ribosomal gene transcription. Nature Genetics. *32* 393 – 396.

Savic V, Yin B, Maas NL, Bredemeyer AL, Carpenter AC, Helmink BA, Yang-Iott KS, Sleckman BP, Bassing CH. (2009). Formation of dynamic gamma-H2AX domains along broken DNA strands is distinctly regulated by ATM and MDC1 and dependent upon H2AX densities in chromatin. Molecular Cell. *34* 298-310.

Schärer OD, Jiricny J. (2001). Recent progress in the biology, chemistry and structural biology of DNA glycosylases. Bioessays. *23* 270-81.

Selzer RR, Nyaga S, Tuo J, May A, Muftuoglu M, Christiansen M, Citterio E, Brosh RM Jr, Bohr VA. (2002). Differential requirement for the ATPase domain of the Cockayne syndrome group B gene in the processing of UV-induced DNA damage and 8-oxoguanine lesions in human cells. Nucleic Acids Research. *30* 782–793.

Shaked H, Avivi-Ragolsky N, Levy AA. (2006). Involvement of the Arabidopsis SWI2/SNF2 chromatin remodelling gene family in DNA damage response and recombination. Genetics. *173* 985-94.

Shogren-Knaak M, Ishii H, Sun JM, Pazin MJ, Davie JR, Peterson CL. (2006). Histone H4-K16 Acetylation Controls Chromatin Structure and Protein Interactions. Science. *311* 844-847.

Stopka T, Skoultchi AI. (2003). The ISWI ATPase Snf2h is required for early mouse development. Proceedings of the National Academy of Sciences of the United States of America. *100* 14097-14102.

Strohner R, Wachsmuth M, Dachauer K, Mazurkiewicz J, Hochstatter J, Rippe K, Langst G. (2005). A 'loop recapture' mechanism for ACF-dependent nucleosome remodelling. Nature structural & molecular biology. *12* 683-690.

Sun LQ, Lee DW, Zhang Q, Xiao W, Raabe EH, Meeker A, Miao D, Huso DL, Arceci RJ. (2004). Growth retardation and premature aging phenotypes in mice with disruption of the SNF2-like gene, PASG. Genes & development. *18* 1035-1046.

Suzuki T, Farrar JE, Yegnasubramanian S, Zahed M, Suzuki N, Arceci RJ. (2008). Stable knockdown of PASG enhances DNA demethylation but does not accelerate cellular senescence in TIG-7 human fibroblasts. Epigenetics. *3* 281-91.

Takata M, Sasaki MS, Sonoda E, Morrison C, Hashimoto M, Utsumi H, Yamaguchi-Iwai Y, Shinohara A, Takeda S. (1998). Homologous recombination and non-homologous end-joining pathways of DNA double-strand break repair have overlapping roles in the maintenance of chromosomal integrity in vertebrate cells. EMBO Journal. *17* 497-508.

Tong JK, Hassig CA, Schnitzler GR, Kingston RE, Schreiber SL. (1998). Chromatin deacetylation by an ATP-dependent nucleosome-remodelling complex. Nature. *395* 917-921.

Troelstra C, van Gool A. de Wit J, Vermeulen W, Bootsma D, Hoeijmakers JH. (1992). ERCC6, a member of a subfamily of putative helicases, is involved in Cockayne's syndrome and preferential repair of active genes. Cell. *71* 939-953.

Umar A, Buermeyer AB, Simon JA, Thomas DC, Clark AB, Liskay RM, Kunkel TA. (1996). Requirement for PCNA in DNA mismatch repair at a step preceding DNA resynthesis. Cell. *87* 65-73.

van Attikum H, Fritsch O, Hohn B, Gasser SM. (2004) Recruitment of the INO80 complex by H2A phosphorylation links ATP-dependent chromatin remodelling with DNA double-strand break repair. Cell. *119* 777–788

Vongs A, Kakutani T, Martienssen RA, Richards EJ. (1993). Arabidopsis thaliana DNA methylation mutants. Science. *260* 1926-1928.

Ward IM, Minn K, Jorda KG, Chen J. (2003). Accumulation of Checkpoint Protein 53BP1 at DNA Breaks Involves Its Binding to Phosphorylated Histone H2AX. J Biol Chem. *278* 19579-19582.

Weberpals JI, Clark-Knowles KV, Vanderhyden BC. (2008). Sporadic epithelial ovarian cancer: clinical relevance of BRCA1 inhibition in the DNA damage and repair pathway. J Clin Oncol. *26* 3259-3267.

Weirich-Schwaiger H, Weirich HG, Gruber B, Schweiger M, Hirsch-Kauffmann M. (1994). Correlation between senescence and DNA repair in cells from young and old individuals and in premature aging syndromes. Mutation Research. *316* 37-48.

Whitehouse I, Flaus A, Cairns BR, White MF, Workman JL, Owen-Hughes T. (1999). Nucleosome mobilization catalysed by the yeast SWI/SNF complex. Nature. *400* 784-787.

Wong AK, Shanahan F, Chen Y, Lian L, Ha P, Hendricks K, Ghaffari S, Iliev D, Penn B, Woodland AM. (2000). BRG1, a component of the SWI-SNF complex, is mutated in multiple human tumour cell lines. Cancer research. *60* 6171-6177.

Wu X, Wilson TE, Lieber MR. (1999). A role for FEN-1 in non-homologous DNA end joining: the order of strand annealing and nucleolytic processing events. Proc Natl Acad Sci USA. *96* 1303-1308.

Yang JG, Madrid TS, Sevastopoulos E, Narlikar GJ. (2006). The chromatin-remodelling enzyme ACF is an ATP-dependent DNA length sensor that regulates nucleosome spacing. Nature structural & molecular biology. *13* 1078-1083.

Yu S, Teng Y, Waters R, Reed SH. (2011). How chromatin is remodelled during DNA repair of UV-induced DNA damage in *Saccharomyces cerevisiae*. PLoS Genetics. 2011 e1002124.

Yu S, Owen-Hughes T, Friedberg EC, Waters R, Reed SH. (2004). The yeast Rad7/Rad16/Abf1 complex generates superhelical torsion in DNA that is required for nucleotide excision repair. DNA Repair. *3* 277–287.

Xiao Z, Chen Z, Gunasekera AH, Sowin TJ, Rosenberg SH, Fesik S, Zhang H. J Biol Chem. (2003). Chk1 mediates S and G2 arrests through Cdc25A degradation in response to DNA-damaging agents. *278* 1767-1773.

Zhang Y, LeRoy G, Seelig HP, Lane WS, Reinberg D. (1998). The dermatomyositis-specific autoantigen Mi2 is a component of a complex containing histone deacetylase and nucleosome remodelling activities. Cell. *95* 279-289.

Zhu H, Geiman TM, Xi S, Jiang Q, Schmidtmann A, Chen T, Li E, Muegge K. (2006). Lsh is involved in de novo methylation of DNA. The EMBO journal. *25* 335-345.

Ziv Y, Bielopolski D, Galanty Y, Lukas C, Taya Y, Schultz DC, Lukas J, Bekker-Jensen S, Bartek J, Shiloh Y. (2006). Chromatin relaxation in response to DNA double-strand breaks is modulated by a novel ATM- and KAP-1 dependent pathway. Nature Cell Biology. *8* 870-876.

The SNF2 family ATPase LSH promotes phosphorylation of H2AX and efficient repair of DNA double-strand breaks in mammalian cells

Joe Burrage, Ausma Termanis, Andreas Geissner*, Kevin Myant‡, Katrina Gordon and Irina Stancheva§

Wellcome Trust Centre for Cell Biology, University of Edinburgh, Michael Swann Building, Mayfield Road, Edinburgh EH9 3JR, UK

*Present address: Max Planck Institute of Colloids and Interfaces, Wissenschaftspark Potsdam-Golm, 14476 Potsdam, Germany
‡Present address: The Beatson Institute for Cancer Research, Garscube Estate, Switchback Road, Glasgow G61 1BD, UK
§Author for correspondence (istancheva@ed.ac.uk)

Accepted 25 July 2012
Journal of Cell Science 125, 5524–5534

doi: 10.1242/jcs.111252

Summary

LSH, a protein related to the SNF2 family of chromatin-remodelling ATPases, is essential for the correct establishment of DNA methylation levels and patterns in plants and mammalian cells. However, some of the phenotypes resulting from LSH deficiency cannot be explained easily by defects in DNA methylation. Here we show that LSH-deficient mouse and human fibroblasts show reduced viability after exposure to ionizing radiation and repair DNA double-strand breaks less efficiently than wild-type cells. A more detailed characterisation of this phenotype revealed that, in the absence of LSH, the histone variant H2AX is not efficiently phosphorylated in response to DNA damage. This results in impaired recruitment of MDC1 and 53BP1 proteins to DNA double-strand breaks and compromises phosphorylation of checkpoint kinase CHK2. Furthermore, we demonstrate that the ability of LSH to hydrolyse ATP is necessary for efficient phosphorylation of H2AX at DNA double-strand breaks and successful repair of DNA damage. Taken together, our data reveal a previously unsuspected role of LSH ATPase in the maintenance of genome stability in mammalian somatic cells, which is independent of its function in *de novo* DNA methylation during development.

Key words: DNA damage, DNA methylation, LSH, Chromatin, Chromatin remodelling

Introduction

Genetic information within the eukaryotic nucleus is organised into a highly conserved structural polymer, chromatin, which supports and controls crucial functions of the genome. The organisation of DNA into chromatin is inhibitory to most biological processes that utilise DNA as a template, such as transcription, replication, recombination and repair. There are several mechanisms by which chromatin structure and composition can be altered. One of the most fundamental of these is ATP-dependent chromatin-remodelling carried out by specialised proteins (Becker and Hörz, 2002; Lusser and Kadonaga, 2003). A number of chromatin remodelling proteins, often organised into large multi-subunit complexes, have been identified in mammalian cells (Lusser and Kadonaga, 2003; Narlikar et al., 2002). The catalytic subunit in these complexes, the ATPase, uses the energy from ATP hydrolysis in order to reposition, reorganize, modify or evict nucleosomes from DNA. Several chromatin-remodelling complexes including INO80, SWI/SNF, CHD4 and ISWI have been implicated in DNA damage repair in yeast, plants and mammalian cells (Polo and Jackson, 2011).

The Lymphoid-Specific Helicase LSH, also known as HELLS or PASG, is a ubiquitously-expressed 100 kDa protein related to the SNF2 family of chromatin-remodelling ATPases. Knockout of *Lsh* (*Hells*) gene in mice leads to postnatal lethality and 50–70% reduction in the global levels of DNA methylation, including repetitive sequences and large chromosomal domains throughout the genome (Dennis et al., 2001; Myant et al., 2011; Tao et al., 2011). In addition, $Lsh^{-/-}$ embryos exhibit defects in male and female meiosis, which are manifested by incomplete chromosome synapses and failure to load crossover-associated foci (De La Fuente et al., 2006; Zeng et al., 2011). It has been hypothesised that LSH remodels chromatin to render DNA accessible to DNA methyltransferase enzymes and therefore it supports *de novo* DNA methylation and stable gene silencing (Zhu et al., 2006). In agreement with this, it has been reported that LSH is required for developmentally programmed DNA methylation during embryogenesis (Myant et al., 2011). Nevertheless, ATP-dependent chromatin remodelling activity of LSH has never been demonstrated *in vitro*. *In vivo*, deletion of exons 10–12 was shown to truncate the catalytic SNF2 domain generating a hypomorph *Lsh* allele. Mice homozygous for the truncated *Lsh* allele also display DNA methylation defects, but they survive longer after birth, exhibit signs of premature ageing and upregulated expression of senescence-associated markers (Sun et al., 2004). It is yet unclear whether the loss of DNA methylation and cellular senescence are distinct or related to each other phenotypes resulting from impaired function of LSH in chromatin remodelling.

Here, we investigate the response of LSH-deficient mouse and human cells to DNA damage induced by ionizing radiation (IR). We find that LSH-deficient cells display reduced survival and inefficient repair of DNA double-strand breaks (DSBs) compared to cells with wild-type levels of LSH. Our characterisation of this

phenotype reveals that the LSH-deficient cells show normal activation of DNA damage-responsive kinase ATM, but weaker and more transient phosphorylation of ATM substrate, the variant histone H2AX (γH2AX). This results in inefficient recruitment and retention of DNA damage response mediator proteins MDC1 and 53BP1 at DSBs and leads to compromised ATM-dependent phosphorylation of checkpoint kinase CHK2. We also show that the DSB repair defects in LSH-deficient cells are independent of changes in DNA methylation and can be reversed by re-expression of wild-type, but not a catalytically inactive, LSH protein in $Lsh^{-/-}$ mouse embryonic fibroblasts (MEFs). Taken together our data imply that, in addition to promoting DNA methylation during development, LSH has a conserved, DNA methylation-independent function in DNA DSB repair.

Results

Inefficient repair of ionizing radiation-induced DNA damage in LSH-deficient cells

In order to investigate whether LSH is required for repair of DSBs in mammalian cells, we plated wild-type and $Lsh^{-/-}$ MEFs at clonal density and subjected them to increasing doses of ionizing radiation (IR). We monitored the survival of non-irradiated and irradiated cells by colony formation assay. Interestingly, the viability of $Lsh^{-/-}$ MEFs after IR was significantly impaired compared to wild-type MEFs, indicating that LSH-deficient cells are more sensitive to DNA damage induced by IR (Fig. 1A,B).

As LSH is involved in the formation of heterochromatin (Myant and Stancheva, 2008; Myant et al., 2011; Yan et al., 2003), it is possible that the same dose of IR generates a greater number of breaks in $Lsh^{-/-}$ fibroblasts than in wild-type MEFs due to general chromatin relaxation. To examine this, we employed single cell electrophoresis (comet assay) to measure the relative extent of DNA damage induced by IR in wild-type and LSH-deficient MEFs. We also examined whether the IR-induced DSBs are repaired equally well in both cell types. As is apparent from the comparable comet tail length after exposure to 10 Gy of IR, the wild-type and the $Lsh^{-/-}$ cells acquired a similar number of DNA breaks (Fig. 1C,D). However, the $Lsh^{-/-}$ MEFs failed to repair ~50% of these lesions compared to wild-type cells when investigated 8 hours after irradiation (Fig. 1C–E). Taken together, these data suggest that reduced viability of $Lsh^{-/-}$ MEFs after IR exposure reflects inefficient repair of DSBs rather than acquisition of greater DNA damage.

LSH-deficient MEFs display normal activation of DNA damage signalling

In mammalian cells, IR-induced DSBs lead to activation of a DNA damage response (DDR) signalling which promotes the recruitment of mediator and repair proteins to the sites of DNA damage and simultaneously orchestrates cell cycle arrest while the breaks are repaired (Polo and Jackson, 2011). DDR signalling cascade in G1 and G2 of the cell cycle is initiated by the ATM (Ataxia telangiectasia mutated) kinase, which undergoes auto-phosphorylation at Serine 329 in response to DNA damage (Bakkenist and Kastan, 2003). ATM subsequently binds to the MRN (MRE11, RAD50, NBS) complex that assembles at DNA breaks (Lee and Paull, 2004; Lee and Paull, 2005). The MRN-bound ATM phosphorylates multiple effectors proteins, including Serine 139 of the histone variant H2AX which is present in approximately every fifth nucleosome throughout chromatin (Burma et al., 2001). Phosphorylated H2AX (γH2AX) appears

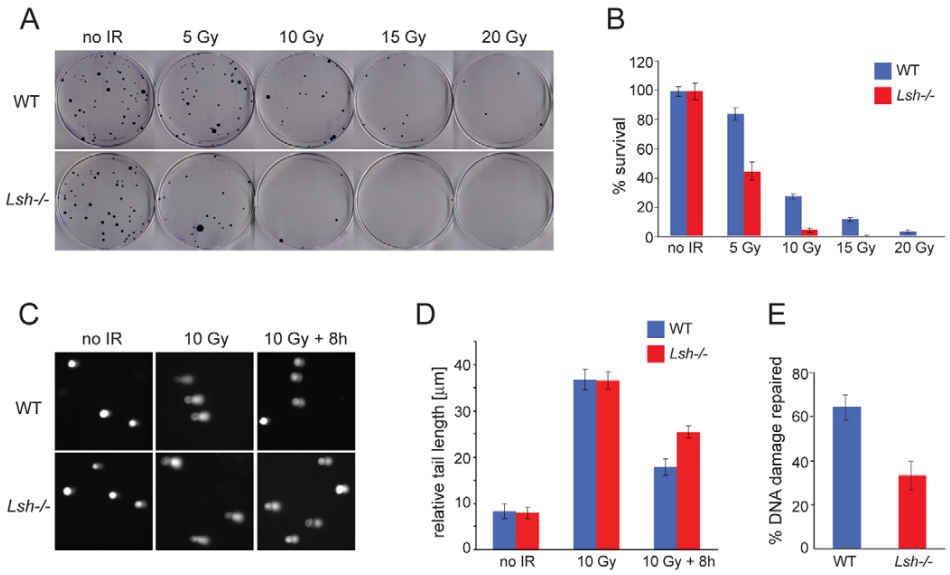

Fig. 1. Inefficient repair of DNA damage induced by IR in $Lsh^{-/-}$ MEFs. (**A**) Wild-type (WT) and $Lsh^{-/-}$ MEFs were plated at clonal density and subjected to increasing doses of IR. The number of colonies appearing after ten days on the irradiated plates indicate the reduced viability of $Lsh^{-/-}$ MEFs after exposure to IR. (**B**) Quantification of experiments (as shown in A) performed in triplicate. '% survival' represents the number of colonies appearing on irradiated plates relative to the number of colonies on non-irradiated plates seeded in parallel. (**C**) Comet assays show DNA fragmentation in wild-type and $Lsh^{-/-}$ MEFs without IR, immediately after treatment with 10 Gy of IR and 8 hours of recovery post-IR. (**D**) Quantification of the relative tail length from the experiments shown in C. A total of 50 cells were examined at each time point for each of the two genotypes. (**E**) The % repaired DNA damage was calculated from the values shown in D for 10 Gy and 10 Gy+8 hours time points. All error bars represent standard deviation (S.D.).

within minutes of DNA damage, spreads over large megabase-long domains flanking the DSB and serves as a platform for the recruitment of DNA damage repair machinery (Iacovoni et al., 2010; Rogakou et al., 1999; Rogakou et al., 1998). Accumulation of γH2AX and repair proteins at the sites of the DNA damage leads to the formation of discrete cytologically detectable foci which disperse as DNA damage is repaired (Polo and Jackson, 2011).

To investigate whether DDR initiates correctly in the *Lsh*$^{-/-}$ MEFs, we monitored the association of MRE11 with chromatin and the phosphorylation and localisation of ATM before and after IR. Chromatin retention assays showed that, unlike LSH, which stably associates with chromatin independently of DNA damage (Fig. 2A), MRE11 was enriched on DNA after exposure to IR and this occurred at similar levels in wild-type and *Lsh*$^{-/-}$ cells (Fig. 2B). Moreover, we detected no difference between wild-type and *Lsh*$^{-/-}$ MEFs in the kinetics of ATM phosphorylation after IR (Fig. 2C), the localisation of ATM to DSBs (Fig. 2D) and the number of ATM foci at the onset of DNA repair (supplementary material Fig. S1A). Collectively, our data suggest that the activation of ATM, detection of DSBs and initiation of DNA damage response are not impaired in the *Lsh*$^{-/-}$ MEFs.

Reduced phosphorylation of H2AX in LSH-deficient cells

To examine the events that take place downstream of ATM activation, we followed the kinetics of γH2AX accumulation after IR in wild-type and *Lsh*$^{-/-}$ MEFs by indirect immunofluorescence and western blots (Fig. 3A–C). In wild-type cells, γH2AX was

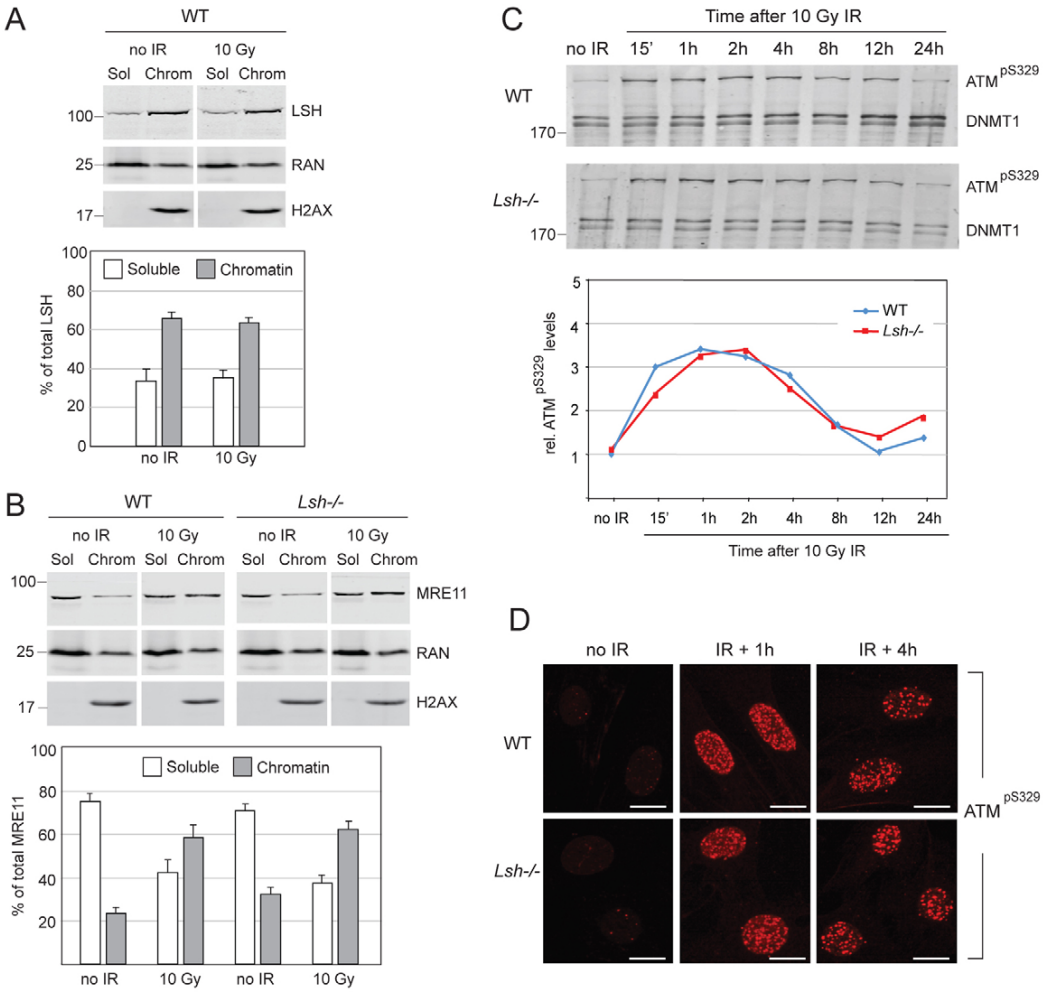

Fig. 2. Normal activation of DNA damage response in wild-type (WT) and *Lsh*$^{-/-}$ MEFs. (**A**) Western blot detecting LSH before and after IR in the soluble (Sol) and chromatin-bound (Chrom) fractions of nuclear proteins. Quantification of western blots from several independent experiments indicates that before and after IR, ~60% of LSH is constitutively bound to DNA/chromatin and ~40% is in the soluble nucleoplasm fraction. RAN and H2AX serve as loading controls for the soluble and chromatin fractions, respectively. (**B**) MRE11 accumulates equally well on chromatin after IR in wild-type and *Lsh*$^{-/-}$ MEFs and is partly depleted from the soluble nucleoplasm fraction. The bar graph shows quantification of MRE11 in the soluble and chromatin fractions from three independent experiments. The error bars in A and B represent S.D. (**C**) The activating phosphorylation of ATM at Serine 329 (pS329) displays similar kinetics after irradiation of the wild-type and *Lsh*$^{-/-}$ MEFs. DNMT1 is a loading control. The numbers on the left indicate molecular weight in kDa. The graph shows quantification of phosphorylated ATM relative to DNMT1 during the time course. (**D**) Phosphorylated ATM is recruited to DNA damage foci after irradiation of the wild-type and *Lsh*$^{-/-}$ MEFs. The scale bars represent 10 μm.

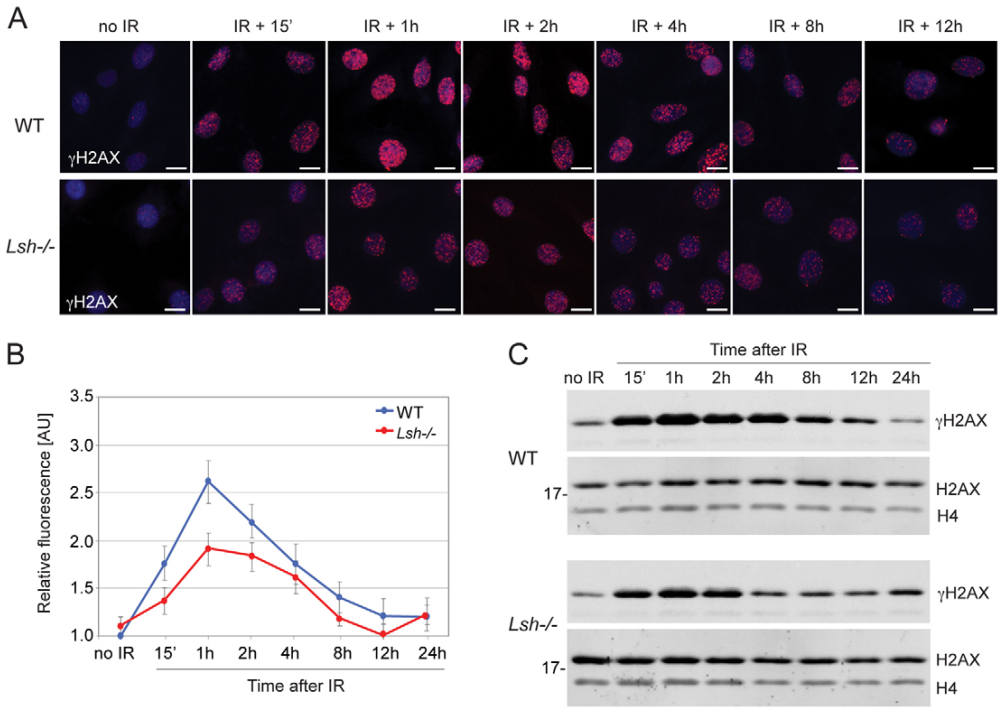

Fig. 3. Reduced phosphorylation of H2AX in *Lsh*$^{-/-}$ MEFs subjected to IR. (**A**) Immunostaining of wild-type (WT) and *Lsh*$^{-/-}$ MEFs with antibodies against γH2AX (red) before and after 10 Gy of IR. The nuclei were counterstained with DAPI (blue). The analysed time points are shown above the panels. The scale bars represent 10 μm. Note that *Lsh*$^{-/-}$ MEFs display significantly weaker staining for γH2AX. (**B**) Quantification of relative intensity of γH2AX staining in the immunofluorescence experiments shown in A. A total of 100 cells of each genotype were analysed at every time point. The error bars represent S.D. (**C**) Western blots showing the kinetics of γH2AX relative to H2AX and histone H4 in wild-type and *Lsh*$^{-/-}$ MEFs. All samples were run on the same gel and detected simultaneously. The numbers on the left indicate molecular weight in kDa.

detectable 15 minutes after the exposure of cells to IR, peaked 1 hour post-IR, persisted at lower, but significant levels at 2- and 4-hour time points, and gradually declined to basal levels by the 24-hour time point (Fig. 3A,C, top panels). In contrast, the accumulation and the persistence of γH2AX in the *Lsh*$^{-/-}$ MEFs were significantly reduced (Fig. 3A,C, bottom panels; see also the graph in Fig. 3B). In the irradiated LSH-deficient cells, γH2AX never reached the same levels as in the wild-type cells at the 1-hour time point and decreased dramatically 4 hours post-IR (Fig. 3A,C, bottom panels). Quantification of γH2AX in immunofluorescence experiments and western blots showed that the phosphorylation of the variant histone is reduced by ~50% in the *Lsh*$^{-/-}$ MEFs compared to their wild-type counterparts (Fig. 3B; supplementary material Fig. S2). The inefficient phosphorylation of H2AX was neither due to a reduced total amount of the variant histone in chromatin of LSH-deficient cells (Fig. 2B, Fig. 3C; supplementary material Fig. S2), nor caused by the overexpression of a known phosphatase that may dephosphorylate γH2AX prematurely (supplementary material Table S1). Thus, despite the normal activation and localisation of ATM kinase to IR-induced DSBs, the phosphorylation of H2AX is significantly impaired in the absence of LSH.

Potentially, the lack of LSH could affect γH2AX either globally, at all DSBs, or locally – only at a subset of DNA lesions. To investigate this, we counted the γH2AX foci in wild-type and *Lsh*$^{-/-}$ MEFs exposed to IR and found that the number of detectable γH2AX foci in *Lsh*$^{-/-}$ MEFs is reduced compared to their wild-type counterparts (supplementary material Fig. S1B). This indicates that LSH may not be required for high levels of γH2AX at all DSBs.

Reduction of γH2AX is independent of DNA methylation levels and is conserved between mouse and human LSH-deficient fibroblasts

In the *Lsh*$^{-/-}$ MEFs, the global levels of DNA methylation are reduced by ~50%, affecting many gene promoters and large chromosomal domains (Myant et al., 2011; Tao et al., 2011). Potentially, DNA hypomethylation may compromise the efficiency of DSBs repair either directly, by altering chromatin structure, or indirectly, by changing the expression of DNA repair genes. In order to investigate whether lack of DNA methylation affects the efficiency of H2AX phosphorylation, we irradiated MEFs genetically null for maintenance DNA methyltransferase DNMT1 and p53 (*Dnmt1*$^{-/-}$*; p53*$^{-/-}$) as well as p53-null MEFs (*p53*$^{-/-}$) (Lande-Diner et al., 2007) as controls and followed the γH2AX levels during DNA damage repair. Despite the almost complete lack of DNA methylation (<10%), *Dnmt1*$^{-/-}$*; p53*$^{-/-}$ MEFs displayed normal kinetics of γH2AX compared to wild-type and *p53*$^{-/-}$ control MEFs (Fig. 4A). This indicates that DNA methylation is not essential for efficient phosphorylation of H2AX near the sites of DNA damage.

In order to determine whether reduced γH2AX in response to IR is specific to LSH-deficient mouse fibroblasts or can be observed in other mammalian cell types, we stably knocked down

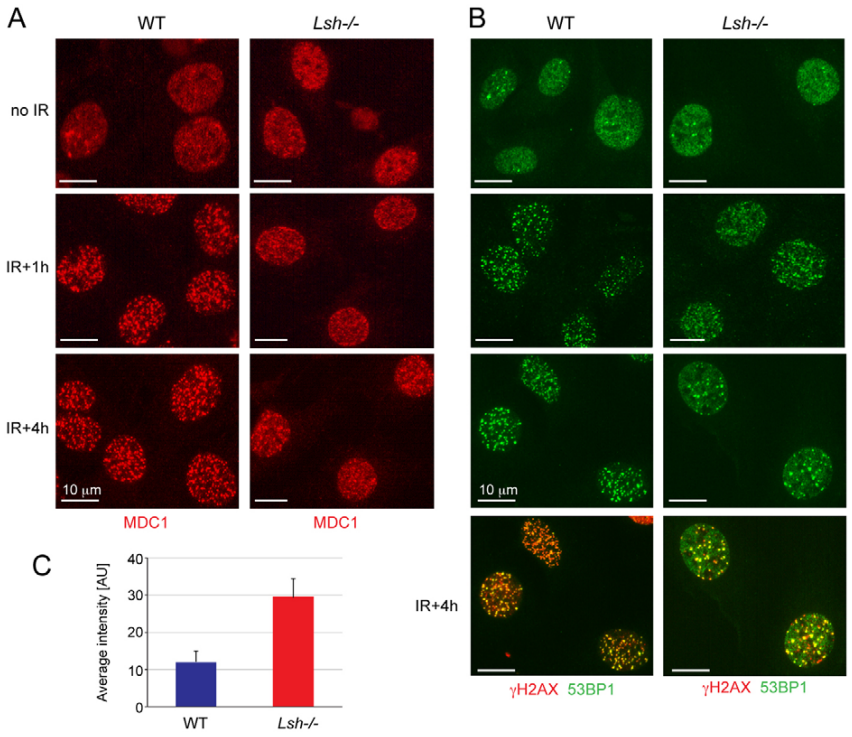

Fig. 5. Impaired recruitment of MDC1 and 53BP1 to the sites of DNA damage in $Lsh^{-/-}$ MEFs. (**A**) Immunostaining of non-irradiated and irradiated wild-type (WT) and $Lsh^{-/-}$ MEFs with antibodies detecting γH2AX binding protein MDC1. Note that diffuse staining for MDC1 can be seen in $Lsh^{-/-}$ MEFs 1 and 4 hours after exposure to IR. (**B**) Immunostaining of non-irradiated and irradiated wild-type and $Lsh^{-/-}$ MEFs with antibodies against 53BP1. Similar to MDC1, there is more diffuse staining for 53BP1 in $Lsh^{-/-}$ MEFs at 1- and 4-hour time points. The co-localisation of 53BP1 with γH2AX shown in the bottom two panels clearly shows diffuse 53BP1 staining in $Lsh^{-/-}$ MEFs that does not overlap with γH2AX. Note the reduced number of γH2AX foci in $Lsh^{-/-}$ MEFs at this time point in comparison to the wild-type MEFs. The scale bars represent 10 μm. (**C**) Quantification of 53BP1 staining in the nucleoplasm in wild-type and $Lsh^{-/-}$ MEFs 4 hours post-IR. The error bars represent S.D.

DSBs to induce cell cycle arrest by inhibitory phosphorylation of CDC25 phosphatase (Lukas et al., 2003; Matsuoka et al., 1998). On the other hand, 53BP1 is required for recruitment to DSBs of other ATM substrates such as BRCA1 and transcription factor p53 (Abraham, 2002). In response to IR, p53 undergoes stabilisation and ATM-dependent phosphorylation at Serine 15 (S15) (Canman et al., 1998). S15-phosphorylated p53 can either induce cell cycle arrest or promote apoptosis in cells that fail to repair DNA damage (Dumaz and Meek, 1999; Lambert et al., 1998).

In order to investigate whether reduced γH2AX and premature dissociation from DSBs of mediator proteins MDC1 and 53BP1 compromise DNA damage checkpoints, we examined the kinetics of CHK2 and p53 phosphorylation after IR in wild-type and LSH-deficient cells. As MEFs often spontaneously immortalize and lose p53 expression, we performed these analyses in human MRC5 fibroblasts infected with either the control non-silencing shRNA vector or MRC5 cells with stable KD of LSH (Fig. 4B). Consistent with γH2AX kinetics and MDC1 recruitment to IRIF, the CHK2 phosphorylation increased gradually after IR and peaked at the 2-hour time point in the control cells (Fig. 6A, Control KD). In contrast, the phosphorylated CHK2 was barely detectable in LSH-deficient cells at all time points after irradiation (Fig. 6A, LSH KD). However, LSH-deficient human fibroblasts displayed relatively normal ATM-dependent phosphorylation of p53 at Serine 15 (pS15) in response to IR. Although in the LSH KD cells the p53 protein levels did not peak as dramatically at 1- and 2-hour time points as in the control cells, we observed earlier and more persistent phosphorylation of p53 at S15 after DNA damage (Fig. 6B). These observations suggest that despite the reduced phosphorylation of CHK2 the LSH-deficient cells either undergo p53-dependent cell cycle arrest or apoptosis.

To investigate whether the control and LSH KD cells can arrest in response to DNA damage we followed their proliferation rate and viability after exposure to IR. Both cell lines showed robust exponential growth and no apparent cell death when grown under normal conditions (Fig. 6C,D, −IR). In response to radiation, both cell lines underwent cell cycle arrest, but resumed proliferation after 48 hours (Fig. 6C, +IR). However, the viability of LSH-deficient cells rapidly decreased after resuming proliferation. 42% of LSH KD cells compared to 24% of controls stained positive with trypan blue 96 hours post-irradiation (Fig. 6D, +IR). This indicates that despite the reduced phosphorylation of CHK2, LSH-deficient cells can undergo transient cell cycle arrest in response to DNA damage, but as they repair DSBs less efficiently, they exit the cell cycle arrest with unrepaired DNA damage which results in accelerated cell death.

The ATPase activity of LSH is required for efficient phosphorylation of H2AX

Despite having a conserved SNF2 domain, the ability of mammalian LSH to hydrolyse ATP and remodel chromatin remains largely unknown. In our hands, recombinant full-length mouse LSH did not reposition nucleosomes *in vitro*, but had a detectable, albeit weak, DNA-dependent ATPase activity (supplementary material Fig. S5). ATP hydrolysis by recombinant LSH *in vitro* was completely abolished by substitution of a highly conserved Lysine to Glutamine (K237Q) in the ATP-binding site (supplementary material Fig. S5C).

Considering this, we asked whether the wild-type and mutant LSH can rescue the kinetics of γH2AX after exposure of $Lsh^{-/-}$ MEFs to DNA damage. To do so, we infected the $Lsh^{-/-}$ MEFs with lentiviral vectors expressing FLAG-tagged either wild-type or K237Q mutant form of LSH at levels close to endogenous (Fig. 7A). $Lsh^{-/-}$ MEFs infected with empty vector (MSCV) served as a control. After exposure of these cell lines to radiation, we found that $Lsh^{-/-}$ MEFs expressing wild-type LSH survived

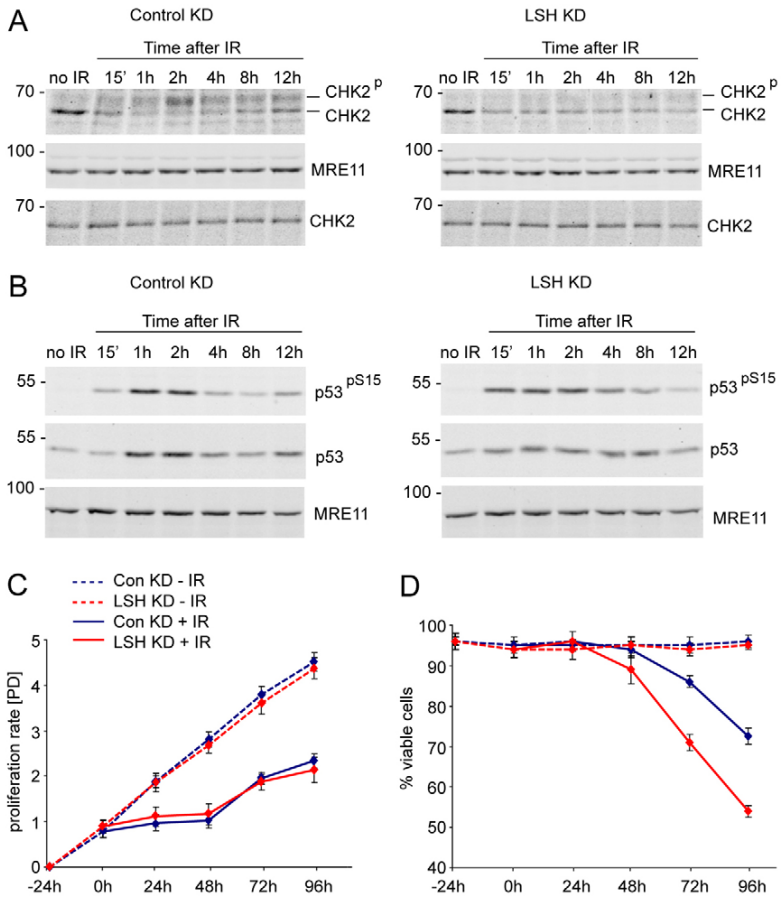

Fig. 6. Reduced phosphorylation of CHK2 in LSH-deficient cells. (**A**) Western blots detecting CHK2, phosphorylated CHK2 and MRE11 in nuclear extracts of non-irradiated and irradiated control KD and LSH KD MRC5 cells. Note that the slower migrating, phosphorylated form of CHK2 is barely detectable throughout the time course of recovery after IR in the LSH KD cells. Extracts prepared without phosphatase inhibitors (bottom panels) do not show the slower migrating phosphorylated form of CHK2. (**B**) The control KD and LSH-deficient cells display stabilisation of p53 and ATM-dependent phosphorylation of p53 at Serine 15 (pS15) after IR. MRE11 serves as a loading control. The numbers on the left indicate molecular weight markers in kDa. (**C**) Proliferation of non-irradiated (−IR) and 2.5 Gy irradiated (+IR) control and LSH KD MRC5 cells at indicated time points. '[PD]' indicates population doublings. (**D**) Viability of non-irradiated and irradiated control and LSH KD cells as detected by trypan blue staining at indicated time points. The error bars represent standard error of the mean.

IR as well as the wild-type MEFs, while cells expressing ATPase-deficient LSH K237Q had reduced survival, similar to *Lsh*$^{-/-}$ MEFs infected with empty vector (Fig. 7B). In addition, the expression of wild-type LSH in *Lsh*$^{-/-}$ MEFs restored to normal levels the phosphorylation of H2AX after IR (Fig. 7C) and the recruitment of 53BP1 to IRIF (Fig. 7D). In contrast, the *Lsh*$^{-/-}$ MEFs expressing the mutant LSH K237Q retained reduced phosphorylation of H2AX post-IR, diffuse localisation of 53BP1 to IRIF and were undistinguishable from *Lsh*$^{-/-}$ MEFs carrying the empty vector (Fig. 7C,D). From these experiments we conclude that the ability of LSH to hydrolyse ATP is required for efficient H2AX phosphorylation and repair of DNA damage.

Discussion

Several chromatin-remodelling proteins are implicated in the efficient repair of DNA damage in mammalian cells, including BRG1, CHD1L/ALC1, CHD4, INO80 and ISWI proteins ACF1 and SNF2H (Ahel et al., 2009; Kashiwaba et al., 2010; Lan et al., 2010; Larsen et al., 2010; Lee et al., 2010; Nakamura et al., 2011; Park et al., 2009; Park et al., 2006; Polo et al., 2010; Sánchez-Molina et al., 2011; Smeenk et al., 2010). Most of the chromatin-remodelling proteins are recruited to DNA breaks in a γH2AX-dependent manner and function to modulate chromatin structure and modifications in order to facilitate the access to either DNA or chromatin of factors involved in DNA damage signalling and repair. The function of chromatin remodellers in supporting DNA repair is often conserved from yeast to mammalian cells, indicating that chromatin reorganization during DNA repair is vital for maintenance of genome stability.

LSH has been extensively studied as a protein that promotes DNA methylation and silencing of retrotransposons and genes in plants and mammalian cells (Dennis et al., 2001; Lippman et al., 2004; Myant et al., 2011; Tao et al., 2011; Teixeira et al., 2009). However, genetics screens in budding yeast (Alvaro et al., 2007; Costanzo et al., 2010), which carry an LSH homologue YFR038W/IRC5 (Flaus et al., 2006), but entirely lack DNA methylation, and experiments in *Arabidopsis thaliana* (Costanzo et al., 2010; Shaked et al., 2006) have suggested that LSH may have additional functions that are independent of its role in DNA methylation and regulation of gene expression. Here, we provide experimental evidence that LSH is essential for efficient repair of DNA DSBs in human and mouse fibroblasts. This function of LSH is neither related to alterations in DNA methylation nor caused by mis-expression of known genes involved in DNA repair (supplementary material Table S1). Thus *Lsh*$^{-/-}$ MEFs, but not *Dnmt1*$^{-/-}$ MEFs lacking DNA methylation, exhibit reduced levels of γH2AX in response to IR. This effect is conserved in human cells as stable KD of LSH in hTERT-immortalized lung fibroblasts compromised the phosphorylation of H2AX in response to DNA damage without detectable change in DNA methylation levels. Our data are consistent with earlier observations in plants (Shaked et al., 2006), and strongly suggest that SNF2 family ATPase LSH has at least two distinct functions *in vivo*, namely, to promote *de novo* DNA methylation during development and to facilitate repair

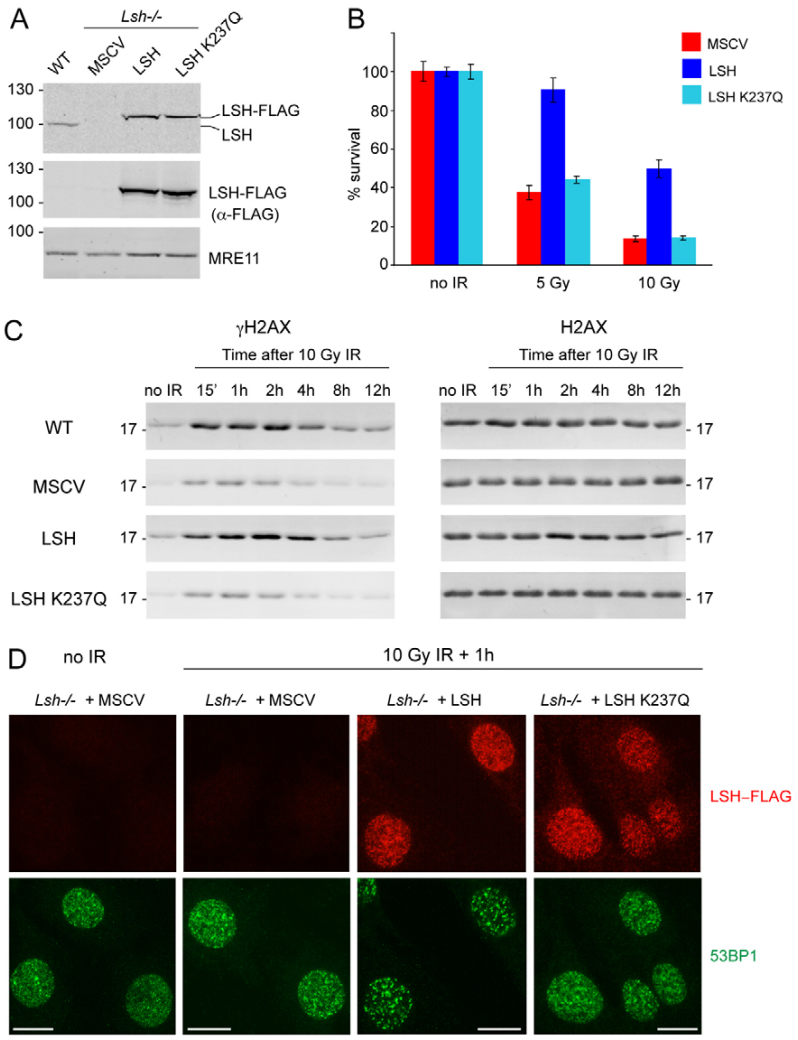

Fig. 7. Wild-type LSH, but not the ATP-binding-deficient LSH K237Q, can rescue the kinetics of γH2AX in irradiated *Lsh*$^{-/-}$ MEFs. (**A**) Western blots with antibodies against LSH and FLAG show the levels of LSH protein in wild-type (WT) MEFs, *Lsh*$^{-/-}$ MEFs infected with empty MSCV lentivirus and cells infected with lentivirus expressing either wild-type or mutant 3× FLAG-tagged LSH protein. MRE11 serves as a loading control. (**B**) % survival after IR of *Lsh*$^{-/-}$ MEFs carrying empty MSCV vector, wild-type LSH and mutant LSH K237Q. The error bars indicate S.D. (**C**) *Lsh*$^{-/-}$ MEFs expressing wild-type LSH, but not cells expressing the K237Q mutant form of LSH, display normal kinetics of γH2AX after IR when compared to control cells. H2AX serves as a loading control. All samples were run on the same gel and detected simultaneously. The numbers on the left indicate molecular weight markers in kDa. (**D**) Immunostaining with anti-FLAG and anti-53BP1 antibodies detect normal localisation of 53BP1 to DNA damage foci in *Lsh*$^{-/-}$ MEFs expressing wild-type LSH. Irradiated *Lsh*$^{-/-}$ MEFs infected either with empty MSCV virus or expressing LSH K237Q show diffuse staining for 53BP1. The scale bars represent 10 μm.

of DSBs in somatic cells. Our KD experiments in human fibroblasts demonstrate that these two functions can be successfully uncoupled from each other.

Whether deficient DNA repair can explain the meiotic defects observed in *Lsh*$^{-/-}$ germ cells (De La Fuente et al., 2006) and premature ageing phenotype in mice expressing hypomorph alleles of LSH (Sun et al., 2004) is yet to be investigated in detail. The formation of synaptonemal complexes during meiosis requires DNA recombination initiated at SPO11-generated DSBs. If such breaks are formed, but not correctly marked by γH2AX, this may compromise recombination between homologous chromosomes and thus impair meiosis (Celeste et al., 2002; Xu et al., 1996). However, γH2AX and RAD51 staining seem to persist longer in pachytene stage *Lsh*$^{-/-}$ oocytes than in their wild-type counterparts (De La Fuente et al., 2006). This may indicate that the lack of LSH confers additional defects in processing of meiotic DSBs during oogenesis and spermatogenesis. On the other hand, accumulation of endogenous unrepaired DNA damage in mice expressing hypomorphic *Lsh* alleles may lead to cellular senescence and premature ageing. Thus, some of the phenotypes resulting from LSH deficiency can be, at least in part, a direct consequence of the defective repair of DNA DSBs.

Although the detection of DNA damage, as evident by ATM activation and binding of MRE11 and ATM to DSBs, are not affected by LSH deficiency, reduced phosphorylation of H2AX at DNA repair sites in LSH-deficient cells indicates that LSH is involved in the early steps of DSB repair. The inefficient recruitment to DSBs of DNA damage signalling mediators MDC1 and 53BP1, compromised phosphorylation of CHK2 and reduced viability are expected outcomes of altered γH2AX levels and patterns in irradiated LSH-deficient cells. However, p53 stabilisation and phosphorylation by ATM remain unaffected by the lack of LSH and may contribute to cell cycle arrest and apoptosis of LSH-deficient cells with unrepaired DNA damage.

How LSH promotes γH2AX accumulation in response to DNA damage is currently unclear. As is evident from our rescue experiments in the *Lsh*$^{-/-}$ MEFs, the ability of LSH to hydrolyse ATP is essential for normal levels of γH2AX and successful DNA repair. Unlike BRG1, which also supports efficient accumulation of γH2AX (Lee et al., 2010; Park et al., 2006), and other chromatin-remodelling proteins implicated in DNA

damage repair (Ahel et al., 2009; Larsen et al., 2010; Polo et al., 2010; Smeenk et al., 2010; van Attikum et al., 2004), LSH neither accumulates at repair foci (Fig. 7D), nor binds more tightly to chromatin specifically after the induction of DNA damage (Fig. 2A). In fact, chromatin retention assays indicate that a significant proportion of LSH is constitutively bound to DNA or chromatin in mammalian cells. Therefore, it is possible that LSH renders the C-terminus of H2AX more receptive to ATM-mediated phosphorylation by acting locally, at DSBs that occur in the vicinity of DNA/chromatin-bound LSH. Alternatively, LSH may not function specifically during DSB repair, but instead facilitate the even distribution of variant histone H2AX in chromatin throughout the genome. It is currently accepted that in mammalian cells on average every fifth nucleosome contains H2AX (Rogakou et al., 1999). However, it is yet unclear when during the cell cycle and how H2AX is incorporated into chromatin. Uneven distribution of H2AX throughout the genome of LSH-deficient cells would result in areas that lack H2AX and repair DSBs less efficiently. Either one of these two hypotheses could explain the reduced levels of γH2AX and number of detectable γH2AX foci in the $Lsh^{-/-}$ MEFs (supplementary material Fig. S1B). Future experiments will aim to investigate the accumulation and spreading of γH2AX at defined DNA lesions (Iacovoni et al., 2010) as well as the distribution of H2AX in the genome of LSH-deficient cells. It will also be essential to determine whether or not LSH and BRG1 have redundant function in promoting γH2AX accumulation in response to IR-induced DNA damage.

Collectively, the data we provide in this report identify LSH as an important and functionally conserved, from plants to mammals, component of DSB repair process. Frequent deletions within the SNF2 domain of LSH have been detected in human lymphoid malignancies and may contribute to stress-induced genomic instability in cancers carrying LSH mutations (Lee et al., 2000). Compared to quiescent cells, LSH is highly expressed in all rapidly proliferating cell types, including most immortalized and cancer-derived cell lines (Lee et al., 2000). Therefore, it is conceivable that development of small molecules that inhibit the ATPase activity of LSH would be beneficial for applications aiming to sensitise cancer cells to DNA damage in order to aid successful radiotherapy.

Materials and Methods

Cell lines and viral infections

Wild-type and $Lsh^{-/-}$ MEFs were cultured in DMEM supplemented with 10% FCS, penicillin, streptomycin and L-glutamine. Vectors expressing 3×FLAG C-terminally-tagged LSH and K237Q mutant LSH were generated by cloning synthetic cDNAs (Life Technologies) into pMSCV-puro vector (Clontech). The vectors were packaged into lentiviral particles in amphotropic Phoenix cell line and used for infection of $Lsh^{-/-}$ MEFs at multiplicity of infection (MOI)=1. The cells were selected with 2.5 μg/ml of puromycin for two weeks and individual stable colonies were expanded and tested for LSH expression. Human foetal lung fibroblast MRC5 (ATCC number: CRL-171) were cultured in MEM supplemented with 10% FCS, non-essential amino acids, sodium pyruvate, penicillin, streptomycin and L-glutamine. MRC5 cells were immortalized by transduction with pBabe-hTERT-Neo plasmid packaged into retroviral particles in Phoenix cells. The infected cells were selected with 400 μg/ml G418 for 10 days. LSH was stably knocked down in $MRC5^{hTERT}$ cells by introducing at MOI=4 two independent pGIPZ-shRNAmir plasmids V2LHS_155499 and V2LHS_155497 packaged into lentiviral particles (Open Biosystems). Control cells were infected under the same conditions with non-silencing pGIPZ-shRNAmir particles RHS4348 (Open Biosystems). The infected cells were selected with 2.5 μg/ml of puromycin for 7 days and the LSH knockdown assessed by western blots and quantitative RT-PCR.

Irradiation experiments

Wild-type and LSH-deficient either mouse or human fibroblasts were plated on 10 cm dishes in triplicate at a density of 200 cells/plate and irradiated with indicated doses of IR in a Torrex X-ray cabinet (Faxitron Ltd). In survival assays, the irradiated cells were left to recover and form colonies for 10–14 days, fixed, stained with Giemsa and counted. For time course experiments, the cells were plated on 20 cm dishes at ~60% confluency, subjected to indicated dose of IR (usually 10 Gy) and collected 15 minutes, 1, 2, 4, 8, 12 and 24 hours after irradiation. Nuclear extracts were prepared as described previously (Myant et al., 2011) in buffers supplemented with phosphatase (Pierce) and protease (Sigma Aldrich) inhibitors. For short-term analyses of cell proliferation and viability, human fibroblasts were plated on 6-well plates (2×10^5 cells/well) irradiated with 2.5 Gy and counted in trypan blue solution by Countess Cell Counter (Life Technologies).

Comet assays

Cells were plated on 10 cm dishes at ~60% confluency, subjected to 10 Gy of IR and either collected immediately or left to recover for 8 hours. Cells were diluted to 6×10^5 cells/ml with PBS, mixed 1:10 with 0.6% low melting point agarose and placed onto glass slides pre-coated with 1% agarose. Slides were placed in lysis buffer (2.5 M NaCl, 10 mM Tris, 1% Triton-X, pH 10) overnight at 4℃. Lysis buffer was removed, the slides washed twice with dH_2O and electrophoresis was carried out in a cold alkaline buffer (300 mM NaCl, 1 mM EDTA, pH 13) at 100 A, 12 V for 20 minutes. Slides were neutralised with 3×5 minute washes with cold 0.4 M Tris, pH 7.5 followed by 10 minute wash with cold dH_2O. Staining was carried out with a 20 μg/ml propidium iodide solution followed by 2×5 minute washes in cold dH_2O. Images were collected by an Olympus BX61 microscope equipped with 20× objectives and AnalySIS software (Soft Imaging Systems). Comet tail lengths were quantified using customized macro in ImagePro 9.0 software (Media Cybernetics).

Chromatin retention assays

Cells were plated on 20 cm dishes at ~60% confluency, subjected to the indicated dose of IR and collected at the indicated time point after irradiation. Nuclei were prepared by disrupting the cells in hypotonic buffer (NE1) as previously described (Myant et al., 2011). Soluble nuclear proteins and those loosely associated with chromatin were extracted using NE1 supplemented with 100 mM NaCl. After centrifugation the pellets containing chromatin bound proteins were resuspended in NE1 buffer supplemented with 25 U of Benzonase nuclease (Merck). Following 1 hour incubation on ice, NaCl was added to a final concentration of 500 mM and incubated at 4℃ for 1 hour. After centrifugation the supernatant containing the chromatin associated proteins was collected. All buffers were supplemented with phosphatase (Pierce) and protease inhibitors (Sigma Aldrich).

Western blots

50 μg of each nuclear extract was resolved on either 8.5% or 15% SDS-PAGE, transferred to nitrocellulose membrane (BioRad) and detected by anti-LSH (Santa Cruz; sc-46665), anti-γH2AX (Millipore; 05-636), anti-H2AX (Active Motif), anti-H4 (Millipore; 07-108), anti-phospho-ATM (Millipore; 05-740), anti-MRE11 (Calbiochem; PC388), anti-CHK2 (Cell Signaling; 2662), anti-p53 (Santa Cruz, sc126 for human cells and Cell Signaling 2524 for mouse cells) and anti-p53 pS15 (Cell Signaling; 9284) antibodies followed by secondary either anti-mouse IR800 or anti-rabbit IR680 (LiCOR Biosciences). The western blots were imaged on Odyssey Imager (LiCOR Biosciences) and quantified where indicated with the aid of Odyssey V3.0 software.

Immunofluorescence

Cells were fixed either with 4% paraformaldehyde or with cold 100% methanol for 5 minutes, permeabilized by incubation in PBS with 0.1% Tween for 10 minutes, blocked with 4% BSA in PBS, incubated with diluted primary antibodies for 2 hours and after washes with secondary anti-rabbit Alexa 488 or anti-mouse Alexa 565 labelled antibodies. The slides were washed with PBS, counterstained with DAPI and mounted in Vectashield (Vector Laboratories). Images were collected by Olympus BX61 microscope equipped with 20× and 40× PlanApo objectives (Olympus), ColourViewII camera and AnalySIS software (Soft Imaging Systems). Where indicated, fluorescent images were quantified using a customized macro in ImagePro 9.0 software (Media Cybernetics). Antibodies used for immunofluorescence were: anti-pATM (Millipore; 05-740) 1:2000 dilution; anti-γH2AX (Millipore; 05-636) 1:4000 dilution; anti-MDC1 (Abcam; ab11171) 1:1000 dilution; anti-53BP1 (Cell Signaling; 4397) 1:1000; and anti-FLAG M2 (Sigma Aldrich) 1:2000.

DNA methylation assays

The global levels of 5-methyl cytosine in the genome of $MRC5^{hTERT}$, LSH KD and control KD cells were investigated by ELISA assays using an Imprint™ kit (Sigma Aldrich) according to manufacturer's instructions.

Quantitative RT-PCR

RNA was extracted from cells with Trizol reagent (Life Technologies). 4 μg of each RNA were treated with RNase-free DNase (Fermentas) and reverse

transcribed using poly-dT primer and SuperscriptIII reverse transcriptase (Life Technologies). Q-PCRs were carried out in triplicate with SYBR Green Master Mix (Roche) and primers detecting LSH and GAPDH mRNA on a Lightcycler 480 instrument (Roche). Relative levels of LSH mRNA were quantified relative to GAPDH using the standard methods (Pfaffl, 2001).

Chromatin remodelling and ATPase assays

Full-length cDNA of wild-type and K237Q mutant mouse LSH were cloned into a shuttle pFastBac vector (Invitrogen) in frame with a N-terminal 6× Histidine tag and introduced into DH10Bac *E. coli* (Life Technologies) to obtain recombinant Bacmids. Expression in SF2 cells and purification by nickel affinity and ion exchange chromatography were carried out using standard protocols. Chromatin remodelling assays were performed as described (Stockdale et al., 2006) with nucleosomes assembled by salt dialysis (Narlikar et al., 2002) on Cy5 labelled 601 nucleosome positioning sequence (Lowary and Widom, 1998) carrying either 54 bp of linker DNA on either site (54A54) or 601 with 54 bp linker DNA on one side and 0 on the other side (54A0) in the presence of either recombinant wild-type LSH or *S. cerevisiae* RSC protein as control. Remodelling reactions were resolved on 5% acrylamide gel in 0.5× TBE buffer and scanned on ProXPRESS proteomics imaging system (Perkin Elmer Life Sciences, UK). ATPase activity assays were carried out with either wild-type or mutant LSH in the presence of ^{32}P-γATP and indicated substrates for 30 minutes at 37℃. The reactions were stopped on ice and spotted on PEI Cellulose TLC plates (Merck). Separation was achieved in 0.5 M LiCl/1 M formic acid buffer. The plates were dried, exposed and scanned on Storm 860 Phosphorimager (Molecular Dynamics). ATP hydrolysis was calculated from the signal intensity of the released free phosphate (^{32}Pi) using ImageQuant software. Detailed protocols of these methods are available upon request.

Acknowledgements

We thank Kathrin Muegge (National Cancer Institute, Frederick, MD, USA) for kindly providing the wild-type and *Lsh*$^{-/-}$ MEFs, Eric So (King's College, London, UK) for MSCV vectors, David Kelly (Wellcome Trust Centre for Cell Biology, COIL facility) for help with imaging and image quantification and the members of Stancheva laboratory for reading the manuscript and helpful suggestions.

Funding

This research was supported by Cancer Research UK Senior Fellowship [grant number C7215/A8983] and Wellcome Trust Centre for Cell Biology Core grant [grant number 077707]; J.B. is a Biotechnology and Biological Sciences Research Council CASE PhD student supported by CellCentric Ltd.; and A.T. is a PhD student funded by Cancer Research UK [grant number C7215/A9218]. Deposited in PMC for release after 6 months.

Supplementary material available online at
http://jcs.biologists.org/lookup/suppl/doi:10.1242/jcs.111252/-/DC1

References

Abraham, R. T. (2002). Checkpoint signalling: focusing on 53BP1. *Nat. Cell Biol.* **4**, E277-E279.

Ahel, D., Horejsí, Z., Wiechens, N., Polo, S. E., Garcia-Wilson, E., Ahel, I., Flynn, H., Skehel, M., West, S. C., Jackson, S. P. et al. (2009). Poly(ADP-ribose)-dependent regulation of DNA repair by the chromatin remodeling enzyme ALC1. *Science* **325**, 1240-1243.

Ahn, J. Y., Schwarz, J. K., Piwnica-Worms, H. and Canman, C. E. (2000). Threonine 68 phosphorylation by ataxia telangiectasia mutated is required for efficient activation of Chk2 in response to ionizing radiation. *Cancer Res.* **60**, 5934-5936.

Alvaro, D., Lisby, M. and Rothstein, R. (2007). Genome-wide analysis of Rad52 foci reveals diverse mechanisms impacting recombination. *PLoS Genet.* **3**, e228.

Bakkenist, C. J. and Kastan, M. B. (2003). DNA damage activates ATM through intermolecular autophosphorylation and dimer dissociation. *Nature* **421**, 499-506.

Becker, P. B. and Hörz, W. (2002). ATP-dependent nucleosome remodeling. *Annu. Rev. Biochem.* **71**, 247-273.

Burma, S., Chen, B. P., Murphy, M., Kurimasa, A. and Chen, D. J. (2001). ATM phosphorylates histone H2AX in response to DNA double-strand breaks. *J. Biol. Chem.* **276**, 42462-42467.

Canman, C. E., Lim, D. S., Cimprich, K. A., Taya, Y., Tamai, K., Sakaguchi, K., Appella, E., Kastan, M. B. and Siliciano, J. D. (1998). Activation of the ATM kinase by ionizing radiation and phosphorylation of p53. *Science* **281**, 1677-1679.

Celeste, A., Petersen, S., Romanienko, P. J., Fernandez-Capetillo, O., Chen, H. T., Sedelnikova, O. A., Reina-San-Martin, B., Coppola, V., Meffre, E., Difilippantonio, M. J. et al. (2002). Genomic instability in mice lacking histone H2AX. *Science* **296**, 922-927.

Costanzo, M., Baryshnikova, A., Bellay, J., Kim, Y., Spear, E. D., Sevier, C. S., Ding, H., Koh, J. L., Toufighi, K., Mostafavi, S. et al. (2010). The genetic landscape of a cell. *Science* **327**, 425-431.

De La Fuente, R., Baumann, C., Fan, T., Schmidtmann, A., Dobrinski, I. and Muegge, K. (2006). Lsh is required for meiotic chromosome synapsis and retrotransposon silencing in female germ cells. *Nat. Cell Biol.* **8**, 1448-1454.

Dennis, K., Fan, T., Geiman, T., Yan, Q. and Muegge, K. (2001). Lsh, a member of the SNF2 family, is required for genome-wide methylation. *Genes Dev.* **15**, 2940-2944.

Dumaz, N. and Meek, D. W. (1999). Serine15 phosphorylation stimulates p53 transactivation but does not directly influence interaction with HDM2. *EMBO J.* **18**, 7002-7010.

Eliezer, Y., Argaman, L., Rhie, A., Doherty, A. J. and Goldberg, M. (2009). The direct interaction between 53BP1 and MDC1 is required for the recruitment of 53BP1 to sites of damage. *J. Biol. Chem.* **284**, 426-435.

Flaus, A., Martin, D. M., Barton, G. J. and Owen-Hughes, T. (2006). Identification of multiple distinct Snf2 subfamilies with conserved structural motifs. *Nucleic Acids Res.* **34**, 2887-2905.

Glover, J. N., Williams, R. S. and Lee, M. S. (2004). Interactions between BRCT repeats and phosphoproteins: tangled up in two. *Trends Biochem. Sci.* **29**, 579-585.

Huyen, Y., Zgheib, O., Ditullio, R. A., Jr, Gorgoulis, V. G., Zacharatos, P., Petty, T. J., Sheston, E. A., Mellert, H. S., Stavridi, E. S. and Halazonetis, T. D. (2004). Methylated lysine 79 of histone H3 targets 53BP1 to DNA double-strand breaks. *Nature* **432**, 406-411.

Iacovoni, J. S., Caron, P., Lassadi, I., Nicolas, E., Massip, L., Trouche, D. and Legube, G. (2010). High-resolution profiling of γH2AX around DNA double strand breaks in the mammalian genome. *EMBO J.* **29**, 1446-1457.

Kashiwaba, S., Kitahashi, K., Watanabe, T., Onoda, F., Ohtsu, M. and Murakami, Y. (2010). The mammalian INO80 complex is recruited to DNA damage sites in an ARP8 dependent manner. *Biochem. Biophys. Res. Commun.* **402**, 619-625.

Lambert, P. F., Kashanchi, F., Radonovich, M. F., Shiekhattar, R. and Brady, J. N. (1998). Phosphorylation of p53 serine 15 increases interaction with CBP. *J. Biol. Chem.* **273**, 33048-33053.

Lan, L., Ui, A., Nakajima, S., Hatakeyama, K., Hoshi, M., Watanabe, R., Janicki, S. M., Ogiwara, H., Kohno, T., Kanno, S. et al. (2010). The ACF1 complex is required for DNA double-strand break repair in human cells. *Mol. Cell* **40**, 976-987.

Lande-Diner, L., Zhang, J., Ben-Porath, I., Amariglio, N., Keshet, I., Hecht, M., Azuara, V., Fisher, A. G., Rechavi, G. and Cedar, H. (2007). Role of DNA methylation in stable gene repression. *J. Biol. Chem.* **282**, 12194-12200.

Larsen, D. H., Poinsignon, C., Gudjonsson, T., Dinant, C., Payne, M. R., Hari, F. J., Rendtlew Danielsen, J. M., Menard, P., Sand, J. C., Stucki, M. et al. (2010). The chromatin-remodeling factor CHD4 coordinates signaling and repair after DNA damage. *J. Cell Biol.* **190**, 731-740.

Lee, J. H. and Paull, T. T. (2004). Direct activation of the ATM protein kinase by the Mre11/Rad50/Nbs1 complex. *Science* **304**, 93-96.

Lee, J. H. and Paull, T. T. (2005). ATM activation by DNA double-strand breaks through the Mre11-Rad50-Nbs1 complex. *Science* **308**, 551-554.

Lee, D. W., Zhang, K., Ning, Z. Q., Raabe, E. H., Tintner, S., Wieland, R., Wilkins, B. J., Kim, J. M., Blough, R. I. and Arceci, R. J. (2000). Proliferation-associated SNF2-like gene (PASG): a SNF2 family member altered in leukemia. *Cancer Res.* **60**, 3612-3622.

Lee, H. S., Park, J. H., Kim, S. J., Kwon, S. J. and Kwon, J. (2010). A cooperative activation loop among SWI/SNF, γ-H2AX and H3 acetylation for DNA double-strand break repair. *EMBO J.* **29**, 1434-1445.

Lippman, Z., Gendrel, A. V., Black, M., Vaughn, M. W., Dedhia, N., McCombie, W. R., Lavine, K., Mittal, V., May, B., Kasschau, K. D. et al. (2004). Role of transposable elements in heterochromatin and epigenetic control. *Nature* **430**, 471-476.

Lowary, P. T. and Widom, J. (1998). New DNA sequence rules for high affinity binding to histone octamer and sequence-directed nucleosome positioning. *J. Mol. Biol.* **276**, 19-42.

Lukas, C., Falck, J., Bartkova, J., Bartek, J. and Lukas, J. (2003). Distinct spatiotemporal dynamics of mammalian checkpoint regulators induced by DNA damage. *Nat. Cell Biol.* **5**, 255-260.

Lusser, A. and Kadonaga, J. T. (2003). Chromatin remodeling by ATP-dependent molecular machines. *Bioessays* **25**, 1192-1200.

Matsuoka, S., Huang, M. and Elledge, S. J. (1998). Linkage of ATM to cell cycle regulation by the Chk2 protein kinase. *Science* **282**, 1893-1897.

Myant, K. and Stancheva, I. (2008). LSH cooperates with DNA methyltransferases to repress transcription. *Mol. Cell. Biol.* **28**, 215-226.

Myant, K., Termanis, A., Sundaram, A. Y., Boe, T., Li, C., Merusi, C., Burrage, J., de Las Heras, J. I. and Stancheva, I. (2011). LSH and G9a/GLP complex are required for developmentally programmed DNA methylation. *Genome Res.* **21**, 83-94.

Nakamura, K., Kato, A., Kobayashi, J., Yanagihara, H., Sakamoto, S., Oliveira, D. V., Shimada, M., Tauchi, H., Suzuki, H., Tashiro, S. et al. (2011). Regulation of homologous recombination by RNF20-dependent H2B ubiquitination. *Mol. Cell* **41**, 515-528.

Narlikar, G. J., Fan, H. Y. and Kingston, R. E. (2002). Cooperation between complexes that regulate chromatin structure and transcription. *Cell* **108**, 475-487.

Park, J. H., Park, E. J., Lee, H. S., Kim, S. J., Hur, S. K., Imbalzano, A. N. and Kwon, J. (2006). Mammalian SWI/SNF complexes facilitate DNA double-strand break repair by promoting γ-H2AX induction. *EMBO J.* **25**, 3986-3997.

Park, J. H., Park, E. J., Hur, S. K., Kim, S. and Kwon, J. (2009). Mammalian SWI/SNF chromatin remodeling complexes are required to prevent apoptosis after DNA damage. *DNA Repair (Amst.)* **8**, 29-39.
Pfaffl, M. W. (2001). A new mathematical model for relative quantification in real-time RT-PCR. *Nucleic Acids Res.* **29**, e45.
Polo, S. E. and Jackson, S. P. (2011). Dynamics of DNA damage response proteins at DNA breaks: a focus on protein modifications. *Genes Dev.* **25**, 409-433.
Polo, S. E., Kaidi, A., Baskcomb, L., Galanty, Y. and Jackson, S. P. (2010). Regulation of DNA-damage responses and cell-cycle progression by the chromatin remodelling factor CHD4. *EMBO J.* **29**, 3130-3139.
Rogakou, E. P., Pilch, D. R., Orr, A. H., Ivanova, V. S. and Bonner, W. M. (1998). DNA double-stranded breaks induce histone H2AX phosphorylation on serine 139. *J. Biol. Chem.* **273**, 5858-5868.
Rogakou, E. P., Boon, C., Redon, C. and Bonner, W. M. (1999). Megabase chromatin domains involved in DNA double-strand breaks *in vivo*. *J. Cell Biol.* **146**, 905-916.
Sánchez-Molina, S., Mortusewicz, O., Bieber, B., Auer, S., Eckey, M., Leonhardt, H., Friedl, A. A. and Becker, P. B. (2011). Role for hACF1 in the G2/M damage checkpoint. *Nucleic Acids Res.* **39**, 8445-8456.
Sanders, S. L., Portoso, M., Mata, J., Bähler, J., Allshire, R. C. and Kouzarides, T. (2004). Methylation of histone H4 lysine 20 controls recruitment of Crb2 to sites of DNA damage. *Cell* **119**, 603-614.
Shaked, H., Avivi-Ragolsky, N. and Levy, A. A. (2006). Involvement of the *Arabidopsis* SWI2/SNF2 chromatin remodeling gene family in DNA damage response and recombination. *Genetics* **173**, 985-994.
Smeenk, G., Wiegant, W. W., Vrolijk, H., Solari, A. P., Pastink, A. and van Attikum, H. (2010). The NuRD chromatin-remodeling complex regulates signaling and repair of DNA damage. *J. Cell Biol.* **190**, 741-749.
Stockdale, C., Flaus, A., Ferreira, H. and Owen-Hughes, T. (2006). Analysis of nucleosome repositioning by yeast ISWI and Chd1 chromatin remodeling complexes. *J. Biol. Chem.* **281**, 16279-16288.
Sun, L. Q., Lee, D. W., Zhang, Q., Xiao, W., Raabe, E. H., Meeker, A., Miao, D., Huso, D. L. and Arceci, R. J. (2004). Growth retardation and premature aging phenotypes in mice with disruption of the SNF2-like gene, PASG. *Genes Dev.* **18**, 1035-1046.
Suzuki, T., Farrar, J. E., Yegnasubramanian, S., Zahed, M., Suzuki, N. and Arceci, R. J. (2008). Stable knockdown of PASG enhances DNA demethylation but does not accelerate cellular senescence in TIG-7 human fibroblasts. *Epigenetics* **3**, 281-291.
Tao, Y., Xi, S., Shan, J., Maunakea, A., Che, A., Briones, V., Lee, E. Y., Geiman, T., Huang, J., Stephens, R. et al. (2011). Lsh, chromatin remodeling family member, modulates genome-wide cytosine methylation patterns at nonrepeat sequences. *Proc. Natl. Acad. Sci. USA* **108**, 5626-5631.
Teixeira, F. K., Heredia, F., Sarazin, A., Roudier, F., Boccara, M., Ciaudo, C., Cruaud, C., Poulain, J., Berdasco, M., Fraga, M. F. et al. (2009). A role for RNAi in the selective correction of DNA methylation defects. *Science* **323**, 1600-1604.
van Attikum, H., Fritsch, O., Hohn, B. and Gasser, S. M. (2004). Recruitment of the INO80 complex by H2A phosphorylation links ATP-dependent chromatin remodeling with DNA double-strand break repair. *Cell* **119**, 777-788.
Xu, Y., Ashley, T., Brainerd, E. E., Bronson, R. T., Meyn, M. S. and Baltimore, D. (1996). Targeted disruption of ATM leads to growth retardation, chromosomal fragmentation during meiosis, immune defects, and thymic lymphoma. *Genes Dev.* **10**, 2411-2422.
Yan, Q., Huang, J., Fan, T., Zhu, H. and Muegge, K. (2003). Lsh, a modulator of CpG methylation, is crucial for normal histone methylation. *EMBO J.* **22**, 5154-5162.
Zeng, W., Baumann, C., Schmidtmann, A., Honaramooz, A., Tang, L., Bondareva, A., Dores, C., Fan, T., Xi, S., Geiman, T. et al. (2011). Lymphoid-specific helicase (HELLS) is essential for meiotic progression in mouse spermatocytes. *Biol. Reprod.* **84**, 1235-1241.
Zhu, H., Geiman, T. M., Xi, S., Jiang, Q., Schmidtmann, A., Chen, T., Li, E. and Muegge, K. (2006). Lsh is involved in *de novo* methylation of DNA. *EMBO J.* **25**, 335-345.

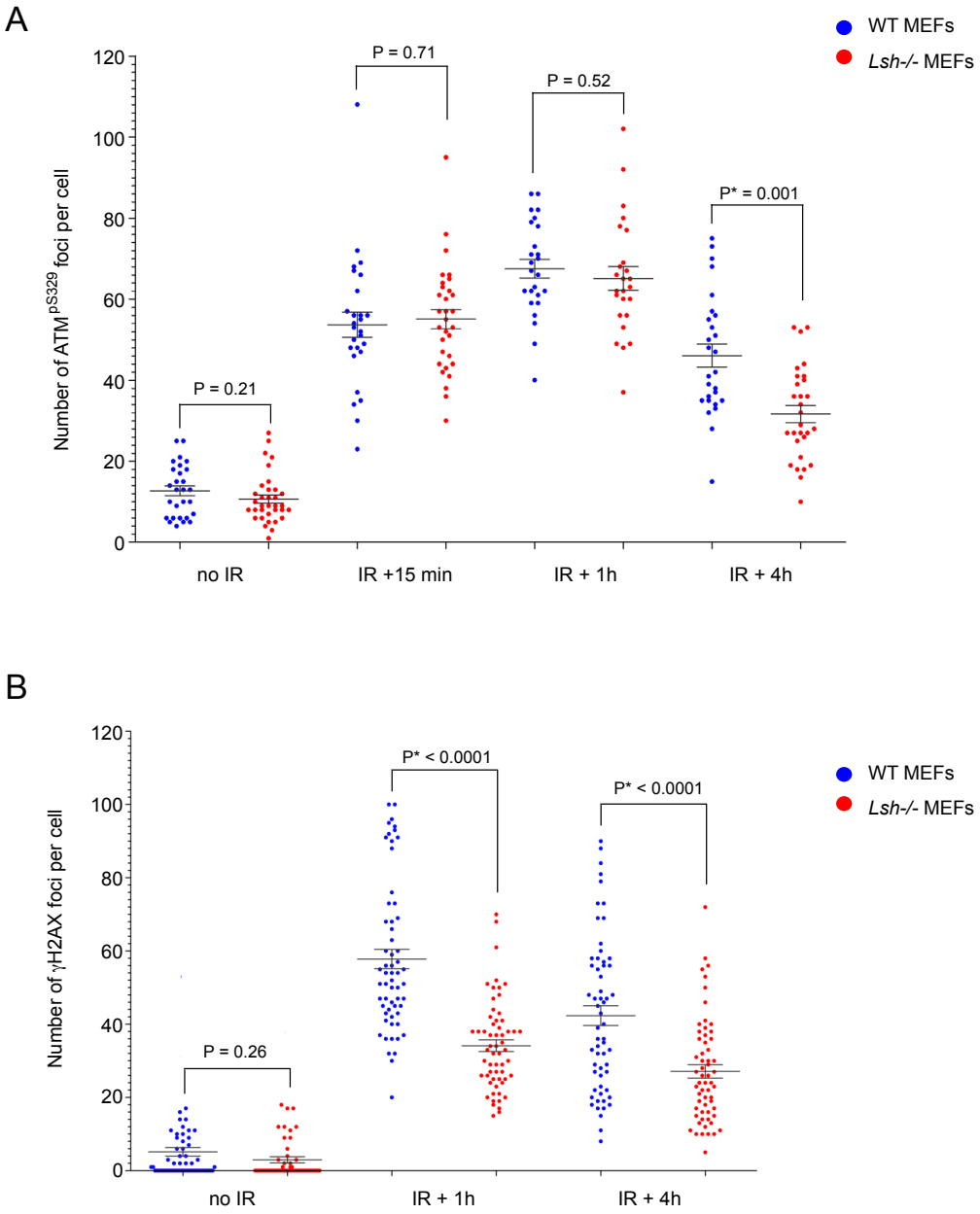

Supplemental Figure 1 Quantification of ATM^{pS329} and γH2AX foci in wild-type and *Lsh-/-* MEFs

A. Counts of ATM^{pS329} foci in non-irradiated and irradiated wild-type and *Lsh-/-* MEFs at indicated time points. Each dot on the graph represents a single cell. The mean value and the standard error of the mean are indicated for each group of cells. Note that there is no significant difference between the wild-type and *Lsh-/-* cells in the number of ATM^{pS329} foci observed 15 minutes and 1 hour post-IR indicating that the initial recognition of DSBs is not impaired in LSH-deficient cells. Comparable number of foci also correlates well with equal amount of DNA damage induced by IR in both cell lines as quantified by the comet assays in Figure 1D. However, the number of ATM^{pS329} foci are significantly reduced in *Lsh-/-* MEFs 4 hours after IR. This is consistent with reduced γH2AX levels in *Lsh-/-* MEFs at this time point and the existence of a feed back loop at later time points after DNA damage where spreading of γH2AX from the break recruits more ATM in MDC1/MRN-dependent manner allowing continuous ATM signalling at slow repairing breaks (Lou et al, 2006; van Atticum and Gasser, 2009).

B. Counts of γH2AX foci in wld-type and *Lsh-/-* MEFs. The mean value and the standard error are indicated. Note that *Lsh-/-* MEFs show reduced number of foci at 1h and 4h time points after IR, which is consistent with the reduced signal observed in Western blots.

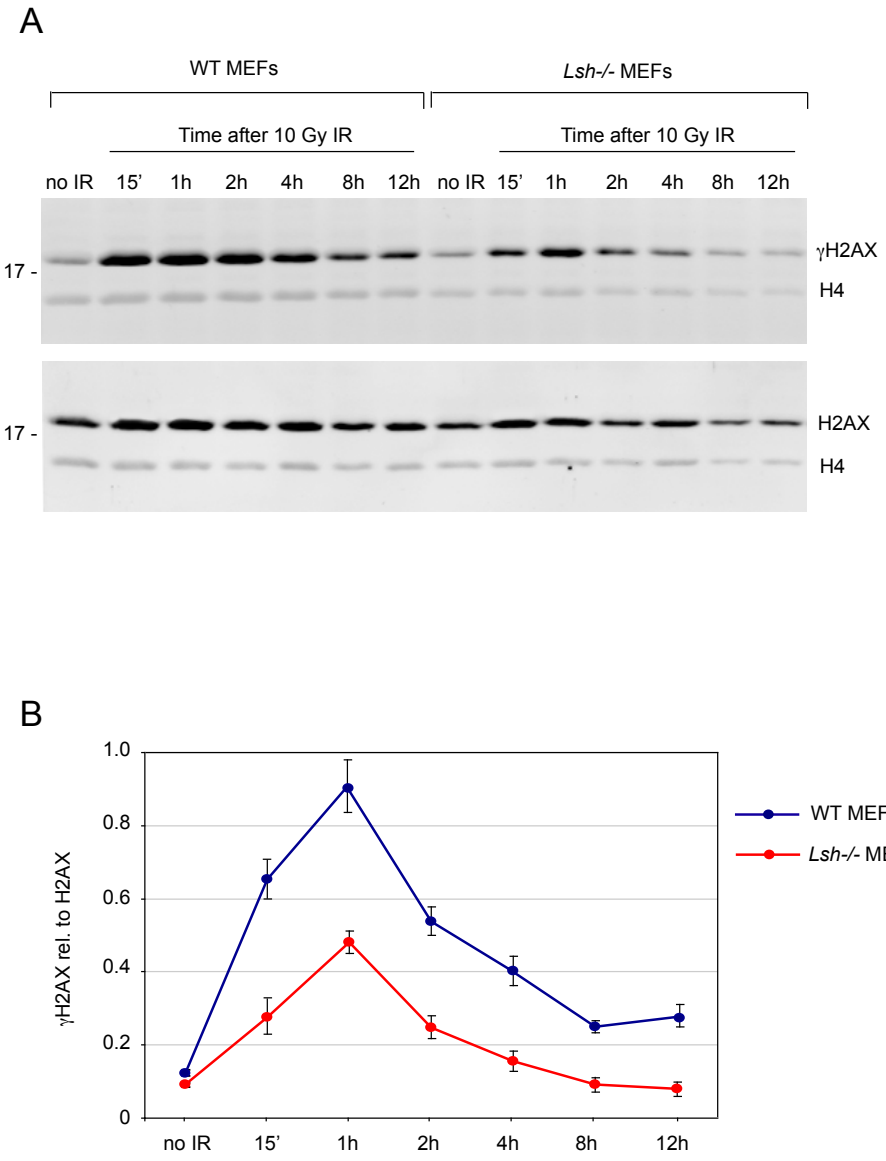

Supplemental Figure 2 Inefficient phosphorylation of H2AX in irradiated *Lsh-/-* MEFs

A. A representative quantitative Western blot detecting γH2AX, H2AX and histone H4 in nuclear extracts of wild type and *Lsh-/-* MEFs before and after exposure to 10Gy of ionizing radiation. Irradiated MEFs were collected at indicated time points.

B. Average levels of γH2AX relative to H2AX in wild-type and *Lsh-/-* MEFs during recovery from IR quantified from Western blots representing three independent experiments (biological replicates). Note that *Lsh-/-* MEFs do not display reduced levels of H2AX. Histone H4 serves as endogenous loading control.

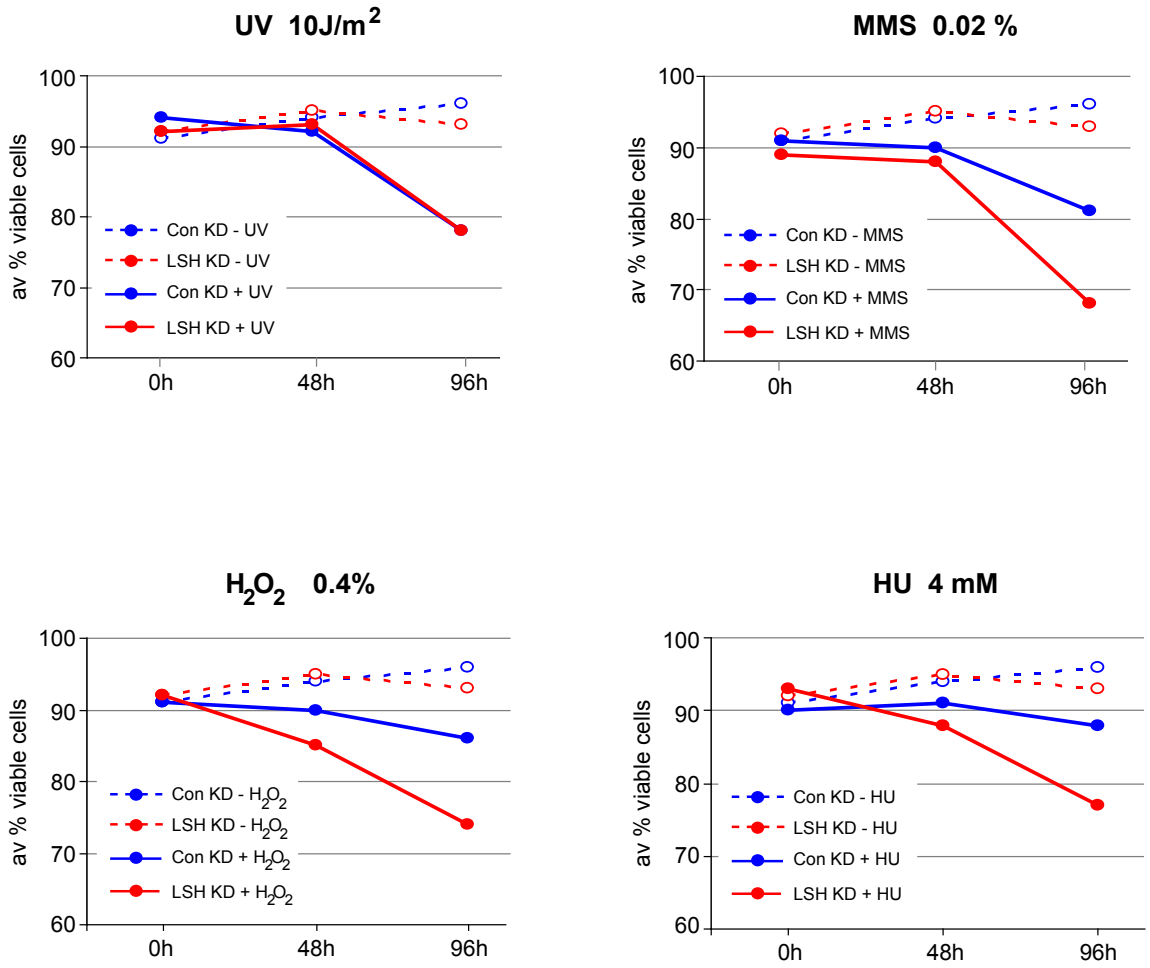

Supplemental Figure 3 Sensitivity of control and LSH-deficient MRC5 cells to DNA damaging agents

Control MRC5 cells expressing non-silencing shRNA and LSH KD MRC5 cells were tested for viability after treatment with UV, MMS, hudroxyurea (HU) and hydrogen peroxide (H_2O_2). Note that LSH KD cells are more sensitive to most DNA damaging agents, but not UV or camptothecin (not shown). The % viable cells was determined as described in Figure 7D.

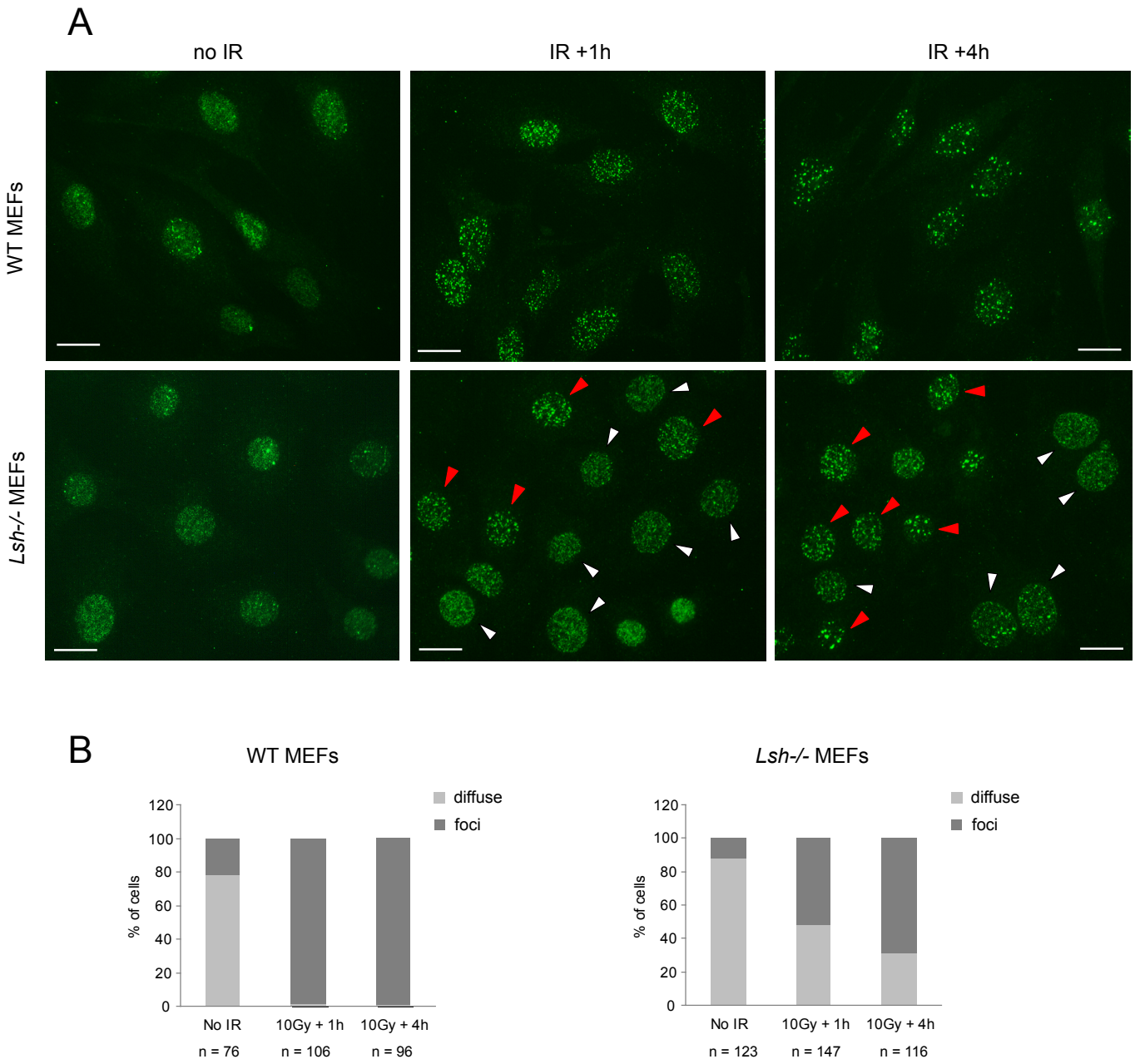

Supplemental Figure 4 Localization of 53BP1 in wild type and *Lsh-/-* MEFs

A. Representative images of wild type and *Lsh-/-* MEFs before and after IR (1- and 4-hour time points) stained with antibodies against 53BP1. In the panels showing irradiated *Lsh-/-* MEFs cells the white arrows indicate cells with diffuse 53BP1 staining and the red arrows point to cells that form discrete 53BP1 foci. The scale bar represents 10 μm

B. Quantification of cells with diffuse and punctated 53BP1 staining. "n" indicates the number of cells counted at each time point.

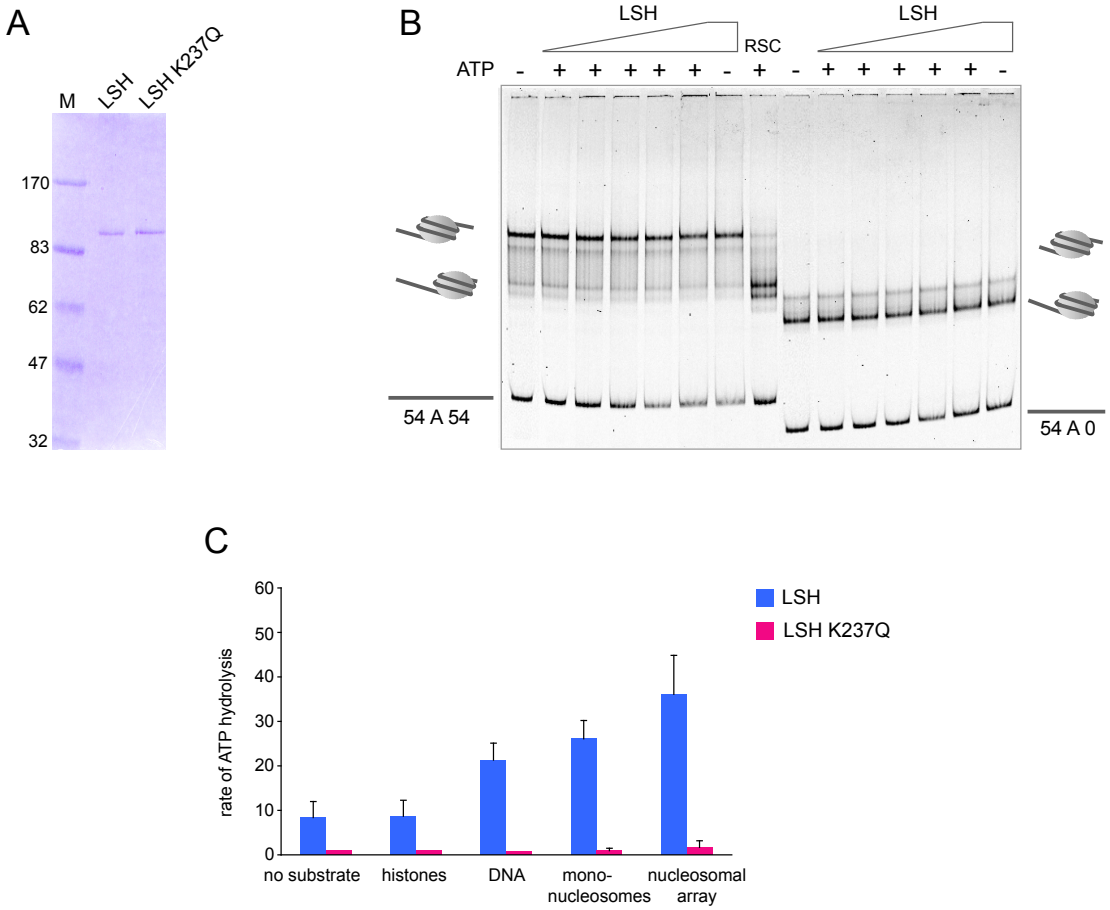

Supplemental Figure 5 Nucleosome repositioning and ATPase activity of recombinant LSH

A. Recombinant wild type and mutant 6xHis-tagged LSH proteins were expressed in insect cells and purified by Ni-affinity chromatography followed by ion exchange chromatography to remove any LSH-bound DNA. M represents molecular weight marker.

B. Recombinant wild type LSH does not reposition either a centrally (54A54) or end positioned nucleosome (54A0) in the presence of ATP. Recombinant yeast RSC protein (100 nM) was used as a control protein that repositions a centrally positioned nucleosome. The triangles indicate increasing concentrations of LSH protein in the reaction (25, 50, 100, 200, 300 nM).

C. LSH shows a weak DNA-stimulated ATPase activity, which is disrupted by the K237Q mutation in ATP binding site. The rate of ATP hydrolysis represents molecules ATP hydrolysed per minute per mol LSH.

Table S1. Expression of DNA repair genes in wild-type and *Lsh-/-* MEFs

The table contains an extract of expression microarray data from Myant et al (2011) *Genome Res* **21**, 83-94 comparing the wild-type (WT) and *Lsh-/-* (KO) MEFs.

M.KO = log2(KO-WT)
FDR.KO = false discovery rate, after p-value adjustment for multiple testing (Benjamini-Hochberg method)
KO = log2(KO)
WT = log2 (WT)

Chr	Gene Name	Gene_ID	Description	M.KO	FDR.KO	KO	WT	Fold change
chr9	H2afx	15270	\H2A histone family, member X\""	-0.2	0.071	13.1	13.0	0.9
chr9	Mre11a	17535	meiotic recombination 11 homolog A (S. cerevisiae)	-0.5	0.052	11.9	12.4	0.7
chr11	Rad50	19360	RAD50 homolog (S. cerevisiae)	-0.1	0.658	12.9	13.0	0.9
chr4	Nbn	27354	nibrin	-0.1	0.573	12.5	12.7	0.9
chr15	Xrcc6 (Ku70)	14375	X-ray repair complementing defective repair in Chine	-0.7	0.013	12.3	12.9	0.6
chr1	Xrcc5 (Ku80)	22596	X-ray repair complementing defective repair in Chine	-0.2	0.551	12.7	12.9	0.9
chr9	Atm	11920	ataxia telangiectasia mutated homolog (human)	-0.3	0.135	11.3	11.5	0.8
chr9	Atr	235533	ataxia telangiectasia and Rad3 related	-0.1	0.743	8.4	8.6	0.9
chr16	Prkdc	19090	\protein kinase, DNA activated, catalytic polypeptide\	0.6	0.008	11.8	11.1	1.5
chr18	Rbbp8 (CtIP)	225182	retinoblastoma binding protein 8	-0.6	0.039	8.9	9.4	0.7
chr1	Exo1	26909	exonuclease 1	-0.5	0.114	8.8	9.3	0.7
chr7	Blm	12144	Bloom syndrome homolog (human)	-1.2	0.000	11.3	12.4	0.4
chr5	Xrcc2 Rad51	57434	X-ray repair complementing defective repair in Chine	-1.1	0.002	8.4	9.5	0.5
chr11	Rad51c	114714	Rad51 homolog c (S. cerevisiae)	-0.4	0.083	7.6	8.0	0.8
chr12	Rad51l1	19363	RAD51-like 1 (S. cerevisiae)	-0.2	0.769	7.5	7.7	0.9
chr11	Rad51l3	19364	RAD51-like 3 (S. cerevisiae)	-0.2	0.626	7.5	7.8	0.9
chr11	Rpa1	68275	replication protein A1	-0.5	0.041	12.2	12.5	0.7
chr6	Rad52	19365	RAD52 homolog (S. cerevisiae)	-0.3	0.153	11.6	11.9	0.8
chr9	Rad54l2	81000	Rad54 like 2 (S. cerevisiae)	0.4	0.102	10.4	10.1	1.3
chr4	Rad54l	19366	RAD54 like (S. cerevisiae)	-0.7	0.011	12.3	13.0	0.6
chr17	Mdc1	240087	mediator of DNA damage checkpoint 1	0.2	0.004	9.8	9.6	1.1
chr19	Rad9 (53BP1)	19367	RAD9 homolog (S. pombe)	-0.3	0.020	12.8	13.0	0.8
chr2	Dclre1c (Atrtemis)	227525	\DNA cross-link repair 1C, PSO2 homolog (S. cerevis	0.0	0.983	7.9	8.0	1.0
chr13	Xrcc4 (Ligase IV)	108138	X-ray repair complementing defective repair in Chine	0.0	0.889	9.9	10.0	1.0
chr7	Xrcc1 DNA lig3	22594	X-ray repair complementing defective repair in Chine	-0.5	0.033	12.6	13.1	0.7
chr12	Xrcc3 HJ resolvase	74335	X-ray repair complementing defective repair in Chine	0.3	0.219	10.2	9.9	1.3
chr15	Rad1	19355	RAD1 homolog (S. pombe)	0.0	0.941	11.3	11.3	1.0
chr15	Rad21	19357	RAD21 homolog (S. pombe)	0.0	0.983	14.0	13.9	1.0
chr13	Rad17	19356	RAD17 homolog (S. pombe)	-0.2	0.420	12.4	12.6	0.9
chr9	Rad54l2	81000	Rad54 like 2 (S. cerevisiae)	0.4	0.102	10.4	10.1	1.3
chr8	Rad23a	19358	RAD23a homolog (S. cerevisiae)	0.6	0.007	13.5	13.0	1.5
chr6	Rad18	58186	RAD18 homolog (S. cerevisiae)	-0.8	0.002	11.1	11.9	0.6
chr5	Rad9b	231724	RAD9 homolog B (S. cerevisiae)	0.7	0.059	7.3	6.7	1.6
chr4	Rad54l	19366	RAD54 like (S. cerevisiae)	-0.7	0.011	12.3	13.0	0.6
chr4	Rad23b	19359	RAD23b homolog (S. cerevisiae)	-0.3	0.245	14.3	14.5	0.8
chr6	Rad52	19365	RAD52 homolog (S. cerevisiae)	-0.3	0.153	11.6	11.9	0.8
chr11	Brca1	12189	breast cancer 1	-0.2	0.001	11.8	11.7	0.9
chr5	Brca2	12190	breast cancer 2	-0.3	0.002	11.0	11.3	0.8
								1.0
chr9	Chek1 (Rad27)	12649	checkpoint kinase 1 homolog (S. pombe)	-0.2	0.000	9.7	9.9	0.9
chr5	Chek2 (Rad53)	50883	CHK2 checkpoint homolog (S. pombe)	-0.9	0.003	8.7	9.6	0.6
chr11	Trp53	22059	transformation related protein 53	0.9	0.002	13.8	12.9	1.9
chr19	Htatip (Tip60)	81601	\HIV-1 tat interactive protein, homolog (human)\""	-0.1	0.821	12.6	12.6	1.0
chr7	Htatip2	53415	\HIV-1 tat interactive protein 2, homolog (human)\""	0.4	0.002	7.8	7.4	1.4
chr19	Ddb1	13194	damage specific DNA binding protein 1	-0.2	0.397	14.8	15.0	0.9
chr2	Ddb2	107986	damage specific DNA binding protein 2	0.5	0.103	10.1	9.7	1.4
chr8	Cul4a	99375	cullin 4A	-0.5	0.031	13.4	13.9	0.7
chrX	Cul4b	72584	cullin 4B	-0.3	0.148	13.1	13.5	0.8
chr17	Rnf8	58230	ring finger protein 8	-0.8	0.003	11.5	12.2	0.6
chr16	Rnf168	70238	ring fnger protein 168	0.0	0.967	10.6	10.6	1.0
chr1	Smarcal1	54380	\Swi/SNF related matrix associated, actin dependent	0.5	0.092	10.7	10.3	1.4
chr2	Inoc1 (Ino80)	68142	INO80 complex homolog 1 (S. cerevisiae)	0.1	0.871	11.1	11.0	1.0
chr3	Smarca3 Hltf	20585	\SWI/SNF related, matrix associated, actin depender	-1.2	0.000	9.9	11.1	0.4
chr3	Smarca3	20585	\SWI/SNF related, matrix associated, actin depender	-0.9	0.002	7.6	8.6	0.5
chr3	Chd1l (ALC1)	68058	chromodomain helicase DNA binding protein 1-like	-1.5	0.000	10.9	12.3	0.3
chr6	Smarcad1	13990	\SWI/SNF-related, matrix-associated actin-dependen	-0.5	0.051	10.5	10.9	0.7
chr8	Smarca5 Snf2h , WCRF13	93762	\SWI/SNF related, matrix associated, actin depender	-0.5	0.059	13.4	13.9	0.7
chr9	Smarca4 (Brg)	20586	\SWI/SNF related, matrix associated, actin depender	-0.2	0.504	13.4	13.5	0.9
chr19	Smarca2 (Brm)	67155	\SWI/SNF related, matrix associated, actin depender	-0.1	0.827	13.6	13.6	1.0
chrX	Smarca1 Snf2L	93761	\SWI/SNF related, matrix associated, actin depender	-2.1	0.001	6.9	8.9	0.2
chr6	Chd4	107932	chromodomain helicase DNA binding protein 4	0.2	0.636	14.4	14.2	1.1
chr19	Ppp1ca	19045	\protein phosphatase 1, catalytic subunit, alpha isofo	-0.4	0.056	14.4	14.8	0.8
chr11	Ppp2ca	19052	\protein phosphatase 2 (formerly 2A), catalytic subur	0.0	0.924	12.7	12.7	1.0
chr7	Ppp4c	56420	\protein phosphatase 4, catalytic subunit\""	0.2	0.477	14.2	14.0	1.1
chr2	Ppp6c	67857	\protein phosphatase 6, catalytic subunit\""	0.5	0.057	13.4	12.9	1.4
chr11	Ppm1d (Wip1)	53892	\protein phosphatase 1D magnesium-dependent, del	0.0	0.924	10.0	10.0	1.0